Effect of Permeation on Discharge Characteristics of Capacitive Deionization Process

By

Ishan Barman

B.Tech., Mechanical Engineering
Indian Institute of Technology, Kharagpur, 2005

SUBMITTED TO THE DEPARTMENT OF MECHANICAL ENGINEERING IN PARTIAL FULLFILMENT OF THE REQUIREMENTS FOR THE DEGREE OF

MASTER OF SCIENCE IN MECHANICAL ENGINEERING
AT THE
MASSACHUSETTS INSTITUTE OF TECHNOLOGY

June 2007

Signature of Author .....
Department of Mechanical Engineering
May 19, 2007

Certified By.....
Nam P. Suh
Ralph E. and Eloise F. Cross Professor of Mechanical Engineering
Thesis Supervisor

Accepted By .....
Lallit Anand
Chairman, Departmental Committee on Graduate Studies
Department of Mechanical Engineering

Effect of Permeation on Discharge Characteristics of Capacitive Deionization Process

by
Ishan Barman

Submitted to the Department of Mechanical Engineering
on May 19, 2007, in partial fulfillment of the
requirements for the Degree of Master of Science in
Mechanical Engineering

Abstract

Cost-effective desalination of seawater can be a panacea for the growing freshwater crisis that ranks alongside the problems of shortage of viable energy resources and global warming in terms of its frightening global spread and magnitude. However, the energy guzzling nature of the existing desalination technologies has resulted in very limited relief characterized by a meager 0.3% contribution to the annual water use. In recent years, capacitive deionization (CDI) has been reported to potentially solve some of the crucial issues that have plagued the classical desalination processes. CDI is a low-pressure, non-membrane desalination technology that employs the basic electrochemical principle of adsorbing ions in a capacitive fashion to high surface-area electrodes such that the outgoing stream becomes devoid of the ions that were present in the incoming stream. Although the power efficiency of CDI is nearly an order-of-magnitude superior to the existing processes, it is plagued by the problem of low water recovery ratio. The costs of pumping and pre- and post-treatment of water added to the rising costs of surface water makes maximizing the recovery ratio a priority. Moreover, the throughput of the plant is related to the water recovery ratio.

To drastically reduce the problem of low water recovery ratio while still maintaining the sizeable power consumption advantage of the CDI process, we propose a capacitive deionization process with permeating flow discharge (PFD). In PFD, the waste water is permeated through the porous electrodes rather than flowing in-between the electrodes as is the case in the conventional axial flow discharge (AFD) process. We hypothesize that the rate of removal of ions from a channel setup is higher for a process that is influenced by solvent drag (PFD) than for one which is diffusion limited (AFD), given the same flow conditions.

A table-top setup, designed to simulate the AFD and PFD processes, is used to obtain precise experimental evidence for the ion removal rate for each process. A mathematical model based on unsteady convection-diffusion process for AFD and membrane transport process for PFD is presented. We find that over smaller time scales, permeating flow is much more efficient in removing the ions detached from the electrical double layer in the porous electrode. Based on our experimental observations, we observe that the use of the PFD process, under conventional operational conditions, can cause a discharge time reduction by at least a factor of two. Numerical simulations carried out on the basis of this model are shown to compare favorably with the experimental observations. The model predicts that the reduction in discharge time translates to an increase in water recovery ratio by approximately 30 percent. Moreover, the clear superiority in power efficiency is not surrendered by employing this new scheme.

Thesis Supervisor: Nam P. Suh
Title: Ralph E & Eloise F Cross Professor of Mechanical Engineering

Acknowledgements

Delving into the intricacies of desalination has been one of the most wonderfully rewarding experiences of my life. It has been challenging at all times to deal with a project of such far-reaching consequences but the intellectual stimulation it has provided me has been worth the journey. And the ride would not be what it has been if not for all the support that I have received from some truly remarkable people.

First and foremost, I would like to acknowledge the unwavering support and insightful guidance of Professor Nam P. Suh. Without his resourcefulness and creative inputs, the project would have faltered many a times. His enthusiasm for the project did not flag even when he shifted to KAIST. It has been a pleasure to work with a man of his stature, understanding and experience. Through my interactions with him, I have grown as a researcher and as a person.

I also owe a great deal of gratitude to Professor Sang-Gook Kim, whose suggestions and advice has proven invaluable in shaping the thesis into its current form. Dr. Taesik Lee deserves a lot of credit for keeping a constant tab on the project, and even undertaking to help out with the experiments performed. He has also provided an excellent sounding board for all our ideas and an able negotiator for the conflicts we have had during the process. Dr. Gyunyoung Heo, for the time he was associated with the project, contributed immensely, especially on the experimental front. He was instrumental in setting up our apparatus, right down to the nuts and bolts.

I would take this opportunity to thank all my labbies: Steve, AJ, Malin, Hrishi, Pete, Jordan and Eric. They have eased the trials and tribulations of adjusting to life at MIT and, of course, of the research itself. Our group meetings have provided me with a ready source of feedback. We have shared much more than a dour academic existence and our bonding has provided me with a source of sustenance on many an occasion. Thanks are also in order for Tony Pulsone for the skillful maneuvering that has been needed at times.

I am indebted to my professors at IIT Kharagpur, especially Professor Sujoy Guha and Professor S. K. RoyChowdhury. Professor Guha taught the ABCs of research, showing me the ins and outs of an academic life. And needless to say, I would not have survived even my freshman year had it not been for the life support system provided by Professor RoyChowdhury.

My friends, from Kolkata and Kharagpur, deserve a special mention. My conversations and emails with each and every one of them has let me lead a normal existence. I cannot thank them enough for that. Two of them deserve a special mention in this regard. Shiladitya, especially for the period when he was at Tufts, has given me a helping hand, right from groceries to MEMS. Our conversations must have made Cingular rethink their phone plans. A special token of thanks needs to go out to Damayanti. She has provided me with a constant sounding board. Her enthusiasm in listening to the electrochemistry of desalination must be commended.

Finally, I do not know where and how to start thanking my parents. There are no words to express my feelings of gratitude and really anything I will put down does not do justice to their efforts. They have always – with a capital A – believed in me and my pursuits. Never have they had anything but words of encouragement and support. Baba and Ma, I would like you to know that one cannot have better mentors, friends and guides than you have been.

Table of Contents

List of Figures

List of Tables

Chapter 1: Introduction

The presence of water is central to the functioning of all living organisms. The human body consists of approximately seventy-five percent water showing the importance of this single component in the sustenance of life forms. The characteristic properties of water, particularly with regard to its solvent ability, dielectric constant, temperature of maximum density, heat capacity and surface tension, make it immeasurably important for all organic life so much so that it is currently theorized that the presence of water on any celestial body might provide the first signs of existence of preliminary life on it. From a biological standpoint alone, water plays vital roles in photosynthesis and respiration, in acid-base reactions and enzyme reactions, as a universal solvent and as an essential part of numerous metabolic processes.

In order to satisfactorily perform most of the aforementioned functions, it is critical that the solute concentration of the water consumed lies within a specific window of tolerance, as required for the particular process or reaction. For example, as the solvent base of the fluids in plants and animals, water is instrumental in the transportation of nutrients to tissues and cells in the body as well as in the removal of waste matter from the body. This requires the periodic replenishment of water in the body, which is accomplished in a large number of organs and tissues by the passage of water through semi-permeable membranes, such as the root covering of plants and the lining of colon in animals. The semi-permeable membranes permit water flow from a dilute solution to a relatively concentrated one by osmosis, while screening the dissolved minerals. The physics of the osmosis process necessitates that the fluids used to replenish the body must be less concentrated than the body fluids. Evidently, each of the fluid transport processes, whether governed by osmosis, convection or diffusion, imposes its own restrictions on the concentration of water that can be used for replenishment.

The most important consequence of the limitations imposed on the water intake concentration by the physics of the various processes governing the physiological phenomena is that seawater and even brackish water, which has a substantially high concentration of ions, is unacceptable for direct human consumption. To overcome this problem, most marine and estuarine life, which have no alternative but to consume saline water, have developed special capabilities to concentrate wastes and retain as much fresh water as possible in the body. While there are a number of factors, such as concentration of particular compounds, alkalinity and pH, that determine the acceptability of water for consumption purposes, a generic figure that is commonly cited as the maximum desirable concentration limit for potable water is 500 parts per million (ppm) of total dissolved solids (TDS) [1]. The other factors mentioned above provide additional stipulations on the 'safety' of drinking water, including upper bounds on concentration of specific chemicals of health significance, such as fluoride, nitrate and pesticide, concentration of substances that give rise to consumer complaints, and bacterial contamination.

While fresh water is absolutely critical in sustaining various life processes, its significance in agricultural uses, particularly in developing countries, cannot be underestimated. Irrigation of crops, particularly in equatorial and tropical climates, account for nearly seventy percent of global water consumption [2]. Given the hot and dry conditions of the developing countries in these regions, it is perhaps not surprising that a disproportionately high amount of water is required to feed the burgeoning population. It is also no coincidence therefore that ancient civilizations, which possessed exclusively agrarian characteristics, flourished in regions with abundant supply of fresh water. Mesopotamia, the ancient Egyptian civilization, and the Indus Valley Civilization developed around the riverine regions watered by the Tigris and Euphrates, the Nile and the Indus and Ghaggar-Hakra rivers respectively. Needless to say, very few of the early human settlements were situated in regions of plentiful saline water (near seas or oceans, for example), where fresh

water from rivers and lakes was not readily available. In addition to irrigation, agricultural water consumption figures also account for the water required for livestock, dairies and fish farms. While the ratio of water used for livestock to that used for irrigation is typically very small, inefficient and labor-intensive irrigation methods can raise both the total amount of water required and the fraction of water consumed by livestock. It is worth mentioning here that given the large amount of water that is needed for irrigation and the skewed distribution of fresh water resources, the piping losses in the water conveyance systems for irrigation can be substantial.

Along with agriculture, domestic and public water consumption, the other major category of de-mineralized water use is industrial. In this classification scheme, industrial water use accounts for not only the water utilized by the electronics, pharmaceuticals and food industries amongst others but also by the power generation stations, where it is used primarily in the form of boiler feed water and coolant. While industrial and energy development use varies widely from the least developed countries to the industrialized nations, it is estimated that industrial water consumption across the globe occupies a twenty-three percent segment of the total water consumption pie [3]. Various industries designate different tolerance ranges for water intake, but power generation plants typically are capable of handling a higher degree of salinity in their water intake than the pharmaceuticals and semiconductor industries. The latter, in particular, demands that the input water is chemically, physically and biologically very pure – and the trend towards further miniaturization of circuit components is imposing even stricter requirements [4]. Moreover, it might also be important to monitor other 'purity' parameters such as water hardness and water activity level (defined as the ratio of the vapor pressure of water in a solution to the vapor pressure of pure water), for example, in the food processing industry. Water activity level is a function of solute concentration and directly affects microbial growth, which in turn impacts the preservation and shelf-life of food items [5].

In the face of such obvious need for ample fresh water supply to generate energy, grow crops, provide for high-tech fabrication and most importantly to sustain life, it is evident that any strain on the global fresh water resources can have major repercussions. As it stands, 97 percent of the earth's water is saline and contains anywhere between 3.1 to 3.8 percent salt by weight, which translates to an average of 35,000 ppm of total dissolved solids [6]. This leaves only 3 percent of the water on the planet in the 'freshwater' category. However, two-thirds of the total freshwater is locked up as ice in the glaciers and frozen polar caps. The remaining 1 percent is carved out approximately in the ratio of 3:7 between surface water resources and groundwater aquifers. In other words, the amount of stored freshwater (as differentiated from the annual precipitation which serves to replenish the water resources) that can be readily treated to yield water suitable for the aforesaid uses is about 0.5 percent of the total water available on Mother Earth. Moreover, the distribution of freshwater resources and rainfall is fairly uneven over the entire land mass. The high cost of water redistribution prohibits the transportation of water over large distances to arid and drought affected regions.

It is worth mentioning that about seven-eighths of the surface freshwater, which requires the least effort to transform to product water both in terms of energy cost as well as quality and quantity of necessary water treatment, is contained in freshwater lakes, with swamps and rivers accounting for the rest. Regions that do not receive sufficient annual precipitation and do not have lakes and rivers in their vicinity are, therefore, prone to serious and recurring droughts. While this has been the prevalent situation for as long as human civilization has existed, the availability of fresh water has taken a sharp downturn in recent decades due to substantial human interference in the natural hydrologic cycle.

Population explosion, coupled with the rising living standards and rapid industrialization, has led to shrinking per capita supplies all around the globe. Overpopulation has also brought about irresponsible practices, such as misuse of available freshwater and pollution of freshwater sources, which have in turn led to unprecedented water scarcity. Flood irrigation, which is extensively used in major agricultural pockets around the world, provides a classic example of appallingly inefficient utilization of water resources. Although this form of irrigation satisfies the primary functional requirement of supplying water to the crops on the field, massive quantities of water are allowed to just trickle away or evaporate before serving any known purpose. The resultant overirrigation causes a multitude of problems ranging from depletion of groundwater aquifers to surface subsidence as experienced in Mexico City [7]. It also has a deleterious effect on sustainable agricultural yields and on the quality of soil surface it leaves in its wake.

The inadequacy of fresh water supplies to meet the demands of the human population locally and globally has meant that the world is facing a crisis of gigantic proportions that ranks alongside the twin problems of shortage of viable energy resources and global warming in terms of its frightening spread and magnitude. This inadequacy exists not only in terms of insufficient quantity of water resources available at a specific location but also in terms of the poor quality of water in places where the availability of 'untreated' water is not a concern. The latter obviously precludes the possibility of human consumption due to the presence of excess amount of chemical, physical or/and biological impurities. Typically, in underdeveloped countries the acute deficiency of basic infrastructure as regards water withdrawal facilities (whether it be from groundwater aquifers or surface water supplies) and water conveyance systems is the root cause of water scarcity. In overpopulated developing countries, on the other hand, the focus of the water crisis is on the lack of proper water treatment particularly for domestic water supplies.

The poor quality of water, characterized by the presence of excess minerals and bacterial contamination, is a crucial issue as evidenced by the fact that waterborne diseases are responsible for the largest number of deaths worldwide and are estimated to cause around 80 percent of all human sicknesses [8]. Diarrhea, while usually thought of as an irritation more than as a medical condition in developed countries, has an annual fatality count in the region of 2 million people worldwide [9]. The spread of acute diarrhea, particularly among infants, has a high degree of correlation with lack of access to safe drinking water and inadequate sanitation facilities. While the incidence and severity of such diseases is primarily restricted to people in underdeveloped and developing nations, specific population pockets in periurban and rural areas of developed countries also face the danger of coming in contact with viral infections and bacterial toxins carried by contaminated water.

The World Water Development Report 2003 [10] delivers the grim prognosis that by the middle of this century, more than 50 nations, constituting a population of about 5 billion, will face a water crisis. The World Resources Institute report [11] estimates that, in 1995, 41 percent of the world's population, or 2.3 billion people, were living in river basins under 'water stress', meaning that per capita water supply was less than 1700 m^3/year. Monitoring surveys, conducted jointly by WHO and UNICEF [12], reveal that, despite slight gains in water coverage during the 1990s, approximately 1.1 billion people still have to depend on unreliable water resources such as ponds, unprotected wells and vendor-provided water to meet their daily needs. The major reason for the unavailability of reliable water supplies can be attributed to the fact that the increase in water coverage (from 77 percent to 82 percent in the decade of 1991-2001) has barely kept pace with the population explosion and migrations in the developing world. The surveys also highlight that arsenic poisoning of groundwater has become a serious problem for a number of Asian countries during the past decade. To complicate matters further, nearly 2 billion people around the globe do not have access to adequate sanitation facilities. These twin issues of shortage of

safe drinking water and inadequate sanitation facilities are inherently inter-linked as improper sewage disposal due to lack of proper sanitation gives rise to contamination of safe drinking water lines. The converse relation is established by the fact that places lacking adequate drinking water resources are unable to afford the 'luxury' of sufficient water for sanitation.

The numbers predict a bleak future for a water-stressed society which increasingly has greater demands for de-mineralized water and lesser supply avenues to satisfy those demands. However, even these figures tend to substantially underestimate the gravity of the problem because they reflect only gross macroscopic averages of annual precipitation, withdrawal and consumption, smoothing out local irregularities and shortfalls. More importantly, however, the statistics fail to reveal the far-reaching consequences of the socio-economic manifestations of limited water resources. It would not be far from the truth if one were to say that control of limited water resources is one of the major destabilizing forces and cause for potential conflicts in many parts of the world. While it might be a little too premature to accept the "next world war will be over water" rhetoric, tensions clearly exist over water as a 'strategic resource' and nowhere more so than in the Middle East, where armies have prepared to go to war over water ownership [13, 14].

The main problem, from a geo-political perspective, is the mindset that local water resource is an absolute territorial matter that must be controlled by people local to the region. In reality, though, few would disagree that water must be a shared resource that necessitates global cooperation to manage appropriately and to benefit all by doing so. Issues pertaining to water use, water ownership and water rights continue to provide an added edge to underlying border tensions in already destabilized regions. Although Helsinki Rules [15] provide a certain framework to negotiate international water disputes, in many a case the fight for water might only provide the ignition for the war for survival, which to all intents and purposes supercedes any logical rationale. International water disputes that fall into this category are familiar to the nations of North and South Korea, Egypt, Ethiopia and Sudan, and Israel and Palestine. In Israel, for example, extraction from water resources has exceeded replenishment by 2.5 billion meters in the past 25 years [16] and given that water needs are only going to spiral up, water use becomes an 'add-on' to the myriad issues that need to be resolved in the region.

Another major water-related flashpoint on the world stage pertains to the withdrawal and nature of use by upstream consumers that has a direct bearing on the quantity and quality of water available to people further downstream. Wrongful dam construction and diversion projects have huge social manifestations since entire villages, towns or even states might need to be relocated as a consequence of the poorly planned action. Typically such construction also comes at a substantial environmental cost, as a result of the widespread damage caused to both vegetation and wildlife in the region. Other unpleasant issues that arise from water scarcity and subsequent tensions arising from water use and ownership include questions on food security for nations starved of water, hugely subsidized water pricing, which hurts regions that have abundant supply of water but little else, and productivity of ecosystems, which have been continuously milked for providing water security, in other sectors.

There is no obvious solution to this increased competition between different sectors, different populations and different nations, particularly in the current climate of limited cooperation at all levels. To tackle a global issue of this magnitude, huge mobilization efforts need to take place to create an international consensus that can provide for water security for generations to come. Measures to inculcate equitable water price, empower international agencies to create basic infrastructure in underdeveloped countries, install wastewater treatment plants, and replace flood irrigation methods by drip irrigation and precision sprinklers, have been proposed to reduce the water crisis. While these and other political, social and economic initiatives would undoubtedly

enable better utilization of the meager freshwater resources, a technological breakthrough that can rapidly alleviate the problem is desperately needed in these dire circumstances.

Desalination stands out as an attractive proposition as, theoretically speaking, it can exploit the earth's seemingly boundless reserves of saline water in the oceans and seas to generate freshwater suitable for human consumption as well for agricultural and industrial use. However, over the years, it has failed to meet up to the lofty expectations primarily because of the energy guzzling nature of the different desalination technologies employed to date. The current opinion regarding desalination is that while it may take on greater significance in the future, existing desalination operations will be restricted to countries, where the local distribution of energy and water resources is significantly skewed in favor of the former (e.g. in the Middle-East).

Currently, about 12,300 desalination plants world-wide strive to fulfill the objective of treating sea water to make it fit for various applications, primarily human consumption [17]. However, their cumulative contribution is only about 0.3% of the world's water use. While the desalination technology roadmap projects that by 2020 "water purification and desalination technologies will contribute significantly to meeting the need to assure a safe, sustainable, affordable and adequate water supply" [18], the current state of the art does not allow desalination to be extensively used. However, if by introduction of some novel 'disruptive' technology one were to scale down the energy costs by an order of magnitude or more, the landscape of the water crisis phenomenon might undergo a sea change. It is pertinent to note that in doing so one must be very careful that the capital and maintenance costs do not spiral out of control, as has been the case for a number of promising, yet ultimately unsuccessful, desalination technologies.

The present global desalination market is dominated by membrane-based technologies and thermal desalination methods. In recent years, the former has rapidly gained impetus as compared to the more traditional thermal desalination techniques that have essentially remained the same as regards the basic process structure over the last century or so. Reverse osmosis (RO), which has a market share of approximately 47 percent of installed capacity worldwide [19], is the foremost proponent of the membrane-based desalination technologies. In this process, saline water is filtered through a semi-permeable membrane by applying pressures well in excess of the osmotic pressure against the natural pressure gradient. The thermal desalination techniques, on the other hand, use the time-tested method of evaporating saline water and then condensing the water vapor, formed in the evaporation step, to obtain pure water. The various thermal processes, such as multi-stage flash (MSF) and multi-effect distillation (MED), vary in the pressures and temperatures employed at different stages, and in the number of chambers and passes utilized for a typical process. The MSF process forms the basis of about 36 percent of the world's desalination plants. Another desalination technology that has been in vogue, since the 1970s, especially for brackish water desalination is electrodialysis reversal (EDR) [20]. In the EDR process, saline water is passed through an electrolytic chamber where an electric field is applied to separate out the ions from the pure water. Table 1 presents a comprehensive list of the desalination methods classified according to the respective physical phenomenon that forms the basis for ion separation from saline water. Some of the key ideas behind these different processes are revisited in greater detail in Chapter 2.

Table 1: Classification of desalination technologies based on the physics of the individual processes

Thermal process	Membrane-based process	Electrochemical process	Miscellaneous
Multi-Stage Flash (MSF)	Reverse Osmosis (RO)	Electrodialysis (ED)	Freezing
Multi-Effect Distillation (MED)	Nanofiltration	Electrodialysis Reversal (EDR)	Geothermal distillation
Vapor Compression (VC)	Forward Osmosis (FO)	Electrodeionization (EDI)	Solar humidification
Evaporation/ Condensation (EC)		Capacitive Deionization (CDI)	"Hurricane-vortex" desalination

Membrane related research [21] has helped in decreasing the energy consumption of the RO and EDR processes and enabled the maturation of the RO process, in particular, to a point where the potable water needs in the Middle-East can be satisfied partially by employing this method. However, neither can it be used in water-stressed regions that do not enjoy the luxury of abundant energy resources, such as in the African continent, nor can the greater share of the market, for industrial and agricultural uses, be satisfied with the high energy requirements inherent in the process.

In recent years, capacitive deionization (CDI) has been reported to potentially solve some of the crucial issues that have plagued the classical desalination processes such as energy cost and membrane fouling (Table 2 and 3) [22]. It consists of flow of saline water through a pair of high surface area electrodes (e.g. activated carbon cloth) across which a small voltage is applied. During the flow the ions in the saline water move towards one of the electrodes depending upon the polarity of the ions. The porous electrode is able to electrostatically absorb the ions in a reversible manner. As a result, during this charging process, capacitive current flows in the external circuit connecting the electrodes. Consequently, the water flowing out of the system is de-ionized. Once the capacitor is fully charged, the ions are regenerated by shorting the electrodes (or by applying a reverse polarity). The discharge process, thus, consists of the flushing of the ions adsorbed during the charging process by means of waste water through the same flow path. The basic electrochemical scheme in the CDI process is distinguished from that used in the EDR process by the fact that the former avails of reversible electrostatic adsorption in the electrical double layer close to the surface of the polarizable electrode while the latter employs electrolysis on the surface of the non-polarizable (or reactive) electrode. Surface adsorption naturally requires much less energy than electrolysis of ions.

Although the capacitive process has shown a lot of promise over the last decade or so, it is yet to be fully implemented in an industrial setup. One of the reasons that affect its suitability in such an environment is the low water recovery ratio (with regards to other processes used for brackish water desalination) (Table 2). Water recovery ratio is defined as the ratio of the amount of desalinated water obtained to the total amount of input water. For a given throughput of a desalination plant/process, the water recovery ratio and the power consumption per unit volume

of water desalinated provide the two most significant metrics for judging the effectiveness of the plant/process. The costs of pumping and pre- and post-treatment of water added to the rising costs of surface water makes maximizing the recovery ratio a priority. It is also accepted that aquifer withdrawals surpass the recharge with resulting drops in water tables, which renders the recovery ratio even more important. In the CDI process, it is observed that the discharge typically takes at least half the time required for charging thereby enabling a maximum recovery ratio of 0.5 – 0.6 (for brackish water desalination) [23, 24]. The corresponding recovery ratios for the RO and EDR processes for brackish water desalination typically exceed 0.85 – 0.94 [25]. In addition, the available energy during the process cycle is not fully utilized as it is really operational for half to two-thirds of the total cycle time. Furthermore, the low ratio constrains the range of input saline water the process can be used for.

Table 2 Performance comparison of the major desalination processes

Process / Parameters	Seawater Desalination		Brackish water Desalination		
	MSF	RO	RO	EDR	CDI
Susceptibility to scaling	Low	High	High	Low	Negligible
Final product salinity (ppm TDS)	Can be <10	On demand <500	On demand <500	On demand <500	-
Energy cost ($kWhr/m^3$)	High (25 – 200)	Moderate (7 – 9)	Moderate (~ 2)	Moderate (~ 2.1)	Low (0.05 – 0.5)
Water recovery	Poor, 10 – 25%	Moderate, 50%	High, >80%	High, 85 – 90%	Low, 50 – 60%

Table 3 Cost comparison of RO and CDI (adapted from [23])

	Reverse Osmosis (RO)	Capacitive Deionization (CDI)
Capital cost	$0.52	$0.26
Operating and Maintenance cost	$0.81	$0.14
Total cost	**$1.33**/1000 gallon	**$0.40**/1000 gallon

To drastically reduce the problem of low water recovery ratio while still maintaining the sizeable power consumption advantage of the CDI process, we introduce a capacitive deionization process with permeating flow discharge (PFD). In PFD, the waste water is permeated through the porous electrodes rather than flowing in-between the electrodes as is the case in the conventional axial flow discharge (AFD) process. It is to be emphasized that this change in flow path is implemented during the discharge period only when the electrodes are regenerating. In this study, a table-top setup to simulate both AFD and PFD is designed and fabricated. The experimental observations for the ion removal rate for each process as a function of time is then presented. To understand the physical mechanisms in a more rigorous manner, a mathematical model based on unsteady convection-diffusion process for AFD and membrane transport process for PFD is built. Numerical simulations are carried out to compare with the

experimental observations. Finally, theoretical predictions of the expected benefit in throughput and water recovery ratio due to utilization of the PFD process are presented.

Chapter 2: Review of desalination technologies

A large number of processes have been proposed for water desalination and a few of these have attained commercial importance. As desalination of water typically takes place in large scale industries, for any new idea to mature requires a huge investment of effort and time, not to mention money. Consequently, numerous promising processes have fettered out for the lack of sufficient research into the physics of the processes and subsequent development of the technology. The state-of-the-art approaches, as noted previously in Table 1, utilize a wide variety of physical principles as well as different forms of input energy that include mechanical energy (reverse osmosis), electrical energy (electrodialysis reversal), thermal energy (multi-stage flash distillation) and chemical energy (ion exchange processes). An excellent review of the engineering principles and various practical aspects of the existing desalination processes can be found in Buros' "ABCs of Desalting" report [26].

The feasibility of employing one of these processes at a proposed location is determined not only by the fundamental characteristics of the process but also by a number of location specific factors, such as the concentration of water that needs to be desalted, type and amount of available energy resources and brine discharge possibilities at the proposed plant site. For instance, given a coastal plant location one would be essentially left with the choice of employing either reverse osmosis or multi-stage flash distillation process. On the other hand, at a location where brackish water comes with an associated price tag and the possibilities of brine discharge are very limited (any place distant from the sea or ocean has these limitations), an electrodialysis reversal process would be more in order. The aforementioned factors are reflected in Fig. 1, where in one finds that despite its energy intensive nature, thermal desalination technologies have approximately a 45 percent share in the global market because of the fact that seawater remains the dominant source for desalting. However, if the focus shifts to the US desalination market, one would observe that thermal desalination accounts for just about 5 percent of the total desalinated water. The reason for this anomaly can be traced to the extensive use of brackish water as source in the US (51 percent) relative to the global market (24 percent).

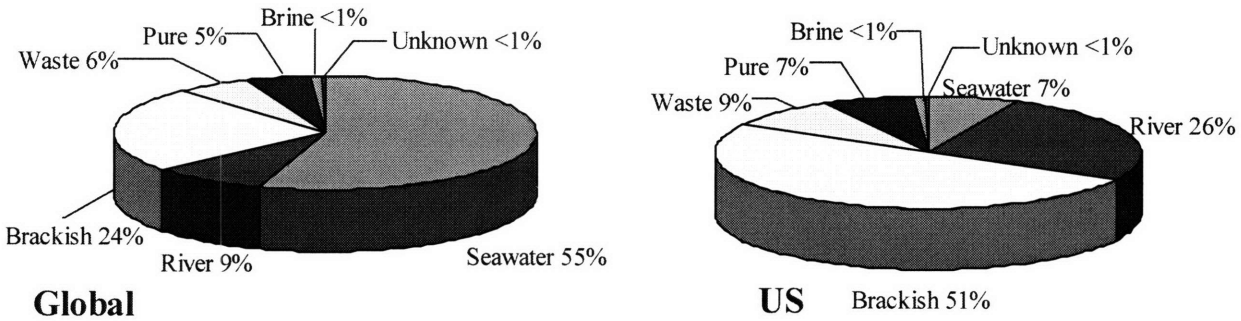

Fig. 1(a): Source water classification: Global market (left) and US market (right) (adapted from [27]).

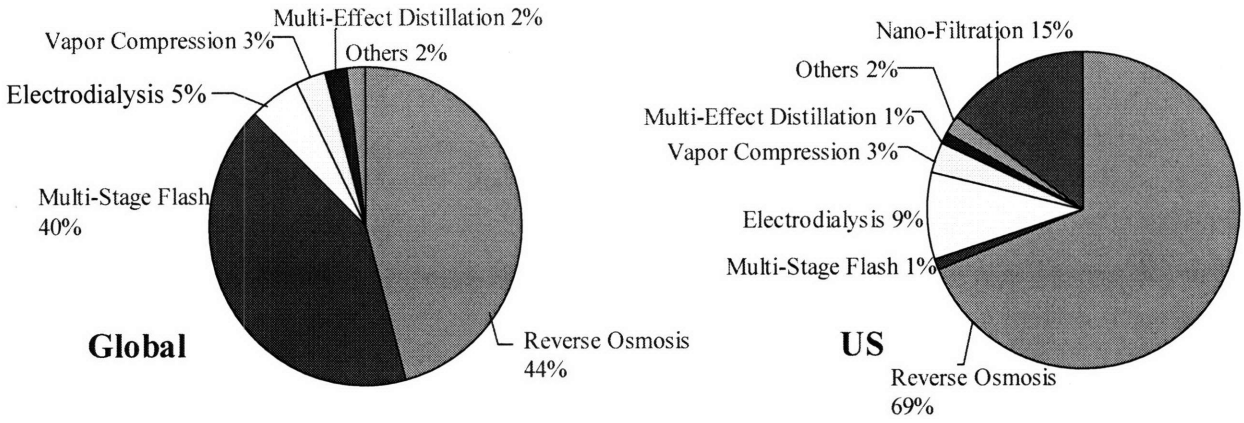

Fig. 1(b): Desalination process classification: Global market (left) and US market (right) (adapted from [27]).

To initiate our review of the existing technologies and the advantages and the pitfalls associated with employing them, let us focus on the key performance characteristics which define the quality of any desalination process. The critical parameters for a desalination plant include throughput (total amount of water desalinated per day), power efficiency (energy required to desalinate unit volume of water), water recovery ratio (ratio of water desalinated to water input) and percent removal of ions. If one imposes an upper bound on the concentration of acceptable (desalinated) water, the percent removal of ions ceases to be a plant performance metric. As the input water has a given salinity (seawater and brackish water have salt concentration in the range of 35000 and 3000 ppm), and the output water must have salinity below 500 ppm to meet human consumption standards, the percent removal of ions becomes pre-specified and is not considered to be a parameter that can be modified or optimized. In other words, the processes must be compared bearing the twin parameters of power efficiency and water recovery ratio in mind, while also accounting for reliability, longevity, fouling characteristics, scalability, and capital and maintenance costs. Finally, a desalination process must also address the issue of brine disposal and the oft associated problem of excess heat rejection.

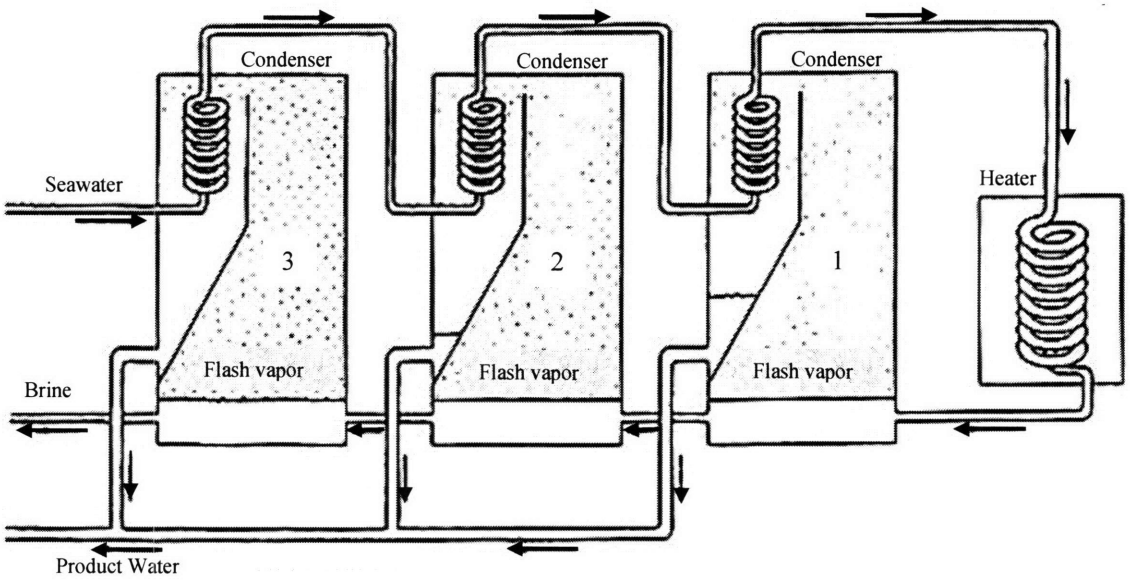

Fig. 2: Multi-Stage Flash distillation (once-through process) (adapted from [28])

Thermal desalination processes typically utilize the concept of evaporation followed by condensation (i.e. distillation) at reduced temperature and pressures (with respect to ambient pressure) for the evaporation step so that less energy is consumed. This is augmented by coupling of the two processes, wherein one feeds energy to the other. Cogeneration configurations, where thermal desalination plants and power plants form dual-purpose facilities, can further reduce the energy requirements of the desalination process as the waste water from the power plant can be used to heat the seawater. Such configurations, however, can only be viable in places where an existing power plant can supply the necessary 'by-products' for the desalination plant. The prominent thermal desalination processes are multi-stage flash, multi-effect distillation and vapor compression desalination.

The multi-stage flash (MSF) desalination process distills sea water by flashing a portion of the water into steam in multiple stages. Seawater is, first, heated in a brine heater (unless a cogeneration configuration is in place). This step is usually achieved by condensing steam on a bank of tubes carrying sea water through the brine heater. The heated water is passed to another container known as a "stage", where the surrounding pressure is lower than that in the brine heater. It is the sudden introduction of the water into a lower pressure "stage" that causes it to boil rapidly and flash into steam. Boiling will continue only until the water cools to the boiling point at the particular pressure after supplying the necessary heat of vaporization. Typically, only a small percentage of this water is converted into steam, depending on the pressure maintained at the stage. The remaining water is subsequently sent through a series of additional stages, each possessing a lower ambient pressure than the previous "stage". The steam generated by flashing is condensed on tubes of heat exchangers that run through each stage. A MSF plant typically consists of more than 15 such stages and operates at a peak temperature of 90-120°C. It is used either in the once-through mode (Fig. 2) or the brine recirculation mode. Although this process has been in vogue for a long time, it has very high energy requirements. Operating the plant at a higher temperature facilitates higher efficiency but increases the possibility of scale formation in the stages.

Multi-effect Distillation (MED), like MSF, exploits the basic evaporation and condensation process in a series of "effects" at reduced pressures to desalt water. However, it tends to have greater scaling issues as compared to MSF and has thus largely been replaced by the latter in most application areas. In the Vapor Compression (VC) technique, compression of vapor before the condensation step provides the necessary heat of vaporization for the entering water. It is typically used in conjunction with other desalination processes or in small scale desalination applications. Although both these techniques, particularly MED, have found suitable application areas (e.g. evaporation of juice from sugarcane for the production of sugar) and have been prominent contributors to the total desalination market over the years, currently neither of them are particularly favored even when thermal desalination is the best way forward.

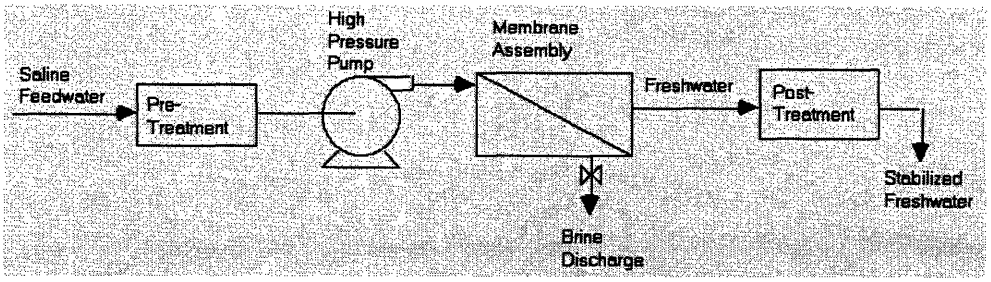

Fig. 3: Schematic diagram of the reverse osmosis process [29]

Membrane processes use semi-permeable membranes to filter out dissolved material or fine solids. In the reverse osmosis process, the permeate (the liquid flowing through the membrane) is forced to flow through the membrane by the pressure differential created between the feedwater and the product water, which is nearly at atmospheric pressure (Fig. 3). The remaining feedwater continues through the pressurized side of the reactor as brine. No heating or phase change takes place. The major energy requirement is for the initial pressurization of the feedwater. For brackish water desalination the operating pressures range from 200 to 400 psi, and for seawater desalination from 800 to 1000 psi. These extremely high pressure gradients are required to offset the osmotic pressure gradient felt by the permeate when it is pressurized against the semi-permeable membrane. Seawater, for example, has a natural osmotic pressure of about 350 psi. Thin film composite membranes, which are typically made of an active thin-film layer of polyimide layered with polysulfone as a porous support layer, act as molecular sieves to filter out inorganic salts as well as non-ionic organic compounds such as fructose (MW 180) and smaller organics such as ethyl alcohol (MW 46). The membranes are rated in terms of rejection rate and flow rate allowed. Nanofiltration is similar to reverse osmosis except that it allows smaller organics and small ions (with lower charges) to go through but requires a smaller pressure gradient to operate. Reverse osmosis has improved significantly due to improvement in membrane characteristics as also improvement in energy recovery and recycling systems. However, it still remains a fairly expensive process due to the high pressure pumps required. Moreover, it is extremely susceptible to scaling and membrane fouling, which decreases the longevity of the process causing major maintenance headaches. Reverse osmosis, also, involves significant amount of pre-treatment (primarily for solid and sediment screening) and post-treatment of the water (mainly for adjustment of pH) further increasing the cost of distributed water.

Forward Osmosis (F.O.) introduces a novel scheme in the spectrum of membrane based desalting approaches. This process employs a passive membrane filter that is hydrophylic (attracts water), slowly permeable to water, and blocks a portion of the solutes. Water is driven across the membrane by osmotic pressure created by food grade concentrate on the clean side of the membrane. Forward osmosis systems are passive in that they require no energy inputs. Although forward osmosis systems have very limited applications on an industry wide scale, they can be useful in emergency desalination purposes in seawater and floodwater settings.

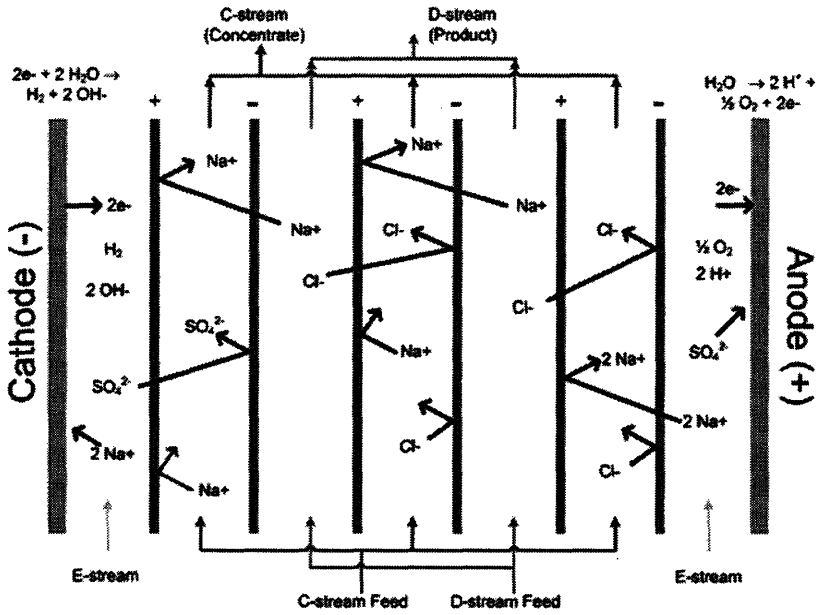

Fig. 4: Schematic diagram of an EDR process in operation (adapted from [30])

The electrodialysis reversal (EDR) process is sometimes clubbed together with reverse osmosis as a commercially successful membrane-based desalination approach. However, the fundamental physics of the EDR process is vastly different from that of the RO process as is the type of input energy utilized to deionize the influx of saline water (mechanical energy for RO as opposed to electrical energy for EDR). In the EDR process, an electric current is employed to force the dissolved salt ions to migrate towards the anode or the cathode, depending on the polarity of the ion, through an electrodialysis stack of alternating cationic and anionic exchange membranes. The ions in their lateral motion are trapped in these concentrate channels leaving alternate channels of fresh water (Fig. 4). EDR systems reduce the fouling tendencies of the saline water by reversing the polarity of the electrodes every 15-20 minutes. This change in polarity causes the scales that may have been formed during one cycle to disassociate from the membranes. Polarity reversal causes the concentrating and diluting streams to switch after every cycle. EDR is a popular process in the domains of industrial process water treatment as also for wastewater reuse projects. The reason it is not favorable for seawater desalination is because the process does not scale up, with respect to the input water concentration, particularly well. The energy requirements of the process rise steeply with the increase in input water concentration that must be treated in the plant. Nevertheless, the EDR process provides a valuable tool for brackish water desalination, primarily because of its high water recovery ratio. General Electric (GE) reports that their EDR systems are able to deliver a water-recovery rate of up to 94 percent [31]. The desirable characteristics of membranes used in electrodialysis applications include selectivity between ions of opposite charge, high ionic conductivity, low electrical conduction, long-term chemical stability, mechanical strength, and resistance to fouling. These characteristics are determined by the membrane matrix polymer and the fixed ionic moiety that affect the ion selectivity of the membrane. Polymer materials such as polystyrene, polyethylene, and polysulfone are often chosen for the membrane matrix and are often cross-linked to ensure stability. Fixed ionic moieties such as SO_3^{2-} and PO_3^{2-} are commonly used for cation exchange membranes, whereas NH_3^+ and RNH_2^+ are common choices for anion-exchange membranes.

In the backdrop of these technologies that have matured over the past few decades, the capacitive deionization technique was proposed to address the predominant problem afflicting the

field of desalination, i.e. the huge cost of desalinated water. Desalinated water currently costs about $2-$9/kgallon. This figure is an order of magnitude higher than the price paid by farmers ($0.2-$0.4/kgallon) and is a factor of two to three higher than that paid by urban users ($1-$3/kgallon) [32]. Although capacitive deionization was first mentioned as a possible method of desalting in 1971 by Johnson and Newman [33], it was not till the early '90s that any substantial efforts were made to develop the promising approach into a practical method of deionizing water. A number of different techniques, using a wide array of electrode materials, flow paths and channel configurations, have since been proposed to take advantage of this energy-efficient deionization technology. In the following paragraphs, we shall outline a few novel schemes that have been actively pursued in terms of characterization and development of the process and the proposed module.

Andelman [34] discloses one of the first inventions relating to spiral-wound (Fig. 5 (a)) and stacked (Fig. 5(b)) flow-through capacitors using high surface area electrodes. In the former, the water enters through the axis of the spirally wound system, comprising of high surface area electrodes 16, 17, 21, 22 that are connected to DC power by means of conductive backing 20 and 14 and are separated from each other by means of insulating material layers 12 and 18. The saline water moves radially outward as well as flowing down along the axis. The desalinated water is then collected from the outer layer as shown in the figure below.

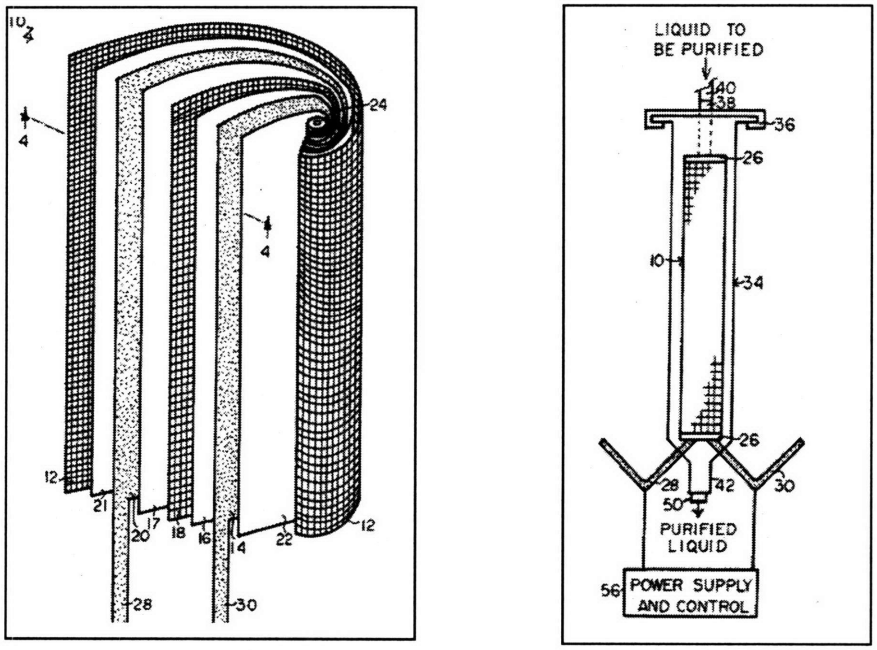

Fig. 5(a) Spiral wound flow-through capacitor as designed by Andelman [34]

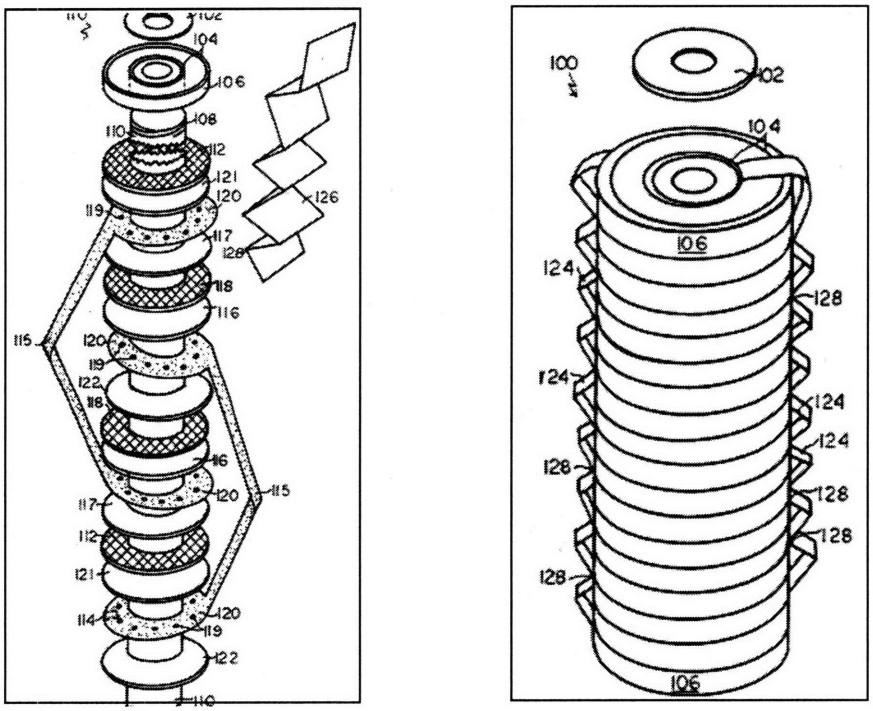

Fig. 5(b) Stacked flow-through capacitor as described by Andelman [34]

Another embodiment of the capacitive deionization scheme is the stacked flow-through capacitor. It consists of a hollow plastic tube that supports the washer parts together. Washer material 116, 117, 121 and 122 provide the high surface adsorption capability while being backed by electrically conductive layers 120. Insulating spacers 112 and 118 separate the electrodes from one another. In a compact form the conductive leads 124 connect the alternating anode and cathode layers in parallel as shown on the right.

Various improvements of the basic flow-through capacitor design have been proposed over the past few years although the principles and flow paths employed remain identical to those stated in [34]. A demonstrative example of the changes can be found in [35], where short solute or fluid flow paths in direct communication with the outside of the capacitor are employed. This invention is said to reduce fouling because the formation of fouling precipitates and crystals is impeded by the lack of spatial dimension over which the flow occurs. Nevertheless, it has not been demonstrated clearly that the introduction of multiple thin strips or open netting instead of porous spacers serve the twin function of providing insulation and minimizing clogging appropriately. In fact the presence of any kind of said spacers decreases the effectiveness of the process in as much as the pressure drop required for fluid flow increases significantly. In the description, the inventor also speaks of the disadvantage of having low water recovery in existing capacitive deionization purification devices. Unfortunately, the designs suggested do not present themselves to any physical mechanism by means of which one can obtain a clear increase in water recovery ratio. Finally, the design necessitates that holes are cut on the electrodes of the flow-through capacitors to align with the perforations on the liquid feeding pipe. This restricts the adsorbing area of the capacitors and complicates the manufacturing and assembly of the system. Both of the effects severely limit the commercial feasibility of the process.

From the investigations carried out at Lawrence Livermore National Laboratory (LLNL), Farmer et al. have described a design where the flow path is strikingly different from that adopted

in Andelman's approach. A flow path that is parallel to the capacitor plates is advocated as opposed to flow through the capacitors. Fig. 6 details the flow path and desorption scheme. In this scheme, saline water flows between the channels created by the aerogel papers (black), which are supported by structural layers of gaskets and frames. As it flows laterally through each of the channels, while also moving down from the input to the output section, so encapsulated between two high surface area electrodes, the ions are adsorbed in the double layer.

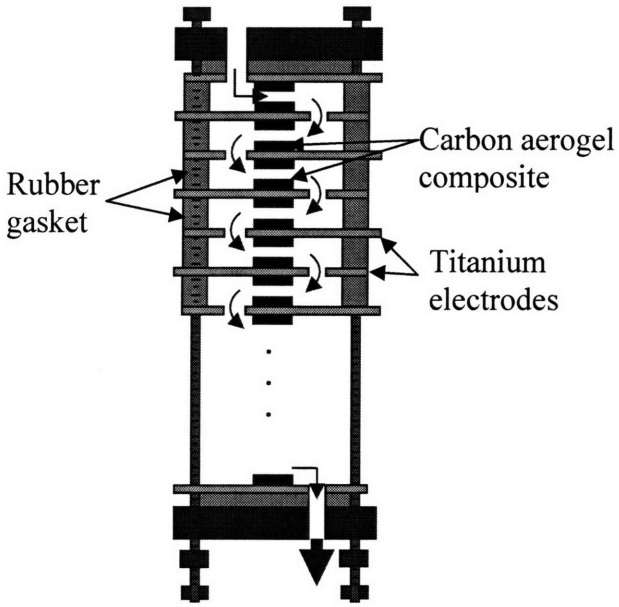

Fig. 6: Flow-along-serpentine-path desalination apparatus, designed by Farmer ([36], [37])

The main advantage of this design is the ease of fabrication and maintenance although, as noted elsewhere [38], the ease of construction does not necessarily imply that the manufacturing process guarantees reliability in satisfying the functional requirements. Another main advantage of this system is that unlike in previous designs where water was made to flow through packed carbon beds, which are not 'immobilized', the carbon aerogel papers do not get entrained in the flow. Consequently, material degradation and erosion is significantly lesser, thereby maintaining efficiency of the process for a longer period of time. Van Konyenburg et al [39] further propose a fuse and filter method for limiting and ameliorating electrode shorting in case a conducting particle is fragmented from a carbon aerogel sheet. While this design also presents exciting possibilities in reducing pressure drops required for water flow through the system in spite of advocating a tortuous serpentine path for solute and water flow, it suffers from substantial fouling problems. Precipitates can form at the bends and corners thereby impeding further flow of fluid. Farmer's design suffers from bulk and cost issues, particularly pertaining to the structural members, as also from severe leak problems from the large number of bends required in such a setup. However, the most significant problem in this design is that the discharge process, which has the same flow path as the charging process, is severely restricted by the convection-diffusion mechanism. This results in a very low water recovery ratio rendering the process not viable in a competitive scenario.

Other methods that have been patented include a process to separate ions by using a combination of electric current and centrifugal force (Hanak [40]) and movable electrode flow-through capacitors (Faris [41]). However, both these ideas while intriguing in themselves and

using very novel approaches incorporate moving mechanical elements (mechanical rotor and movable belt structure or roller respectively) which would be very difficult not only to incorporate in a water purification setup but would also reduce the efficiency and longevity of the system.

In all the patents we have considered thus far it has been noted that a common thread of problems arise from the fact that too much water is used for reclamation or regeneration of the electrodes once they are saturated. While it has been a well-documented fact over the last few years, very few researchers have actively sought to address this issue. Tran et al [42] describe a method of regeneration which uses less of the 'useful' water being deionized. They employ shorting or reverse polarity, the latter due to the possibility of increased rate of ion desorption from the electrodes. Moreover, the design uses a second regenerant fluid to remove ions while slowing down or stopping the flow of 'useful' fluid such that it is not wasted. However, the use of reverse polarity might mean that while ions of one type of charge are repulsed from an electrode, the oppositely charged ions will get immediately attracted to the electrode causing the saturation of the electrode rather than regeneration. Moreover, using a second regenerant fluid gives no additional advantages particularly when one considers that introduction of the new fluid gives no benefits in as far as the first fluid is not wasted. In fact in most cases the saline water is the cheapest resource and if any fluid needs to be used to take away the ions from the saturated electrodes, it must be the incoming saline water.

A method of improving the efficiency of flow-through capacitors by using charge barrier membranes has been proposed by Andelman et al [43]. The inventors disclose a method of placing charge barrier membranes next to the electrodes so as to compensate for pore volume losses caused by adsorption and expulsion of pore volume ions. The "charge barrier" is described as a permeable or semi-permeable membrane which retains the co-ions that migrate into the cell, thereby considerably improving the quality of water produced. It is reported that this results in a large gain in ionic efficiency (defined as the coulomb of ionic charge purified per coulomb of electrons used). Consequently, the capacitive deionization process with the additional charge barrier pieces can be utilized to desalinate seawater which otherwise proves uneconomical. In this method, when a charge cycle is completed the flushing takes place only in the layer between the electrodes and the charge barrier membranes thereby reducing the water used for discharge to an extent. Although this does open up new avenues, it is still untested and has several disadvantages if the extent of benefit, as described in the patent, is not realized. For example, the presence of additional membrane implies the increase in the value of the internal resistance of the RC circuit. The 10% microporous membranes, advocated in the patent, is also likely to cause a severe pressure drop for the flow-through capacitor setup. A significant adverse osmotic pressure gradient would also develop for such a membrane necessitating the application of a much higher hydrostatic pressure. Evidently such membranes would also have the potential for detrimental scale formation and would add to the maintenance cost as well as to the capital cost.

In a recently reported work, Max [44] proposes a segregated flow, continuous flow deionization technique by means of which it is claimed that deionization continues unabated even when polarity reversal takes place. The invention consists of placing membranes next to electrically attractive devices thereby creating segregated sections of concentrated and fresh water flow. The membranes permit ions of the same charge to flow through them but do not let them move back due to resistance in diffusion. However, this design has multiple problems. Firstly, it is difficult to find a membrane that fits the description in the patent. Secondly, in the given design deionization of the concentrated channels occurs in parallel with deionization of the fresh water channels. The ions from the concentrated channels take up substantial surface area of the electrodes thereby

restricting the amount of ions that can be removed from the dilute water channels. Finally, even if one could obtain continuous flow of fresh water by this method, the amount of concentrate water that is thrown away simultaneously would severely restrict the feasibility of the process. In other words, a low water recovery ratio could be expected depending on the relative flow rates in the concentrate and fresh water channels.

The above discussion clearly outlines a significant need for the design and development of a process, which while retaining the energy efficiency of the capacitive deionization process, is able to improve the water recovery ratio substantially such that it can compete with reverse osmosis and EDR for brackish water desalination as well as seawater desalination. It would be desirable that such a process does not entail the use of additional membranes, spacers and such elements that increase power consumption and pressure drops reducing the efficacy of the process. Finally, it should be simple to fabricate and assemble the setup. In an ideal scenario, existing off-the-shelf parts can be brought together to improve the performance metrics by utilizing a novel technique or/and employing a new flow path. It is to be noted that the latter must refer to a totally different scheme that could lead to a paradigm shift in our understanding and warrant the development of the capacitive deionization technique as an industrial process. A quantum leap in water recovery ratio would definitely be a huge step towards that goal.

Chapter 3: Proposed Approach

In the previous chapter, we primarily dwelt on the pitfalls associated with the existing technologies (thermal and membrane-based approaches) as well as some of the proposed capacitive deionization schemes. In this chapter, we begin with a qualitative analysis of why capacitive deionization technique has not been accepted on an industrial level. Subsequently, we introduce the Axiomatic Design (AD) methodology to help in identification of the weak link(s) of this technique as it currently stands. The charting of the functional requirement (FR) – design parameter (DP) matrix should enable us to come up with a new approach that can address one or more of the challenges associated with the large-scale implementation of capacitive deionization process. Finally, the approach that will be pursued in this investigation will be substantiated along with the possible benefits of applying this approach.

It was briefly mentioned in Chapter 1 that low water recovery ratio is one of the major challenges that has hindered the commercialization of the CDI technology. It is pertinent to mention here that the importance of this parameter comes into play mainly because CDI has not demonstrated the capability of desalinating seawater. Water recovery ratio has a far diminished role if seawater can be used as source in the desalination process. This is because the abundance of seawater ensures that the input water almost comes with a negligible price tag and because brine (waste water) can be discharged back into the sea. The latter enables a significant reduction in the final discharge estimates. On a world-wide scale, thus, one would have to say that the limited surface area of the carbon aerogel paper, which is state-of-the-art as regards high surface area ideally polarizable electrode, with respect to the number of ions that need to be removed from seawater forms a critical barrier.

If CDI had to desalinate from a concentration of 35,000 ppm (seawater) to a concentration of 500 ppm (drinking water), one would need to provide much higher surface area per unit flat area electrodes – far higher than is currently provided for by the carbon aerogel electrodes. Otherwise, one would need to employ a ridiculous length of high surface area electrodes such that the ions can find sufficient surface area to diffuse and attach to while the saline stream is passing through the almost-infinite length of the channel. Recycling numerous times for a design employing limited length of high surface area electrodes would also eventually culminate in the removal of the large number of ions that are present in seawater. However, the latter two 'brute-force' approaches are undesirable in terms of convenience and practicality and adversely affect the economics of the process - because of the substantial capital costs necessitated by the employment of large lengths of the high surface area electrodes as detailed in the first approach and the limited throughput capability of the second approach, wherein recycling multiple times means waste of available energy and time to desalinate a fresh stream of saline water. Consequently, the only feasible solution to this problem is the design and fabrication of even higher surface area (per unit flat area) electrodes. While the idea of employing carbon nanotube sheets as extremely high surface area capacitive electrodes is very exciting, it is still very much in the brainstorming domain to be actively considered as a realistic solution at this stage.

At this stage of the discussion, it might be worthwhile to understand the extent of the adverse impact brought about by the inability of the CDI process to desalinate input water having a large number of ions (~30,000 ppm). On the face of it this shortcoming would seem pretty significant as it cripples the process from being used in coastal areas where any form of source water, other than the seemingly endless reserves of seawater, is in short supply. However, despite this obvious drawback, it turns out that the potential of CDI to enter the commercialization phase is immense. The primary reason for this is that seawater desalination, even if done in a very cost-effective fashion, can help coastal regions and places in their immediate neighborhood only as

transportation of water over long distances is expensive and often wasteful. In other words, the prohibitive transportation expense leaves a large vacuum that can only be filled by brackish water desalination as reflected in Fig. 1, especially in the pie-charts for the US desalination market. In large countries such as the US or in regions that are far away from the coast such as a substantial portion of sub-Saharan Africa brackish water desalination is possibly the best way out of the freshwater crisis. Brackish water can have total dissolved solids' concentration varying from 500 ppm to 35,000 ppm but typically a reference concentration number of around 3,000 ppm is widely accepted. In such a scenario, desalination to the tune of 2,000 ppm concentration difference between the input and the product water would be required as opposed to the 34,000 ppm difference necessitated by using seawater as the source. Just to emphasize the point, that is more than an order of magnitude reduction in the amount of desalination required per unit volume of input water. Furthermore, studies reveal that nearly 80 percent of the global water consumption is in the sector of agriculture (irrigation) which can inherently tolerate a slightly higher concentration level (1,200 ppm) with respect to the tolerance limit for potable water (500 ppm). This further reduces the number of ions that need to be removed per unit volume of source water to transform the latter into usable product water. The bottom-line therefore is that capacitive deionization can be used very effectively in places where brackish water forms the predominant source and the product water is primarily used to supply agricultural fields.

The application of the capacitive deionization technology is therefore not limited by its potential market but by its performance parameters in such a market. Compared to the other brackish water desalination processes (as noted from Table 2), the low water recovery ratio of the CDI process has a detrimental effect on the final product water pricing by reducing total throughput per day and increasing pumping, pre-treatment and post-treatment costs. In the capacitive deionization process, product water is produced only during the charging period of the total cycle as depicted in Fig. 7 below. The discharge time enables recharging of the electrodes but the water that flows through the channel during the discharge half cycle cannot be utilized. The discharge cycle can thus be considered to be a 'necessary evil'. In other words, one would like to reduce the downtime (discharge time) as much as possible while retaining the equivalent functionality of regenerating the electrode.

In regard to the stepwise function in one complete cycle of the CDI process when it employs the AFD scheme (Fig. 7), there are a couple of points that deserve special mention. Firstly, since most of the high surface area electrodes, including carbon aerogel, are fairly porous the ions adsorbed in the electrical double layer (EDL) not only appear in the flat surface region but also in the interior where they are adsorbed to the EDL of the inner particle clusters or fibers. The EDL is typically considered to occur within a few nanometers of the actual charged layer. The ions (counter-ions) that form the EDL help to neutralize the charge and the potential in the bulk of the fluid is seen to be almost zero after a couple of Debye lengths (Debye length is the characteristic length for the EDL). Life inside the EDL is very complex indeed, but for our purposes, it is sufficient to understand that such a layer typically consists of a stagnant inner layer of counter-ions and a diffuse outer layer of counter-ions. It is pertinent to mention that electroneutrality is not observed inside the EDL but is restored after a couple of Debye lengths.

In the charging step (2^{nd} snapshot shown in Fig. 7), the saline water progressively becomes 'cleaner' ultimately exiting the channel as product water. This also implies that the high surface area electrodes will probably be more rapidly charged, at least initially, towards the beginning rather than towards the end of the channel. Nevertheless, each ion taken away is equally important as it eventually results in the requisite number of ions to give acceptable water salinity.

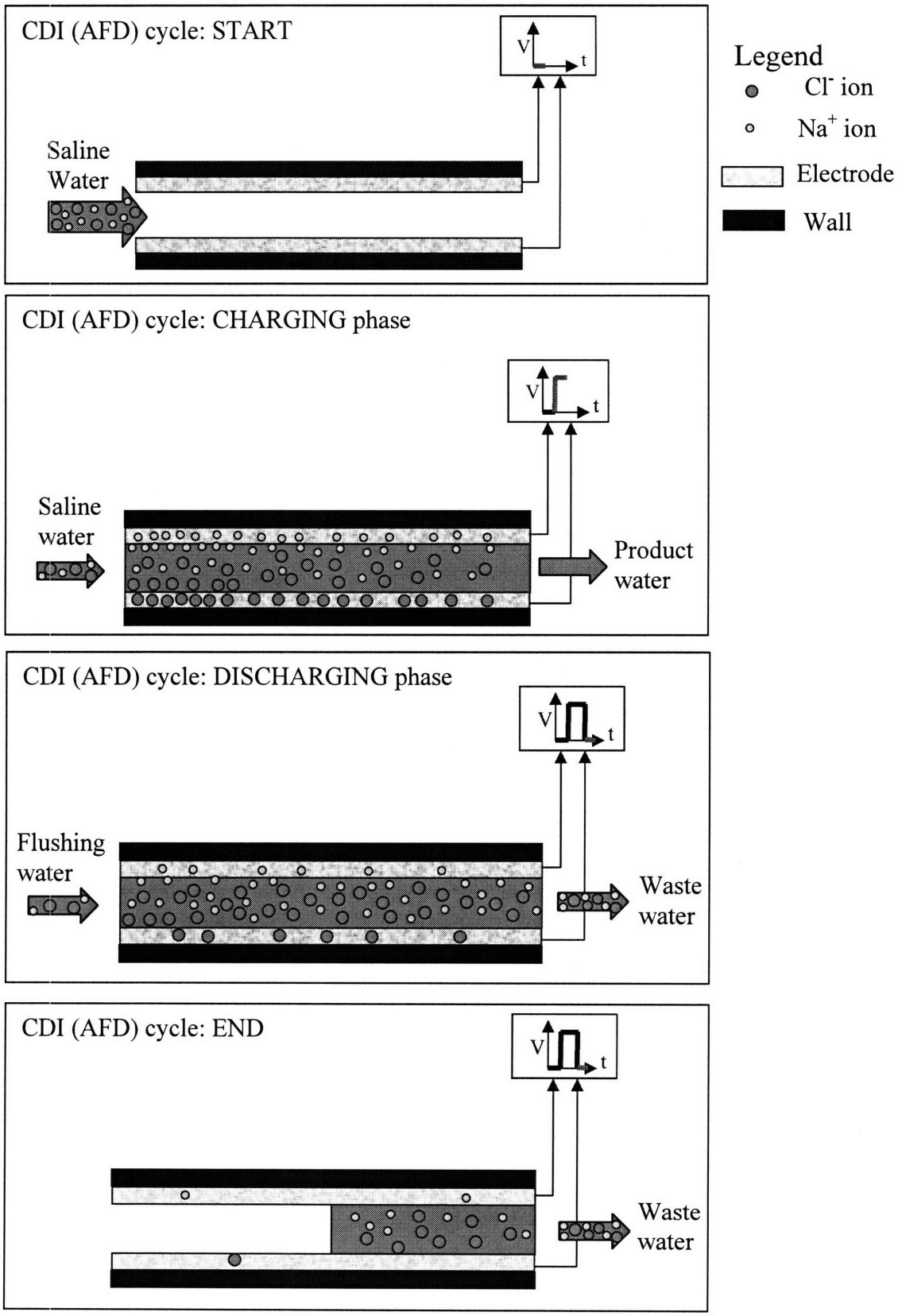

Fig. 7: Representation of one complete cycle of the capacitive deionization process working in axial flow discharge (AFD) mode.

In the discharging phase (3rd snapshot in Fig. 7), one can clearly observe that the ions are starting to detach from the electrode – rather from the EDL region in the vicinity of the electrode - and moving into the bulk of the channel. The voltage across the electrodes at this point of time is zero (i.e. the electrodes are shorted), as opposed to the specific voltage applied during the charging phase. The applied voltage (across the electrodes) at each stage is visualized in the V-t graph shown in each snapshot. With regard to the discharging cycle, it is also to be noted that the flushing water mentioned is nothing but the saline water that is deionized during the charging phase, as the latter has the smallest price tag attached to it. Introduction of a different fluid, including the freshly obtained product water, does not make much economic sense.

The final point of emphasis is that the 'start of cycle' (1st snapshot in Fig. 7) and 'end of cycle' (4th snapshot in Fig. 7) phases do not productively contribute to the water throughput for the plant. Although there is no way to work around this problem, one would need to factor in this 'wasted' time into the calculations for water recovery ratio and final throughput. We shall term this cumulative 'wasted' time as switching time because, in essence, this is the time that is required to switch from the discharging phase to the charging phase. The reason it is not necessary to 'switch' from the charging phase to the discharging phase is because the flushing water (as long as it is the same saline water that is being desalinated during the charging phase) is flowing continuously through the system so it is just a question of shorting the electrodes, once the electrodes are sufficiently saturated.

Knowledge of the functioning of any process and its drawbacks is necessary but usually not sufficient to identify the primary challenge facing the designer or the fatal flaw inherent in a poorly designed system. We are faced with an identical situation in trying to further develop the capacitive deionization process. In order to help in identification of this weak link in the existing process, we introduce the Axiomatic Design methodology [45]. Axiomatic design provides a scientific foundation for design by systematically analyzing customer attributes (CA) and mapping them successively into three generic domains - functional requirements (FR), design parameters (DP) and process variables (PV). By using two fundamental axioms that govern the decision making process, one can create a rigorous interplay between "what we want to achieve" and "how we plan to achieve it". The first axiom, or the Independence Axiom, states that the functional requirements of a design should be independent of one another. The independence implied herein is functional as opposed to physical (indeed it is often desirable to have a physical integration of parts). It should be noted that the clear definition of the functional requirements in a solution-neutral environment is one of the challenges faced by the designer. The second axiom, or the Information Axiom, states that the information content of a specific design must be minimized. In essence, if multiple designs satisfy the Independence Axiom, their suitability for the particular task at hand can be determined by calculating their respective information content. The design having the least information content is considered to be the most appropriate candidate to establish the design goals.

The main step in axiomatic design is to establish what is commonly called a design matrix between the characteristic vectors that define the design goals and the corresponding solutions. The design matrix at the highest level might only consist of a set of Xs and Os to understand which design parameters affect which functional requirements (where an 'X' indicates significant impact on the FR by the given DP and a 'O' indicates little or no impact on the FR by the corresponding DP). In other words, at the top level of design, the design equations are only meant to state the design intent. It is only after decomposition, which is performed by zigzagging between the FR and DP domains for example, that the design details can be incorporated. At this leaf level of the design, the design equations can be representative of true mathematical equations.

For our particular case study, we subject the conventional capacitive deionization process to the highest level statement of FRs and DPs only.

The first step in formulating the crucial FR-DP mapping is to identify the FRs, which in this case is a relatively simple task given that the existing design had been envisioned to serve a particular set of functions. It would have been much more difficult for one to fashion a suitable set of FRs given a broader collection of customer needs. Nevertheless, to identify the actual FRs in this case requires a detailed understanding of the phenomena involved in the entire capacitive deionization process when it employs the conventional axial flow discharge (AFD) scheme. The capacitive deionization process is based on a physical-chemical reaction, which takes place only in a restricted region, i.e. on the surface of the carbon aerogel electrodes. A reaction of this kind is commonly termed as a heterogeneous reaction, as opposed to a homogeneous reaction where the reaction takes place in the bulk of the fluid.

The heterogeneous reaction, under consideration here, consists of three primary steps. The first step involves the transport of the reacting species (ions) to the surface (carbon aerogel). The second step entails a series of substeps including diffusion of ions through the aerogel, adsorption on the surface, subsequent desorption, and diffusion of ions through and out of the surface. The third step is a direct reversal of the first step and deals with the transfer of ions away from the reaction surface and its neighborhood into the bulk phase. This description of the phenomenon is fairly generic and can be associated with chemically catalyzed reactions at solid surfaces, enzyme-substrate reactions at interfaces and electrode reactions in electrochemical cell. The second step is the significant step in the actual desalination process but is rate-limited by the transfer phenomena of steps one and three. In this phenomenological depiction, the first half of the second step (i.e., diffusion of ions through the aerogel and adsorption on surface) completes the charging portion of the cycle while the latter half of the same step (i.e. desorption of ions from the surface and subsequent diffusion of ions through and out of the surface) initiates the discharging part. Based on this understanding, we establish the appropriate FR-DP relations as shown in Table 4.

Table 4 FR-DP mapping for capacitive deionization with axial flow discharge

FR \ DP	DP1 Diffusion	DP2 Electromigration
FR1 Transport ions from bulk to electrode	X	X
FR2 Attach (Remove) ions from electrode	0	X
FR3 Transport ions from electrode to bulk	X	0

We observe from Table 4 that there are only two design parameters at the highest level to satisfy the three top-level functional requirements. In a scenario where the number of FRs exceeds the number of DPs, the design becomes 'coupled'. A coupled design does not satisfy the Independence Axiom and consequently successful attainment of design goals becomes an improbable task, if not an impossible one. The capacitive deionization process design involving axial flow discharge is not a desirable solution and one must look to either 'uncouple' or 'decouple' the design. A decoupled design is characterized by a triangular (either upper or lower triangular) design matrix while for an uncoupled design, the design matrix assumes a diagonal form.

It is evident that uncoupled design is the best possible form since each FR is independently satisfied by its corresponding DP (FR1 by DP1, FR2 by DP2 and so on). However, it is not always possible to attain a simple uncoupled form. In such a scenario, a decoupled design works equally effectively as long as the DPs are implemented in the sequence dictated by the triangular form of the design matrix. The easiest way to decouple the design, presented in Table 4, is to either add a DP or reduce a FR. However, the reduction of a FR is an unacceptable practice as that would mean the reduction of functionality of the system and consequently an inability of the system to attain its required goals. Thus, our new design should incorporate an additional DP such that the new design is able to satisfy the Independence Axiom. Loosely speaking, the new DP should significantly influence its corresponding FR while having limited or no impact on the other FRs. It is to be noted that this is not a strict requirement but given multiple possible DPs one would like to introduce a DP that follows the above stated guideline.

Motivated by the above phenomenological bottleneck, we propose a novel discharge technique that can eliminate the source of coupling in the capacitive deionization technique. In terms of practical benefit, such a design should be able to significantly reduce the downtime enabling an increase in water recovery ratio to the levels of the existing brackish water desalination processes. For this situation, it also means that a higher throughput is obtained for the same system as charging time, relative to the discharging time, is higher for the new approach as compared to the conventional approach.

In the proposed discharge scheme, which we call the permeating flow discharge (PFD), the waste water is permeated through the porous electrodes (Fig. 8 below) rather than the conventional flow path of in-between the electrodes in the axial flow discharge (AFD) process. Essentially, this new flow path introduces a new DP that can directly address FR3 ("Transport ions from electrode to bulk") while not affecting any other FR in any manner whatsoever. The confidence in the latter half of the statement arises from the fact that this flow path is utilized during the discharging time period only as shown in Fig. 8. Consequently, it cannot have any influence on FR1 ("Transport ions from bulk to electrode"). Furthermore, FR2 is restricted to the involvement of electrochemical phenomena only (and is independent of any ion transport process), i.e. adsorption and desorption of ions from the high surface area electrodes.

Before we proceed any further, it needs to be clarified that the product water obtained during the charging process is through the middle channel only as the water exiting through the outer channels are devoid of only one type of ions, i.e. the water exiting the top channel still retains the chloride ions. This is not a property of the flow scheme as much as it is of the particular design used to explain the PFD process. In other words, one can easily envision a PFD system where there is no flow in the outer channels during the charging phase or another system which consists of a series of dilute water channels separated by electrodes having alternate polarity.

The permeation, as seen in the 3rd and 4th snapshots of Fig.8, is controlled by either forcing a fixed amount of fluid through the porous electrodes (e.g. having a fixed displacement pump attached to the middle channel and closing the middle channel outlet valve as soon as discharging starts) or by maintaining a given pressure differential across the middle and outer channels (e.g. having a pair of centrifugal constant-pressure pumps connected to the middle and outer channels). In the latter case, the pressure differential actively regulates the permeation flow velocity, which also depends on the material properties of the porous electrode. One of the obvious consequences of adopting this flow scheme is that the volume flow rate through the outer channels increases (as visualized by the bigger arrow) while that through the middle channel decreases (as depicted by the much smaller arrow).

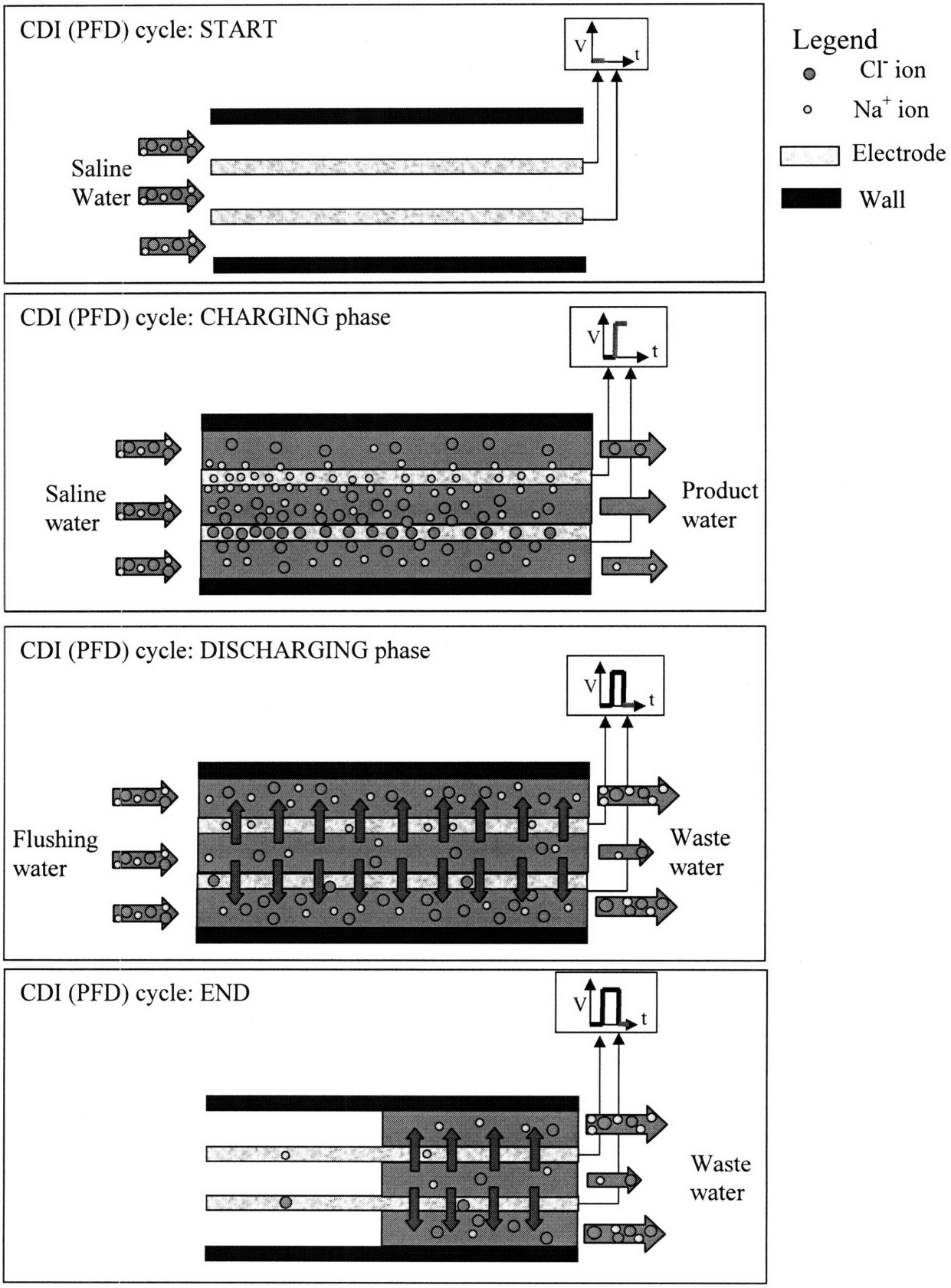

Fig. 8: Representation of one complete cycle of the capacitive deionization process working in permeating flow discharge (PFD) mode.

The new DP introduced by permeation of the waste water through the porous electrodes is called solvent drag. It represents the generic phenomena of ion transport through a membrane (the porous electrode in this case) due to constant solvent flux through the same. In other words, the solute is carried with the solvent as the latter perfuses through the carbon aerogel electrodes. It must be emphasized that the solvent drag phenomena is completely distinct from the diffusion of the ions across the porous electrode due to the concentration difference that exists across it. The solvent drag term and the diffusion term together account for all of the ions transported across the aerogel electrode. The new FR-DP mapping based on the deionization process with the PFD scheme is represented in Table 5.

Table 5 FR-DP mapping for capacitive deionization with permeating flow discharge

FR \ DP	DP1 Diffusion	DP2 Electromigration	DP3 Solvent drag
FR1 Transport ions from bulk to electrode	X	X	0
FR2 Attach (Remove) ions from electrode	0	X	0
FR3 Transport ions from electrode to bulk	x	0	X

The relative magnitude of the solvent drag, diffusion-across-membrane and internal diffusion terms - where the first two regulate the PFD ion transfer phenomena and the last term accounts for ion transport in the AFD scheme - will determine the effectiveness of the new process. Although it is not imperative to have solvent drag to be substantially higher than diffusive permeation across the aerogel electrode, one could reason that this will probably be true unless the permeation velocity is extremely small. This intuitive prediction forms the basis of the smaller 'x' (denoting smaller influence) in the 1st column of the 3rd row as compared to the larger 'X' (depicting significant influence) in the 3rd column of the same row. We shall test this prediction in a quantitative manner in Chapter 5 of this thesis. Please note that even if this prediction is not valid, the design matrix is decoupled.

What is of far greater consequence, however, is the ratio of the sum of the PFD ion transfer terms to the AFD ion transfer term. For maximum beneficial impact, the former should be much higher than the latter - preferably an order-of-magnitude higher, if not more. In other words, the new scheme will be able to cause a quantum leap in the performance metrics of the capacitive deionization process if and only if the ions that are desorbed from the aerogel electrode are removed much faster with the help of the permeating flow path. The understanding that the ion removal rate is inherently linked to the performance metrics, primarily water recovery ratio and throughput, gives rise to the underlying hypothesis of our work, which can be formally stated in the following manner:

The rate of removal of ions from a channel setup is higher for a process that is influenced by solvent drag (PFD) than for one which is diffusion limited (AFD), given the same flow conditions.

In the following chapters, we design a battery of experimental and theoretical tests to understand, analyze and characterize the above hypothesis with respect to different geometric parameters, flow conditions and material properties. We seek to put some numbers on the

qualitative hypothesis presented above such that the theoretical bounds of both AFD and PFD processes can be brought to light. These bounds should aid us in estimating the optimal operation conditions for each process. Finally, the extent of benefit that can be derived by using the PFD process, instead of the conventional AFD flow path, in the original capacitive deionization technique is determined.

Chapter 4: Materials and Methods

To test the hypothesis proposed in the previous chapter, we seek to design an experimental setup that can provide accurate quantitative results in as simple a manner as possible. While the basic hypothesis makes a qualitative prediction about the relative magnitudes of the solvent drag and the diffusion terms for the PFD and AFD processes respectively, it is important to be able to generate quantitative results in order to determine the extent of benefit of employing one versus the other, i.e. whether there is a small percentage increment, a factor of two difference, or even an order of magnitude improvement. The necessity for a reference extent-of-benefit value arises because of the trade-off that might appear between executing a flow path that has less power needs (AFD) and another path which provides better water recovery ratio and throughput performance (PFD). The excess power required in the PFD process is because of the additional pumping that would be necessary to push the (flushing) water across the porous electrode. The consequence of the trade-off is that if PFD enjoys only a miniscule advantage over AFD in terms of its water recovery ratio and throughput parameters, the excess power requirements might more than offset the benefit of employing such a process.

Given the basic flow concept of the PFD process, a number of experimental setups, exhibiting different physical arrangements, could be employed to test the hypothesis. The scheme presented in Fig. 8 previously is just one design embodiment that could be adopted. Another possible embodiment (Fig. 9 (a)) could be a setup using three concentric tubes where saline water is deionized by flowing (axially) through the annular space between the porous electrodes lining the first and the second tube. During the discharging phase, waste water is permeated through the inner (first) tube and the annular space between the second and third tube. This embodiment could also be modified into a large shell containing multiple pairs of concentric tubes mirroring the shell-and-tube type heat exchanger design. In this setup (Fig. 9 (b)), the large shell forms a universal outer (or third) tube for the multiple pairs of concentric tubes inside which deionization takes place in the same fashion as described for the three concentric tube design.

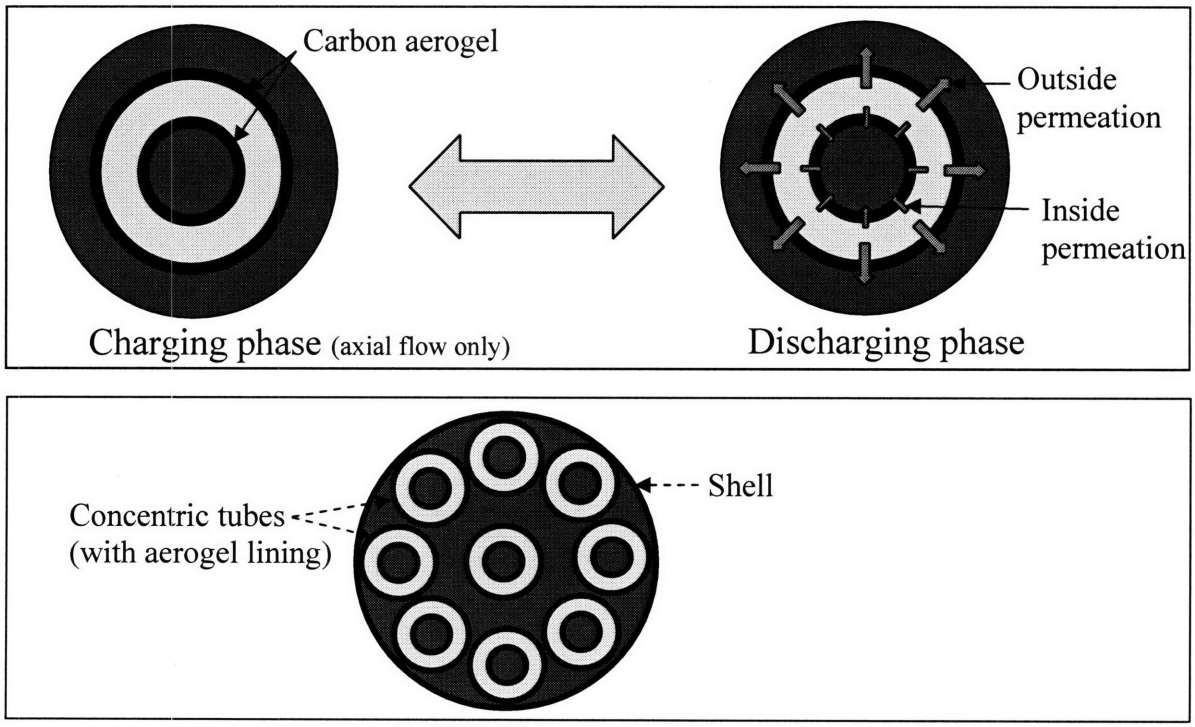

Fig. 9: (a) Three concentric tubes' embodiment (Top); (b) Shell-and-tube design (bottom).

For our experimental studies, we adopted a simpler variation of the three channel setup to test the hypothesis. The schematic diagram of our apparatus in AFD and PFD processes is displayed below in Fig. 10. In the AFD setup, we used just a single channel that was surrounded on either side by carbon aerogel paper. In the PFD setup, we required three channels to simulate the permeating flow conditions. Please note that Fig. 10 shows the discharging flow path only. Charging was done in the no-flow condition (i.e., water was allowed to stand inside the chamber) although the setups shown for both AFD (single channel) and PFD (three channels) remained same for the charging and discharging phases.

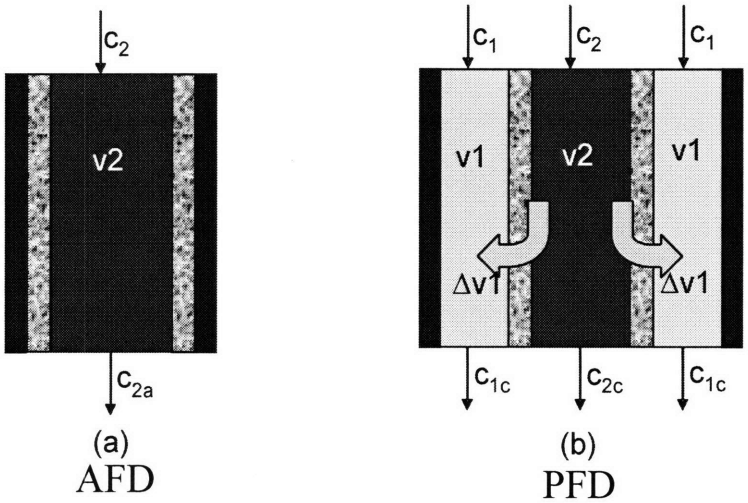

Fig. 10: Schematic diagram of the AFD and PFD setups employed. Flow velocities shown are relevant to the discharging phase only.

Both the single channel and the three channel setups were manufactured and assembled in the same manner, so we will in the following paragraphs describe the materials and fabrication techniques pertaining to the somewhat more complex three channel PFD setup only. Subsequently, we will discuss the deployment of the setup in the actual experiments and the methods employed to study the proposed hypothesis.

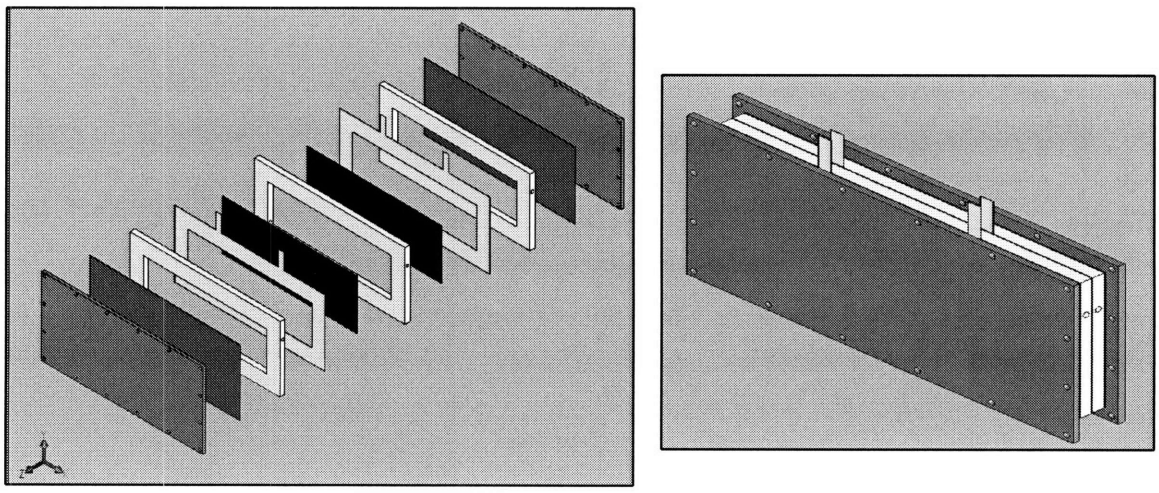

Fig. 11: CAD model of the three channel setup (exploded view – left; isometric view - right). The parts clearly visualized are: polypropylene sheets (purple); rubber gasket (brown); aluminum foil (yellow); polypropylene channel frames (white); carbon aerogel (black).

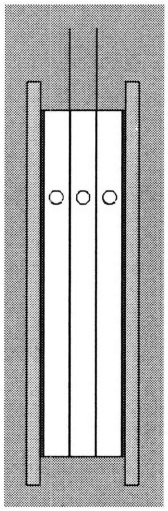

Fig. 12: CAD model of the three channel setup – front view

The channel frames (white rectangular strips shown in Fig. 11) were carved out from polypropylene sheets, having thickness of 8 mm. The channel frames provided the space for the water chambers, each of which was 23 cm long and 7 cm high. The width of the chambers was obviously the same as the thickness of the frames, i.e. 8 mm. Two holes were drilled in each frame to facilitate for piping connections from the pump to the input side and from the outlet to flow control valves. The middle channel was surrounded by carbon aerogel papers (0.25 mm thick), which formed the porous electrodes. Aluminum foils, which were directly connected to the external electrical circuit, were put in direct contact with the carbon aerogel papers. The contact resistance between the conductive foil and the aerogel paper was negligible when the entire setup was sufficiently squeezed by tightening the screws on the outermost retainer plates. Strips of rubber gasket were interposed between the outer channels and the retainer plates to minimize water leakage through the sectional gaps.

No adhesives were used to bond any part of the setup to another. Physical compression was found to be adequate in minimizing leakage and contact resistances in the setup. While this made it more convenient to assemble and disassemble the setup (and add or subtract a particular component, if so desired), there were a couple of concerns with this manner of assembly. The primary difficulty was to impart a uniform level of compression throughout the perimeter of the retainer plates that could be transmitted through the entire assembly. Although it might sound insignificant, it is worth noting that the aerogel papers are less than a centimeter apart and a slight alteration in this distance could have major implications, particularly in the extreme case that the two papers touch each other. The second concern was that during flow through the outer channels the aerogel papers would bend appreciably. This, again, might induce shorting of the electrodes at specific contact points or at the very least change the distance between the electrodes by 10-20%. Indeed these problems would take on even greater significance for shorter distance between the electrodes, say of the order of a millimeter or so. In such a scenario one might have to employ a spacer or attach a conductive mesh to the aerogel paper so as to ensure the positional stability of the latter throughout the experiment. For a channel width of 1 cm, shorting of the electrodes was not a problem, particularly because our carbon aerogel papers were only 7 cm high. Imagine the amount of buckling necessary to facilitate a 0.5 cm deflection in a 7 cm high structure that is fixed to a wall at both ends! However, it was important for our theoretical models to account for the variability in geometrical dimensions of the channel in light of the difficulty in maintaining a constant width as discussed above.

Before moving on to review the methods employed in our experiments, we will undertake a brief discussion on carbon aerogel, which is the material of choice for our capacitive electrodes. It is perhaps appropriate to say, at the very outset, that the introduction of carbon aerogel [46] provided the mainspring for development of capacitive deionization systems. Carbon aerogel is a class of porous carbon material that is manufactured by pyrolyzing carbon fibers impregnated with resorcinol-formaldehyde aerogel (aerogels are solid-state materials derived from gels by substituting the liquid portion with gas). It displays characteristic properties of high surface area, low resistance and high relative capacitance. The cumulative contribution of mesopores

(characteristic dimension between 2 to 50 nm) and micropores (characteristic dimension less than 2 nm) in a typical carbon aerogel sample results in a porosity value of at least 50% (and typically more in the range of 70-80%). While the material is highly porous, its internal structure displays a definite continuity.

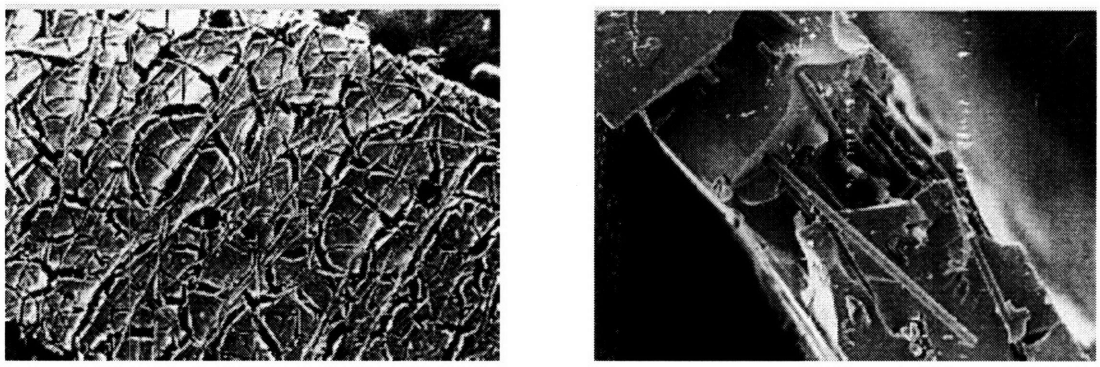

Fig. 13: SEM images of carbon aerogel paper: SEM 22x (left); SEM 200x (right) [47]. At smaller magnification, the paper has a planar appearance. At higher resolutions, distinct fibers traversing through the pores in the material are visible.

The carbon aerogel sheets used in this study, RF paper (MarkeTech International Inc., Port Townsend, WA), came with the following manufacturers' specifications: Density: 0.4-0.5 g/cc, Surface area: 400-500 m^2/g, Capacitance: 15-19 F/g and Specific electrical resistivity: 0.01-0.04 Ω-cm. Prior researchers investigating the pore size distribution of identical aerogel papers had noted that micropores account for 77% of the total surface area but only 25% of the total pore volume [48]. The remaining contribution was from the mesopores present in the material. It is interesting to note that the study found no pores over 100 nm. While it is true that the extremely high surface area of carbon aerogel coupled with its low electrical resistance makes it an attractive choice for electrode material in supercapacitors or deionization systems, it might be of some interest to note that increasing the absolute value of the surface area might not always provide for greater electrosorption. If the additional contribution to the overall surface area comes from increase in the number of micropores, the electrosorption capacity of two materials having widely different surface areas might turn out to very similar. The reason for this discrepancy is that overlapping of electrical double layers (EDL) or self-shielding might prevent the ions from entering the micropores. In other words, micropores smaller than a cutoff width, say 0.6 nm, might not be able to contribute to the overall electrosorption capacity due to the EDL overlapping effect.

The low specific resistivity of carbon aerogel is also beneficial as it would have been difficult to create a uniform potential at the surface of the entire electrode if this had not been the case. A non-uniform potential would create massive difficulties in analyzing the system, primary amongst which would the non-specific electrical forces that each ion inside the channel would experience. In other words, one could envision a chaotic situation where parts of the electrodes are heavily saturated whereas other portions remain relatively untouched by ions. Such an operational state would lead to poor utilization of the aerogel surface area and consequently to poor efficiency of the overall system.

Finally, even though carbon aerogel has proved fairly successful, albeit at the proof-of-concept phase, a quick literature survey reveals that other materials have been investigated to determine their suitability for application in deionization systems [49]. In our experiments, we have tried to

incorporate woven carbon-fiber electrodes as well as different varieties of carbon paper (for example, TGP-H-060 Toray carbon paper, Toray Industries, Inc.). Our research in this direction has been largely unsuccessful. Nevertheless, research towards developing a new electrode material might make a significant impact if such a material can either drastically reduce capital costs of deionization systems (e.g. woven carbon fibers) or increase the possibility of seawater desalination by providing a much larger electrosorption capacity (e.g. carbon nanotube sheets).

Having discussed the essential flow paths and the channel apparatus employed, we are now in a position to detail the experimental procedure followed to test the proposed hypothesis. The first step for both the AFD and PFD processes is the common charging step. To start the charging process, saline water was pumped into the single channel setup for the AFD process and the three channel setup for the PFD process. During the charging period, water was allowed to stand still inside the chamber rather than flow through it. The primary motivation in letting no flow occur during the charging phase was to obtain sufficient desalination (concentration difference) even when the functional area of the electrodes was not remarkably high. The table-top setup in our experiment used carbon aerogel electrodes, each having a flat surface area of 161 cm^2. In order to get a measurable concentration difference, or the maximum possible concentration difference, between the deionized water and the input saline water with this small surface area, it was necessary to maintain the no-flow state. Otherwise, in the continuous flow condition, even after saturating the electrodes, we might not have been able to detect a significant concentration difference due to the fact that the same number of ions would have been removed from a larger volume of water.

In the no-flow state, the setups were charged till the potential difference across the electrodes reached a pre-established value, which for our experiments was 430 mV. It is pertinent to mention that the battery connected for charging must have a potential difference less than or equal to 1.3V to ensure that the water in the channels does not ionize. The time needed to complete the charging operation was 12 minutes and 16 minutes for the AFD and PFD setups respectively. After the completion of the charging phase, the contents of the chamber were emptied and the final concentration of the deionized water was measured with the aid of a TDS meter (TDS4, Industrial Test Systems, Inc., SC). Since the TDS meter used was most sensitive in the 1-999 ppm range (1 ppm resolution in this range), the water fed to the system, produced by mixing distilled water and table salt, had salinity in the range of 600-900 ppm. The mass of ions removed during the charging phase was then calculated using the final concentration value and the concentration value of the saline water input to the system. The charging current, which was measured as a function of time during the experiment, provides an additional check on the deionized mass value.

After the charging phase was completed, the electrodes were shorted and the distinct flow paths for AFD and PFD were implemented. While the AFD flow path is a very simple scheme that can be carried out by simply connecting a pump to the single channel, the implementation of the PFD flow path is not a trivial task. To implement the permeating scheme, we used the fluidic circuit shown in Fig. 14. Two peristaltic (positive displacement) pumps (43045K36, McMaster-Carr, CA) able to feed water at flow rates ranging from 7 ml/min to 207 ml/min were connected to the middle channel and the outer channels as shown in Fig. 14. We performed our experiments at permeation flow rates of 8, 16, 32 and 64 ml/min respectively. The pump was able to handle a maximum pressure of 20 psi (138 kPa), where our maximum pumping requirement was only around 6 psi (41 kPa). To determine a one-to-one equivalence with the AFD procedure (since we want to find the rate of ions removed in each process for the same flow rate employed), we shut off the pump connected to the outer channel and operated the pump connected to the middle channel at the same flow rate as the pump connected to the single channel AFD apparatus.

Further, we completely closed the middle channel valve so that the entire water was permeated through the porous electrodes.

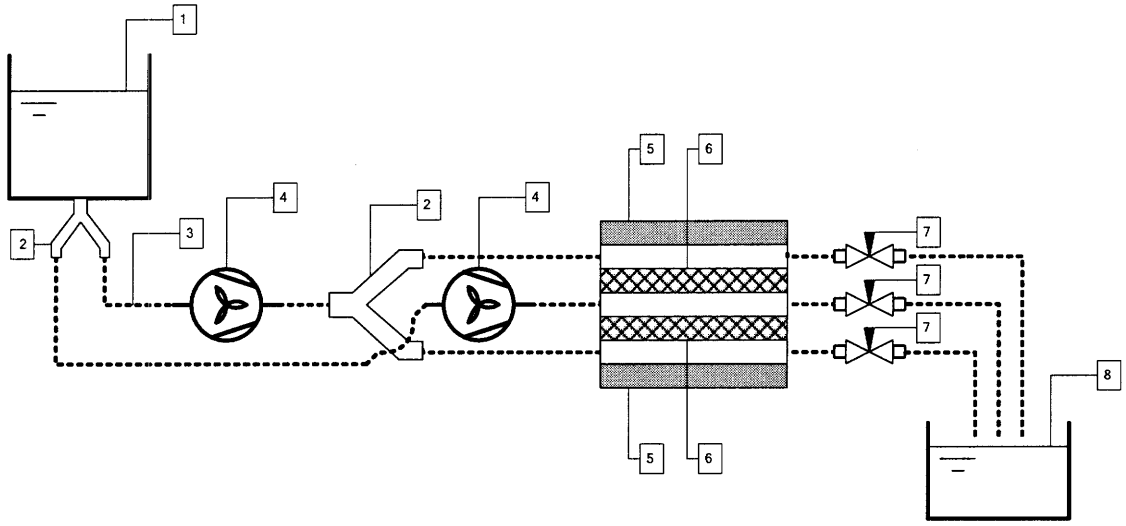

Fig. 14: Schematic diagram of fluidic circuit employed in PFD process.
The components indicated in the figure are: reservoir (1); wye (2); connecting tube (3); peristaltic pump (4); retainer plate (5); carbon aerogel electrode (6); valve (7); collecting beaker (8).

The permeated water moving through the aerogel paper and subsequently through the outer channels was collected in a beaker. The two outer channel outlet streams were collected together and the combined volume flow rate was obviously the same as the flow rate of the outlet stream in the AFD setup. The outlet concentrations in each case were measured at definite time intervals. The experiments were carried out till the discharging current fell to less than 5% of its initial value. Due to its exponentially decaying nature, the discharging current never falls to zero - theoretically, it decays to zero after infinite time – and a criterion must be set to signal the completion of the discharging experiments, such as the decay of the discharging current (as in our case) or the potential difference across the electrodes below a pre-assigned value or below a certain percentage of its initial value. In practice, deionization systems discharge for a 'given amount of time' that enables them to recharge for a 'sufficiently long time'. Both these time intervals are described ambiguously and a feel for the values of the charging and discharging time periods is frequently gained through experience.

The input water used for our discharging processes was tap water (~300 ppm) so that even after carrying the ions from the channel or through the electrode as the case maybe, there was only a remote possibility that the collected water would cross the 999 ppm mark. Crossing the mark would mean loss of resolution in our metrology although the TDS meter could function up to 9990 ppm at a decreased resolution of 10 ppm. To ensure repeatability, all the concentration values were measured five times and after each reading the TDS meter was cleansed with distilled water. After measuring the inlet concentration and the outlet concentrations (at definite time intervals), the mass of ions removed per unit time and the cumulative mass of ions removed for each process (AFD and PFD) was calculated.

The measured discharging current provided an estimate of the number of ions that had been detached from the electrodes. In essence, this could be thought of as the upper bound to the

cumulative mass of ions removed because the transfer of ions from the surface to the bulk (where bulk could mean either the middle channel or the outer channels) is preceded by the reaction at the surface (desorption).

It must be stressed that in our experimental results all calculations pertaining to the mass of ions removed per unit time have an inherent averaging in the time interval over which the measurements were made. In other words, even though we use the phrase 'per unit time', we do not claim to know the variations, taking place on a shorter timescale, within each macroscopically averaged value. Obviously, this problem is reduced if one gathers outlet concentration data at a higher frequency (shorter time intervals). The upper bound to the frequency of data acquisition is provided by the TDS meter, which can only make accurate measurements if sufficient amount of water (~30 ml) has been collected. This led to a lower bound on the time of water collection before each measurement. Evidently, this time period is inversely proportional to the employed flow rate in the system. However, the determination of the cumulative number of ions does not have any such averaging concerns as it is essentially obtained by integrating the mass of ions removed per unit time, i.e. integration of the local variable provides a global parameter that masks localized defects. Consequently, it is more meaningful to draw inferences using the plots of cumulative mass of ions removed as a function of time.

Chapter 5: Model formulation

In this chapter, we will formulate theoretical models to represent and analyze the phenomena occurring in the capacitive deionization systems. We shall begin by developing a simple model for the charging process – the goal of which is to predict the variation in charging time period as a function of the system parameters. Subsequently, we will undertake the analysis of the mass transfer characteristics of the discharging processes. We will then use the finite difference approach to solve the governing equations, formulated in the discharging models, with the help of appropriate boundary conditions. While we shall briefly touch upon some of the electrochemical aspects of the deionization process in our discussion, the primary focus in this section will be to develop predictive equations for water recovery ratio and throughput for deionization systems employing AFD and PFD schemes.

At this juncture, it is necessary to rigorously define the system performance metrics, namely water recovery ratio and throughput, for the sake of clarity in our ensuing discussion. The water recovery ratio (WRR) for any desalination process (or plant) can be written as:

$$WRR = \frac{V_{desal}}{V_{input}} = \frac{V_{desal}}{V_{desal} + V_{waste}} \quad (1)$$

where, V_{desal}, V_{waste} and V_{input} are the volumes of desalinated water, wastewater and input water respectively. If one considers the desalination process to be a black box, water recovery ratio can be aptly described as a transfer function between the acceptable water output and the total water input. The plant throughput can be defined as the amount of desalinated water obtained in a day, i.e. V_{desal} over the whole day. One could just as well describe the throughput on a per-year or a per-month basis, but we will consistently follow the above definition in our discussion.

Adapting the above definitions to the capacitive deionization process one can express WRR in the following manner:

$$WRR = \frac{V_C}{V_C + V_D + V_s} \quad (2)$$

where, V_C is the volume of water desalinated during the charging phase of one cycle, V_D is the volume of water required to flush out the saturating ions during the discharging phase of the cycle and V_s is the volume of water 'wasted' during the time required to switch from the discharging phase of the cycle to the charging phase of the next cycle. The throughput, in this case, is the net volume of water obtained during the charging phase of all the cycles run during the day, i.e. summation of V_C over all the cycles executed in the whole day.

Please note that the above expression for the water recovery ratio would need to be changed if one can stop the intake of water during the switching time period. The water flow during the switching time period is completely wasted and one would like to eliminate it, provided the addition of an extra mechanical component to the existing design is not unduly troublesome. For example, if upstream valves that could cause cessation of flow during the switching phase were added, the expression for the modified water recovery ratio (WRR_m) would be given by:

$$WRR_m = \frac{V_C}{V_C + V_D} \quad (3)$$

Finally, one can simplify the water recovery ratio expressions further if the flow rate during all the phases remains constant. In that case the water recovery ratio expressions can be rewritten by substituting the volumes with the corresponding time periods, e.g. WRR will be equal to the ratio of the charging time period to the sum of the charging, discharging and switching time periods.

5. (a) Analysis of the charging process

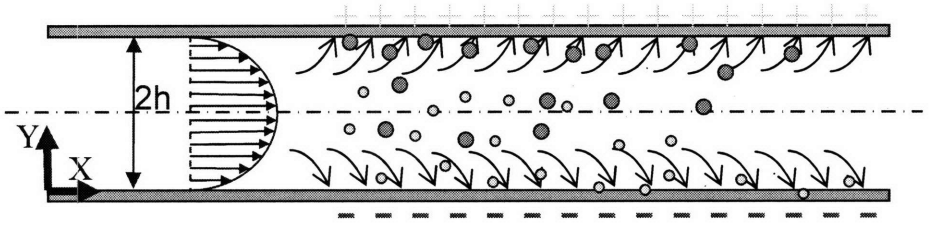

Fig. 15: Schematic diagram of the charging process showing the electromigration phenomenon. Positively charged ions (green) move towards the negatively charged electrode and the negatively charged ions (orange) migrate towards the positively charged electrode.

The charging process involves the diffusion-migration transport of the ions in the electrolyte (saline water), which flows through the system with a parabolic velocity profile (Poiseuille), and the non-steady-state process of the charging of the electrical double layer (EDL) at a developed electrode/electrolyte interface in the pores of the carbonaceous material. The chemical reactions involved in the EDL formation can be represented as:

On the positive electrode:

$$E_s + A^- \leftrightarrow E_s^+//A^- + e^-. \quad (4)$$

On the negative electrode:

$$E_s + C^+ + e^- \leftrightarrow E_s^-//C^+. \quad (5)$$

The overall reaction can then be written as:

$$E_s + E_s + A^- + C^+ \leftrightarrow E_s^+//A^- + E_s^-//C^+. \quad (6)$$

where, E_s represents the electrode surface area in its unpolarized state, A^- and C^+ are the anions and cations in the system, and the // symbol denotes the coupling between the ions and the electrode in the EDL (Fig. 16).

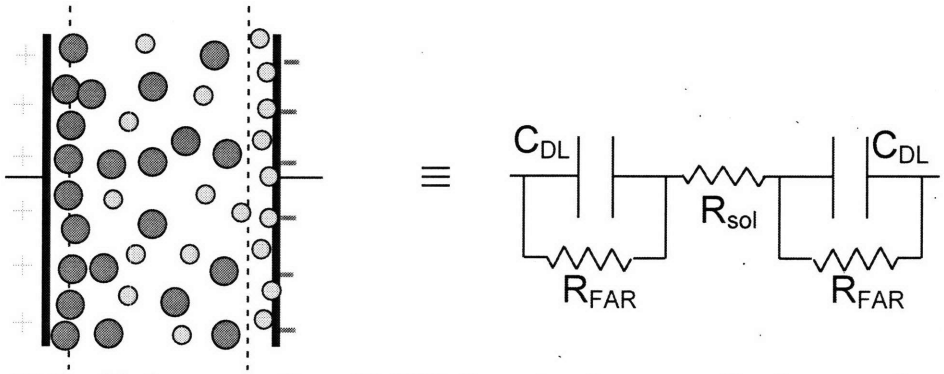

Fig. 16: Double layer capacitor with EDL formation due to coupling between electrode and ions. The dotted lines, on either electrode, depict the Debye length (not drawn to scale) within which the EDL forms. A simple circuit representation of the DLC is shown on the right, where C_{dl} is the capacitance in the EDL, R_{FAR} is the faradaic parallel resistance and R_{sol} is the electrolyte resistance.

While carbon electrodes can usually be approximated as the ideal electrochemical double layer capacitors, contributions from other functional groups which are generally present on activated carbon cannot be completely ignored. The latter, commonly termed as pseudocapacitances, store electric charge at the expense of a reversible faradaic reaction (for example, a redox reaction) that exhibit voltage-current response similar to a capacitor.

A lot of work has been reported, primarily in the electrochemical community, on the characterization and analysis of EDL and double layer capacitors (DLC) [50]. The details of the mathematical models formulated for the DLC are beyond the scope of this work but the interested reader might consult the works of Newman [51], Farahmandi [52], Weidner [53] and Serdyuk [54]. Some interesting results on the potential drop and mass transfer characteristics of flow-by and flow-through electrodes, particularly in limiting current conditions have also been published [55]. Characterization of mass transfer has, however, been primarily on an experimental scale and further developments have been stunted due to the use of generic mass transfer correlations, which provide little insight into the phenomena occurring in the system.

The aim of this section is to determine the amount of time a system can charge for before it needs to be regenerated, i.e. the permissible charging time per cycle. In the charging process, the ion transport from the bulk to the surface of the electrode is succeeded by the ion-electrode interaction in the EDL. Consequently, the extent of EDL charging is the true measure of the quantity of ion removal from the electrolyte and one can calculate the permissible charging time without accounting for the ion transfer characteristics. In other words, since regeneration is necessitated by the saturation of the EDL, the charging current characteristics should provide sufficient information to detect when one needs to switch from the charging phase to the discharging phase. Please note that this is very different from the discharging case, where the extent of ion removal from the system is not given by the discharging current characteristics but by the ion transport characteristics because in discharging, detachment of ions from the electrode is the initial step and is followed by the ion transfer step.

It is clear that the charging process is stopped when the water coming out of the channel(s) has higher than the permissible level of concentration. Since the water being input has the same concentration throughout the charging phase, the amount of desalination in the capacitive deionization system must have dropped off during the elapsed time. This drop off must mirror the decline in the charging current, as explained in the previous paragraph. In other words, when the current in the external circuit falls below a certain value, it means that the capacitor plates (the EDL, in this case) is gradually nearing saturation – as a consequence of which it is not attracting or interacting with the same number of ions as earlier in the charging phase. Thus, one could state that when the charging current falls below a threshold value we must stop the charging phase and move over to the discharging phase. Assuming that the charging current in the DLC has the classical exponentially decaying profile, it is clear that we must have knowledge of the following parameters to enable us to determine the permissible charging time period for the deionization system:

(a) The permissible level of concentration in the output (product) water (c_{perm} ppm),
(b) Flow rate of water in the system (Q ml/min),
(c) Time constant for charging the capacitor (τ sec),
(d) Initial value of the charging current (I_0 A).

The first parameter, the tolerable level of concentration in the product water, is specified by the end user. Naturally, for higher permissible levels of output concentration, the charging can take place for a longer period. The second parameter (flow rate) is a system parameter. In ideal conditions, we would like our system to have as high a flow rate as possible to ensure maximum

throughput. However, higher flow rates would mean the ions are being pushed through the channel at a faster pace and are getting much less 'residence time' (defined as the time of stay of an ion inside the channel). This leads to lesser chances of ion migration and subsequent removal at the electrode surface. Consequently, more number of ions will tend to remain in the product water. To put it a little more mathematically, we can write for two different flow rates, say Q_1 and Q_2 ml/min (where $Q_2 > Q_1$), the following:

For the same input water concentration, we have for a 1 min time period,

$$c_0 = \frac{n_1}{Q_1} = \frac{n_2}{Q_2}, \tag{7}$$

where n_1 and n_2 are the number of ions carried in Q_1 ml and Q_2 ml of the input water respectively. If the same charging current characteristics hold for both higher and lower flow rate deionization, then we can express the two product water concentrations as:

$$\text{Output concentration for lower flow rate } c_1 = \frac{n_1 - \Delta n}{Q_1} \tag{8}$$

$$\text{Output concentration for higher flow rate } c_2 = \frac{n_2 - \Delta n}{Q_2} \tag{9}$$

where Δn is the number of ions removed by the deionization system in both the cases in the 1-min time interval.

As $\frac{\Delta n}{Q_1} > \frac{\Delta n}{Q_2}$, the output concentration for the lower flow rate (c_1) must be smaller than the output concentration for the higher flow rate (c_2). As a consequence, having a higher flow rate would mean having to recharge earlier, i.e. smaller permissible charging time, given a fixed current characteristic profile. This trend between the flow rate and the permissible charging time must be mirrored in the final expression, which must also account for the other parameters.

The final two parameters (c) and (d) stated previously pertain to the variation in the charging current with time. We have assumed that the current in the charging phase exhibits an exponential decay and thus only these two parameters, the initial value and the time constant, are sufficient to determine its value at any point of time. Our experiments reveal, as shown in the Chapter 6, that the exponentially decaying profile provides an excellent approximation to the real charging current characteristics.

Based on the above discussion, we can now write the following:

$$\text{Rate of removal of ions at any time } t = \frac{I(t)}{F}, \tag{10}$$

where I(t) is the current at that time instant and F is the Faraday constant (96,485.3383 C/mole).

Given that the flow rate in the system is Q ml/min,

$$\text{The reduction in concentration } (\Delta c)_t \text{ at time } t = \frac{60\, I(t)}{F\, Q} \text{ moles/ml} \tag{11}$$

Converting this value to a ppm (mg/l) concentration, we have:

$$(\Delta c)_t = 60 \cdot 10^6 \frac{M\, I(t)}{F\, Q} \tag{12}$$

where, M is the molecular weight of the salt (for NaCl, M = 58.442 g/mol).

It is evident that $(\Delta c)_t$ is the critical parameter in making the decision when charging must end, because if $(\Delta c)_t$ falls below a minimum threshold value, the product water concentration will cross the permissible levels. The threshold value for the desalination required is given by:

$$(\Delta c)_{threshold} = c_{input} - c_{perm} \quad (13)$$

where, c_{input} is the concentration of the input water in ppm.

Since, $(\Delta c)_t$ must be greater than or equal to $(\Delta c)_{threshold}$, we can write from Eqn. (12) and (13):

$$c_{input} - c_{perm} \leq 60 \cdot 10^6 \frac{M\, I(t)}{F\, Q} \quad (14)$$

Substituting for I(t) the exponential decay profile, given the initial charging current (I_0) and the charging time constant (τ), we get:

$$c_{input} - c_{perm} \leq 60 \cdot 10^6 \frac{M\, I_0}{F\, Q} \exp(-\frac{t}{\tau}) \quad (15)$$

Simplifying the above expression in the limiting case when equality holds and putting M equal to 58.442 g/mol, we have:

$$t_{critical} = \tau \left[10.5 - \ln\left(\frac{Q \cdot (c_{input} - c_{perm})}{I_0} \right) \right] \quad (16)$$

where $t_{critical}$ is the maximum time for which the charging phase can be continued in one cycle.

The above relationship tells us that the permissible charging time goes down with an increase in flow rate, which matches with our intuitive understanding and the discussion elaborated with the help of Eqn. (7)-(9). It also states that an increase in initial charging current value or an increase in the permissible level of output water concentration (i.e. when higher number of ions in unit volume of water is tolerated) implies a rise in the permissible charging time.

To get an idea of how much larger or smaller this time is compared to the charging time constant of the circuit, we put the following reference numbers from our experiments:
$c_{input} - c_{perm}$ = 10 ppm, I_0 = 20 mA, Q = 10 ml/min.
For these values, we get $t_{critical}$ equal to 1.6 times the charging time constant. Since for a charging capacitor, the current drops down to about 36.7 percent of its original value after one time constant, it would seem reasonable that after 1.6 times this time period, when the current reaches 20 percent of original value, we can no longer keep on charging due to lesser number of ions being removed by the deionization circuit.

5. (b) Analysis of the Axial Flow Discharging (AFD) process

The discharging process can be broadly described as a two step process, where generation of ions (i.e. detachment of ions from the EDL) is followed by transportation of the ions to the bulk and through the channel. In the axial flow discharging (AFD) scheme, the ion transport step is facilitated by diffusion and convection. The aim of this analysis is to study this ion transfer step and the relevant transport phenomena occurring in the AFD process. The ultimate goal is to find the amount of ions that are being removed from the system as a function of time. This result can then be compared to our experimental observations to gain further insight into the system behavior.

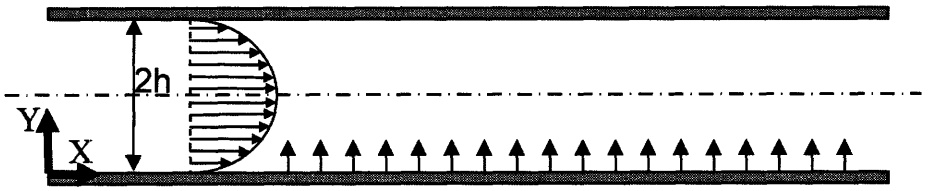

Fig. 17: Schematic diagram of the axial flow discharging process showing diffusion from the walls and axial convection.

In order to achieve the above-stated goals, we need to first know the concentration distribution inside the channel as a function of spatial position and time. The first step in this direction is to identify the different phenomena that contribute to the flux of the ions in the system. In this case, the relevant physical phenomena that may affect the concentration distribution in the system are diffusion, convection and electromigration. One can write the molar flux of component i (ions of the i^{th} species) in a dilute multi-component solution (i.e., in the electrolyte media in the channel) in the following manner (when measured with respect to a fixed coordinate system):

$$\mathbf{N}_i = -D_i \nabla c_i + c_i \mathbf{v} - \left(\frac{z_i}{|z_i|}\right) u_i c_i \mathbf{E} \qquad (17)$$

where, N_i is the molar flux of the i^{th} component,
D_i is the diffusion coefficient of the i^{th} component,
c_i is the concentration of the i^{th} component,
$\mathbf{v}$ is the flow velocity of the solvent,
z_i is the charge on the ion of the i^{th} species,
u_i is the mobility of the i^{th} component, and
$\mathbf{E}$ is the applied electric field in the system.

Eqn. (17) is referred to as the Nernst-Planck equation. This equation expresses the total flux as the sum of the fluxes due to diffusion (first term), convection (second term) and electromigration (third term). The mobility of each ion species, u_i, is related to its diffusivity, D_i, by the Einstein relationship, but we do have to worry about the third term on the RHS of our equation as there is no applied electric field in the system during discharging. In our analysis for both AFD and PFD, we shall assume that during the discharging phase, the electrodes are shorted such that electromigration does not play an active role in the transportation of ions. It is pertinent to note that electromigration could be a major player in the transport phenomena if a reverse polarity was applied to the electrodes to expedite the discharging process.

To relate the above-stated flux to the concentration in the channel, we apply the conservation of mass principle to any arbitrary control volume inside the channel. This operation yields the following equation (when written in terms of a fixed coordinate system):

$$\frac{\partial c_i}{\partial t} = -\nabla.\mathbf{N}_i + G_i \tag{18}$$

where, G_i is the number of moles of ions of the i^{th} species generated inside the control volume.

Eqn. (18) states that the rate of change of concentration of any species within a control volume is equal to the sum of the net flux (i.e., influx – efflux) into the control volume and the net generation of the species inside the control volume. Since the discharging process is a heterogeneous reaction, where the electrochemical reaction only takes place at the surface of the electrodes, no sources or sinks exist inside the channel. In other words, the net generation term for every control volume drawn within the channel confines is zero. Combining Eqn. (17) and (18) then gives us:

$$\frac{\partial c_i}{\partial t} + \mathbf{v}.\nabla c_i = D_i \nabla^2 c_i \tag{19}$$

The velocity profile of the flow in the channel is strictly in the x direction and assuming that diffusion in the x direction is much less significant than the convection along the same, we can further simplify Eqn (19) to the following form:

$$\frac{\partial c_i}{\partial t} + v_x \frac{\partial c_i}{\partial x} = D_i \frac{\partial^2 c_i}{\partial y^2} \tag{20}$$

This is the governing equation for the concentration distribution as a function of space (x, y) and time (t) inside our channel setup. It is to be noted that for our previous assumption to be valid, i.e. for axial convection to be significantly larger than axial diffusion, we must have:

$$v_x >> \frac{D_i}{L^2} \tag{21}$$

where L is the characteristic length scale in the x direction.
Eqn. (21) comes from scaling the corresponding convection and diffusion terms and is true for all systems where the velocity in the axial direction is not negligibly small.

The flow inside the channel is induced by the external pressure gradient, produced by the pump. In analyzing the velocity profile, the following assumptions are made:

a) Fluid characteristics: Newtonian and incompressible (water exhibits both these characteristics to a very large extent),
b) Flow characteristics: Steady, laminar and fully developed. Please note that a steady-state velocity profile does not mean that the concentration distribution will be steady. Since the Reynolds number in our system is around 10, our flow is bound to be laminar unless any active source of turbulences exist in the setup. Finally, the entrance length is equal to the 0.16 times the product of the channel half-width and the Reynolds number [56]. For our setup, the entrance length turns out to be about 8 mm. This is much smaller than the channel length of 230 mm and thus we can safely assume that fully developed flow occurs throughout the channel.

The governing equation for the velocity in the channel is the Navier-Stokes equation given by:

$$\rho \frac{D\mathbf{v}}{Dt} = -\nabla p + \mu \nabla^2 \mathbf{v} + \mathbf{f}_b \tag{22}$$

where ρ is the fluid density, μ is the fluid dynamic viscosity, p is the pressure applied on a fluid element inside the control volume and f_b is the net body forces per unit volume.

In the framework created by the above assumptions, the Navier-Stokes equation can be solved, given the no-slip boundary conditions at either electrode surface, to yield the following axial flow velocity:

$$v_x = \frac{1}{2\mu}\left(-\frac{\partial p}{\partial x}\right) y(2h-y) \tag{23}$$

Please note that the applied pressure gradient is constant and thus, the axial velocity is a function of y only (fully developed flow). Thus, the velocity distribution in the channel is given by the parabolic Poiseuille profile, as sketched in Fig. 17.

Eqn. (23) can be combined with Eqn. (20) to give the final governing equation for the concentration distribution in the system.

$$\frac{\partial c_i}{\partial t} + \frac{1}{2\mu}\left(-\frac{\partial p}{\partial x}\right) y(2h-y)\frac{\partial c_i}{\partial x} = D_i \frac{\partial^2 c_i}{\partial y^2} \tag{24}$$

Eqn. (24) needs to be solved over half of the channel only because our system is symmetric about the centerline. This equation holds for each individual species in the electrolyte media. Consequently, in order to understand the total ion transport one would need to solve this equation for all the ions present in the system. In our case, we shall assume that Na^+ and Cl^- are the only ions present in the input water.

The final piece of the puzzle is to set up the boundary conditions needed to solve this governing equation. In order to solve Eqn. (24) we need two boundary conditions in y, a boundary condition in x and an initial condition in t.

Initial condition in t: $(c_i)_{t=0} = c_{i,0}$ (25a)

Boundary condition in x: $(c_i)_{x=0} = c_{i,\text{input}}$ (25b)

where $c_{i,0}$ is the concentration of water in the channel at time t= 0 and $c_{i,\text{input}}$ is the concentration of input water.

Boundary condition (1) in y: $\left(\frac{\partial c_i}{\partial y}\right)_{y=h} = 0$ (25c)

This arises from symmetry, as the concentration on each side of the half channel must share a common profile and therefore the derivative of the function about the symmetry line must be zero.

Boundary condition (2) in y: $\left(\frac{\partial c_i}{\partial t}\right)_{y=0} = \frac{1}{V\varphi}\left[-D_i A_f\left(\frac{\partial c_i}{\partial y}\right) + R_i\right]$ (25d)

where V is the volume of the electrode, φ is the porosity of electrode, A_f is the flat surface area of the electrode and R_i is the number of moles of ions generated at the electrode surface.

The above equation gives the boundary condition at the electrode surface. The LHS of Eqn. (25d) gives the rate of change of concentration at the surface of the electrode. The expression with the square brackets on the RHS calculates the net number of moles 'appearing' at the surface, by subtracting the number of moles leaving through diffusion from the number of moles being generated at the surface of the electrode via detachment from the EDL. The dividing factor on the RHS, $V\varphi$, is used to convert the number of moles appearing at the surface to an equivalent concentration. We assume for the convenience of further analysis that the ions generated at the EDL surface increase the concentration within the effective volume of the porous electrode uniformly. We cannot accurately predict how much of the volume is actually influenced by the new ions. In some sense therefore the volume factor, $V\varphi$, is introduced to bridge the gap between the known number of moles that have appeared in the particular time instant and the unknown

value of concentration at the electrode. Finally, for the sake of avoiding confusion, we must stress that R_i is different from the G_i term of Eqn (18) because the former predicts the number of moles generated at the surface while the latter is used to describe the molar concentration produced inside a control volume. R_i at any instant of time is obtained by dividing the discharging current in the external circuit at that point in time by Faraday's constant (F).

Typically, convection-diffusion equation solutions are obtained through the use of linear operator theory, such as separation of variables, eigenvector expansions and Fourier transforms. Often an important approximation applied to similar mass transfer problems is the short contact time assumption. By focusing on short times of residence, where the time of residence is given by the length of the channel divided by the average axial velocity, an analytical solution can be obtained by converting a steady-state convection-diffusion partial differential equation to an ordinary differential equation using similarity analysis. However, this approximation is not valid in our case because our residence times are in the order of 10 minutes. Further more, to the best of our knowledge none of the analytical methods described above can be suitably applied to this problem, especially due to the complications arising from the boundary condition at the electrode surface (Eqn. (25d)). Thus, we will endeavor to solve these equations numerically using a finite difference approach, detailed in Section 5(d).

Once we know the concentration distribution in the channel, we can easily determine the amount of ions removed from the system at any instant of time. The latter quantity is equal to the product of the concentration at the channel outlet at the instant of time under consideration and the flow rate, which can be mathematically expressed as:

$$(m_i)_{(t\to t+\Delta t)} = \int_t^{t+\Delta t}\int_0^{2h} c_i(L,y,t)\, v_x(y)\, dy\, dt \qquad (26)$$

where the term on the LHS represents the mass of ions removed from time t to $(t+\Delta t)$ and L is the length of the channel (i.e. the abscissa of the channel outlet) . The net mass of ions removed can then be calculated by summing the masses removed for each ion present in the system.

5. (c) Analysis of the Permeating Flow Discharging (PFD) process

The discharging process, for the PFD process, is also a two-step process, very much similar in its operational hierarchy to the discharging process utilizing the AFD scheme. The primary phenomenological difference in the PFD scheme arises from the manner in which the second step, i.e. the ion transfer from the EDL, is achieved. The design parameter employed to satisfy this second step is radically different from the approach in the conventional AFD scheme. Flow of the solvent media through the porous electrodes is used to carry away the ions from the channel setup, as sketched in Fig. 18.

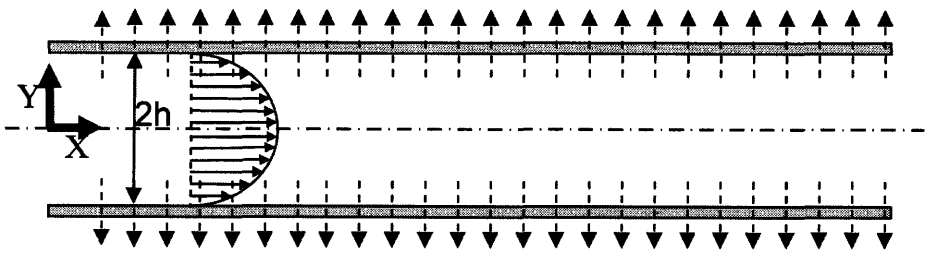

Fig. 18: Schematic diagram of the permeating flow discharging process showing permeation through the porous electrodes.

Internal diffusion, coupled with axial convection, might also account for the transfer of some ions from the electrode surface to the bulk of the middle channel and subsequently out of the channel. Consequently, without carefully analyzing or scaling the relative magnitudes of the internal diffusion-convection flux term and the permeating flux term, one cannot ignore the convection-diffusion phenomena in the middle channel. It is evident, however, that the effect of internal diffusion and axial convection will reduce significantly with the increase in the total volume of water permeated through the electrodes. In the limiting case for the PFD flow path, all the water is permeated through the porous electrodes, i.e. no water flows out of the middle channel outlet. This limiting case is satisfied provided the following condition holds:

$$L \geq \frac{u_{avg} h}{v_w} \tag{27}$$

where, L is the channel length, u_{avg} is the average axial velocity and v_w is the permeation velocity.

The analysis in this section is carried out in two parts. First, we solve for the velocity distribution – both axial and lateral velocity – in the system. Unlike in the AFD analysis where the velocity distribution was a simple Poiseuille profile that remained constant in magnitude throughout the channel, the PFD velocity profile is more complex due to the permeating flow induced at the porous electrodes. After the velocity distribution is obtained, we determine the concentration distribution in the middle channel (convection-diffusion) and more importantly, the ion transfer characteristics through the electrodes. The goals of this analysis mirror those of the AFD analysis presented in Section 5 (b).

For this analysis, we assume that the fluid is Newtonian and incompressible and the flow is steady. The governing equations for the axial velocity u(x, y) and lateral velocity v(x, y) are given by the x-momentum and y-momentum conservation equations (Navier-Stokes).

$$u\frac{\partial u}{\partial x}+v\frac{\partial u}{\partial y}=-\frac{1}{\rho}\frac{\partial p}{\partial x}+\nu\left(\frac{\partial^2 u}{\partial x^2}+\frac{\partial^2 u}{\partial y^2}\right) \tag{28}$$

$$u\frac{\partial v}{\partial x}+v\frac{\partial v}{\partial y}=-\frac{1}{\rho}\frac{\partial p}{\partial y}+\nu\left(\frac{\partial^2 v}{\partial x^2}+\frac{\partial^2 v}{\partial y^2}\right) \tag{29}$$

where ν is the fluid kinematic viscosity, which is the ratio of the dynamic viscosity μ to the density ρ.

The continuity equation is given by:

$$\frac{\partial u}{\partial x}+\frac{\partial v}{\partial y}=0 \tag{30}$$

The velocity boundary conditions required to solve the above equations are:

$$u(x,\pm h)=0 \tag{31a}$$

$$\left(\frac{\partial u}{\partial y}\right)_{y=0}=0 \tag{31b}$$

$$v(x,\pm h)=v_w \tag{32a}$$

$$v(x,0)=0 \tag{32b}$$

where, v_w is the permeation velocity.

Eqn. (31a) is a no-slip condition for the axial velocity at the electrode surfaces. Eqn. (31b) and (32b) are symmetry conditions. In the statement of Eqn. (32a), we assume that the velocity of the

fluid permeating through the electrodes bounding the channel is independent of position. It is a reasonable approximation, if the pressure gradient across the electrodes is much higher than the pressure drop along the length across the electrode (because these pressure differences controls the velocity across and along the channel). In other words, if the difference between p_{outer} (average pressure in the outer channel) and p_{middle} (average pressure in the middle channel) is significantly higher than the difference between the inlet pressure p(0, h) and the outlet pressure p(L, h) along the middle channel, we can safely assume that there is a constant permeation velocity across the electrodes. The osmotic pressure difference across the electrodes was around 20-60 kPa for our setup, whereas the pressure drop along the channel varied in the range of 1-10 Pa only - signifying the soundness of the constant permeation velocity approximation.

The solution in this case will be investigated over the half-channel only (similar to the AFD case) because the flow is symmetrical about a plane midway between the electrodes. There exists a classical solution to this problem, first proposed by Berman [57] while investigating laminar flow in channels with porous walls. In this approach, he introduces the following stream function $\psi(x, y)$:

$$\psi(x,y) = \left[h\bar{u}(0) - v_w x\right] f\left(\frac{y}{h}\right) \tag{33}$$

where $\bar{u}(0)$ is the average axial at the inlet to the middle channel and f is an unknown function.

This stream function is used to reduce Eqn. (28) and (29) to the following ordinary differential equation:

$$R\left[f'^2 - ff''\right] + f''' = k \tag{34}$$

where $R \equiv v_w h/\nu$ (Reynolds number based on permeation velocity), and k is an integration constant.

The transformed boundary conditions are:

$$f(0) = 0 \tag{35a}$$

$$f(1) = 1 \tag{35b}$$

$$f'(1) = 0 \tag{35c}$$

$$f''(0) = 0 \tag{35d}$$

The governing equation for the velocity profile, Eqn (34), is a third-order, non-linear ODE that requires four BC because k is an undetermined constant of integration. These BC are given by Eqn. (35a) – (35d). To solve this problem, Berman introduced a perturbation approach which is valid for $R \leq 1$. Subsequently, the problem has also been solved for $R > 1$ [58]. For our system, R was of the order of 0.01 and thus Berman's solution can be applied without any reservations. The details of the perturbation solution are beyond the scope of this work but we will state the final results obtained for the axial and lateral velocities.

$$u\left(x,\frac{y}{h}\right) = \left[\bar{u}(0) - \frac{v_w x}{h}\right]\left[\frac{3}{2}\left(1-\left(\frac{y}{h}\right)^2\right)\right]\left[1 - \frac{R}{420}\left(2 - 7\left(\frac{y}{h}\right)^2 - 7\left(\frac{y}{h}\right)^4\right)\right] \tag{36}$$

$$v\left(\frac{y}{h}\right) = v_w\left[\frac{1}{2}\left(\frac{y}{h}\right)\left(3-\left(\frac{y}{h}\right)^2\right) - \frac{R}{280}\left(\frac{y}{h}\right)\left(2 - 3\left(\frac{y}{h}\right)^2 + \left(\frac{y}{h}\right)^6\right)\right] \tag{37}$$

Knowledge of the velocity distribution in the channel permits us to move to the second step, i.e. determination of the concentration distribution and the ion transfer characteristics across the

electrodes and at the outlet to the middle channel. The concentration distribution in the middle channel has a similar governing equation as in the AFD scheme, with an additional lateral convection term. The boundary conditions in y are distinct from those stated in Section 5(b) because of the translation of the coordinate system origin from the electrode surface to the channel mid-section and, more importantly, because of the permeation flux at the electrode surfaces.

Governing equation:

$$\frac{\partial c_i}{\partial t} + u\frac{\partial c_i}{\partial x} + v\frac{\partial c_i}{\partial y} = D_i \frac{\partial^2 c_i}{\partial y^2} \tag{38}$$

where we once again assume that axial convection is much more dominant than axial diffusion; no such assumption is made in the lateral direction.

Initial condition in t: $(c_i)_{t=0} = c_{i,0}$ (39a)

Initial condition in x: $(c_i)_{x=0} = c_{i,\text{input}}$ (39b)

where $c_{i,0}$ is the concentration of water in the channel at time t= 0 and $c_{i,\text{input}}$ is the concentration of input water.

Boundary condition (1) in y: $\left(\frac{\partial c_i}{\partial y}\right)_{y=0} = 0$ (from symmetry) (39c)

Boundary condition (2) in y: $\left(\frac{\partial c_i}{\partial t}\right)_{y=\pm h} = \frac{1}{V\varphi}\left[-D_i A_f\left(\frac{\partial c_i}{\partial y}\right) + A_f c_i v - J_{iS} + R_i\right]$ (39d)

where the only new term introduced is J_{iS}, which is the solute flux of the i^{th} component through the porous electrode. All the other notations retain their meanings from our previous discussions.

Evidently, we can solve Eqn. (38), in the framework created by the BC (Eqn. (39a) – (39d)), using the finite difference approach as long as we know the permeating solute flux J_{iS}. Unfortunately, determination of this term is not trivial by any means. One would need to adopt an irreversible thermodynamics approach to come up with the appropriate equations relating the permeating solute flux term to known quantities, such as the pressure difference and the concentration difference across the electrode, and the material properties of the electrode.

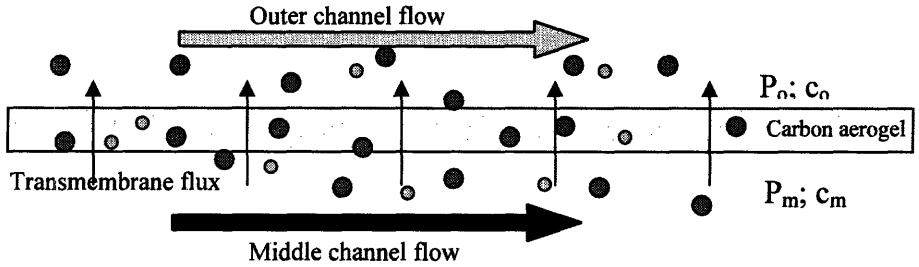

Fig. 19: Permeating flow discharge across a carbon aerogel paper, which was positively polarized during the charging phase.
$\Delta P = P_m - P_o$; $\Delta c = c_m - c_o$.

We will now lay down the basic groundwork, using irreversible thermodynamics theory, for the derivation of the transmembrane flux equations. The following methodology was first proposed by Kedem and Katchalsky [59]. Irreversible thermodynamics states that the fluxes in the system,

J_i, tending to restore equilibrium are functions of the driving forces, X_i, present in the system. If the forces are sufficiently small, one can write linear relationships for each of the fluxes in terms of the driving forces, as expressed below:

$$J_i = L_{i,1} X_1 + L_{i,2} X_2 + \ldots L_{i,j} X_j + \ldots L_{i,N} X_N \quad (40)$$

The factors L multiplying the driving forces are phenomenological constants. In the case under consideration, therefore one can write:

$$\frac{J_V}{S} = L_P \Delta P + L_{PD} RT\Delta c \quad (41a)$$

$$\frac{J_D}{S} = L_{DP} \Delta P + L_D RT\Delta c \quad (41b)$$

where S is the surface area over which the transport phenomena takes place. Eqn. (41a) and (41b) are written for the bulk solvent flux (per unit area) and the exchange flux of the solute (per unit area) relative to the bulk solvent flux (per unit area) respectively. The first driving force arises from the hydrostatic pressure and the second driving force is due to the concentration difference across the electrodes (and thus from the resultant osmotic pressure).

These equations can be further simplified by application of the following constraint provided by Onsager's reciprocity relationship:

$$L_{PD} = L_{DP} \quad (42)$$

The introduction of the equality of the cross-coupling phenomenological constants completes the framework required to develop the Kedem-Katchalsky equation. This equation provides deep insight into the physics of the system by converting the phenomenological constants in Eqn. (41b) to readily identifiable and quantifiable physical parameters. Moreover, the Kedem-Katchalsky equation restates the solute flux in terms of a fixed coordinate system. This is in sharp contrast to Eqn. (41b) where the solute flux is expressed as an exchange flux relative to the bulk solvent flux.

The final equations for transmembrane flow can be expressed as:

$$J_V = L_P S\left(\Delta P - \sigma_S RT\Delta c\right) \quad (43)$$

$$J_{iS} = J_V\left(1-\sigma_f\right)\overline{c_i} + PS\Delta c_i \quad (44)$$

where, J_V is the solvent flux and J_{iS} is the i^{th} solute flux relative to a fixed coordinate system.

There are four phenomenological constants in the system: hydraulic conductivity (L_p), osmotic reflection coefficient (σ_S), filtration reflection coefficient (σ_f) and permeability coefficient of the solutes (P). $\overline{c_i}$ is the average molar concentration of the particular solute in the electrode and can be mathematically expressed as the ratio of the difference in concentration (Δc_i) to the natural logarithm of the ratio of middle channel concentration to the outside channel concentration ($\ln(c_{im}/c_{io})$). This expression is valid for a dilute solution, which is one of the primary assumptions in the above formulation. It is also assumed that transport is at the steady-state.

Eqn. (43) is sometimes referred to as Starling's law of filtration. It states that the solvent flux is proportional to the driving force, given by the hydrostatic pressure difference minus the osmotic pressure difference. The proportionality constant is the hydraulic conductivity of the permeable electrode. In this equation, the value of σ_S varies between 0 and 1, depending on the properties of the solutes and the electrode. While a value of σ_S equal to zero means that the electrode does not retain the solute at all, a value of one implies that the electrode is impermeable to the corresponding solute particles. Please note that the concentration difference term in this equation is not for a particular solute as the net osmotic pressure difference is felt due to all the solutes present in the system.

The solute flux equation, better known as the Kedem-Katchalsky equation (Eqn. (44)), identifies that the solute flux has two distinct contributions. The first term on the RHS arises from the solute flux coupling with the solvent flux whereas the second term designates a diffusive flux term. The former is frequently referred to as the solvent drag term because it quantifies the amount of solute carried away from the electrode by the net solvent flux. In this equation, two more phenomenological constants are introduced, namely the filtration reflection coefficient σ_f and the permeability coefficient P. The filtration reflection coefficient is equal to 1 – f, where f is the retardation coefficient that characterizes the hindrance of convective transport of the solute across the electrode. The difference between σ_f and the previously mentioned σ_S is that the former is constant only for the particular solute under consideration while the latter remains the same for any solute that maintains the same level of osmotic pressure difference across the electrodes. However, when one is dealing with the same solutes, the two reflection coefficients become identical. Finally, the permeability coefficient P is defined as the effective diffusion coefficient (D_{eff}) of the solute in the porous structure per unit thickness.

From our above discussion, it is evident that the molecular properties of the solutes, especially size and charge, and the material parameters of carbon aerogel paper are of paramount importance in the determination of the phenomenological constants. The important material parameters for the electrode are its microstructure and the nature and distribution of charge throughout its volume. In this context, it is pertinent to mention that the Kedem-Katchalsky equation was originally developed to model the permeability of infinitesimal thin membranes to non-electrolytes. The problem of finite width membranes was first addressed by Patlak [60], who integrated the solute flux equations to obtain the following expression:

$$J_{iS} = J_V(1-\sigma_f)c_{im} + PS\Delta c_i \frac{Pe}{\exp(Pe)-1} \qquad (45)$$

where, $Pe = \frac{J_V(1-\sigma_f)}{PS}$.

The Peclet number provides an estimate of the relative importance of convection and diffusion across the electrodes. Please note that the convection mentioned here relates to the solvent drag term, not the axial convection in the channels. It has been observed that Eqn. (45) varies significantly from Eqn. (44) if the convection through the electrodes is larger than the diffusion across the electrodes. Since we are unaware about the scaling behavior of these two terms, we must employ the modified Kedem-Katchalsky equation to calculate the solute flux through the electrodes.

The second concern in adapting the Kedem-Katchalsky equation to our particular system is that we are inherently dealing with electrolyte media where ions abound, whereas the equation was formulated for non-electrolytes. In a subsequent paper [61], Kedem and Katchalsky had formulated equations for the permeation of ions through charged membranes. Based on the Teorell-Meyer-Sievers (TMS) model [62, 63] for the charged membranes, they were successful in relating the phenomenological constants to the ion concentration in electrolyte media and the charge density on the membrane. One would be tempted therefore to switch to this model that accounts for the electrical charge interactions between the ions and the charged membranes, or in this case, the porous electrodes. However, we must remind ourselves that during the discharging process the ions, which are detached from the EDL at any particular moment of time, do not feel any attraction to the electrode due to the decreasing charge on the latter. In other words, the ions that are still attached to the electrode shields any electrical charge interactions between the detached ions and the electrode. This is similar to the shielding of membrane charge by a large background of counter-ions such that the co-ions flow only by diffusion (and convection, if present in the system). The latter provides a classical example of the reduction of the governing

ambipolar diffusion equation in the TMS model to a simple co-ion diffusion equation. In our case, too, we can effectively ignore the charge interactions during the transport of detached ions through the electrode that has just sufficient number of charges to retain the attached ions in the EDL. As a consequence, we can retain the formulation for the permeation characteristics of non-electrolyte media and use Eqn. (43) and (45).

The final step that needs to be completed before we can incorporate the transmembrane flux equations (Eqn. (43) and 45)) into the boundary condition at the electrode surface (Eqn. (39d)) is the determination of the phenomenological constants for the solute-electrode combination in the considered case. The three constants that need to be determined are L_p, σ and P. It is to be noted that we have removed the subscript from the reflection coefficient. As we are interested in studying the transport characteristics of sodium and chloride ions which are nearly identical in size with respect to the much larger pores in the aerogel, the filtration reflection coefficient and the osmotic reflection coefficient assume identical values. One more important simplification can be made at this juncture by recalling that in our experiments, we used positive displacement pumps that supply fluid at a constant flow rate. Since in our PFD experiments we permeated all of the feed water through the porous electrodes, the value of J_V remained constant for the discharging phase. Evidently, this assumption is valid provided the maximum pressure that can be handled by the pump is significantly greater than the pressures in the channel setup. In our case, the peristaltic pump was able to feed water against a maximum pressure of 138 kPa which is larger than the 20-60 kPa pressures required to overcome the cumulative pressure drop in the channel and across the electrodes. In such a scenario, we can decouple the solute flux equation, Eqn. (45), from the solvent flux equation (Eqn. (43)). As a consequence, we can shift our focus to identifying the phenomenological constants relevant to the solute flux equation only, i.e. σ and P. In order to compute these constants, however, one must be able to characterize the electrode.

Carbon aerogels are three-dimensional dendritic structures formed by covalent bonding of nanometer sized particles [64]. On closer inspection, they seem to form foam like structures, consisting of a continuous solid phase with interconnected channels or isolated pores. One can also view fiber like strands running through the pores, as shown in Fig. 13 in the Chapter on Materials and Methods. In other words, one sheet of carbon aerogel paper is constituted by not one but several types of porous structures, such as the foam structure and the fiber matrix. This creates a problem as the determination of the phenomenological constants can proceed along two parallel paths, depending on whether we consider it a predominantly foam structure or a fiber matrix. One can also determine the desired coefficients for a composite material, which has the fiber matrix structure embedded in the foam structure. However, it turns out that such an involved calculation is not necessary because in typical manufacturing processes the fabricated carbon aerogel is seen to possess a macroporous network only [65]. The fibers that are observed in our sample were simply added to enhance the conductivity and stability of the manufactured sheet. Moreover, the proportion of fiber by weight in our sample was less than 20 percent [66]. Consequently, we will compute the reflection coefficient and the permeability of the aerogel sample, assuming that it is composed exclusively of the foam structure.

The next question that needs to be resolved is what percentage of the pores actually contributes to the transport of ions. A typical foam structure can consist of penetrable pores, which can be further classified into passing and nonpassing pores, and isolated pores. The passing pores are connected to two or more domains of the outer surface of the aerogel paper, whereas the nonpassing pores are connected to only one domain. In engineering applications, the former are frequently classified as through holes and the latter as blind holes. The isolated pores have no connections to any outer surface whatsoever. It is evident that only the passing pores contribute to the actual transport phenomena. Moreover, it is observed that the aerogel consists of both

micropores and mesopores. It is evident that the two different pore sizes will correspond to distinctly different values for the phenomenological constants. There is no easy solution to either of the issues. In our analysis, we assign a fudge factor to the total porosity value in order to establish the porosity due to the passing pores. This helps tackle the problem of computing the appropriate porosity for the transport phenomena. It should be noted that the isolated pores are not accessible to external solutes or solvents and thus do not crop up in our analysis for any of the determined porosities. The fudge factor helps resolve the porosity component due to passing pores from that due to nonpassing. To tackle the second problem of the pore size variation in the aerogel, we develop a weighted average of the phenomenological constants for the different pore sizes, as elaborated in the following paragraphs.

Before discussing the determination of the phenomenological constants, we must clearly define two quantities, porosity and partition coefficient. Porosity (ε) can be expressed as the ratio of the void volume to the total volume. Partition coefficient (Φ), the other important parameter in the ensuing analysis, is defined as the ratio of the available volume to the void volume. It must be noted that there are a number of scenarios wherein this ratio is smaller than one, i.e. the available volume is smaller than the void volume, such as when some of the void space is smaller than the solute molecules. Another important reason that the available volume for the solute molecules is typically smaller than the void volume is the finite distance between the solute center and the surface of the pore. The minimum separation distance is given by the radius of the solute molecule. However, this distance could be much larger depending on the charge interactions between the solid surface and the molecules itself.

$$\varepsilon = \frac{\text{void volume}}{\text{total volume}} \tag{46}$$

$$\Phi = \frac{\text{available volume}}{\text{void volume}} \tag{47}$$

$$\varepsilon_p = \xi\,\varepsilon \tag{48}$$

where ε_p is the porosity due to the passing component and ξ is the applied fudge factor.

For the sake of convenience, we will now model the carbon aerogel as a regular porous structure with a rectangular array of cylindrical pores, where porosity of the latter (ε_s) is equal to the porosity due to the passing component (ε_p) in the aerogel. One must point out that in switching from the aerogel to the regular porous structure we are neglecting the tortuosity parameter of the former, which is given by the ratio of the actual path length between two points on connected pores in the aerogel to the shortest geometrical distance between the two points. Substantial tortuosity of a porous media is manifested in the form of an additional hindrance to solute flux through the media. In other words, in neglecting this parameter, we run the risk of overestimating the permeability coefficient and underestimating the value of the reflection coefficient. For the regular porous media with uniformly distributed cylindrical pores, one can develop the following expressions for the porosity and the partition coefficient:

$$\varepsilon_s = \frac{\pi\left(\frac{d^2}{4}\right)LN}{AL} = \pi\left(\frac{d^2}{4}\right)\left(\frac{N}{A}\right) \tag{49}$$

where, L is the thickness of the porous structure and therefore the length of the cylindrical pores, d is the diameter of the pore, and N is the total number of pores present in the structure.

$$\Phi = \frac{\pi\left(\frac{d}{2}-\frac{b}{2}\right)^2 LN}{\pi\left(\frac{d^2}{4}\right)LN} = \left(1-\left(\frac{b}{d}\right)\right)^2 = (1-\lambda)^2 \quad (50)$$

where b is the radius of the solute molecule and λ is the ratio of solute radius to pore radius. Please note that we have neglected all charge interactions by the same rationale used earlier to argue the absence of electrical interactions between the detached ions and the aerogel electrode during the discharging phase.

At this juncture, we invoke the hindered transport theory, first proposed by Deen [67]. It has been shown that for convective-diffusive transport of solutes in a liquid filled pore of the porous structure, one can define two hydrodynamic resistance coefficients H and W, which are related to the pore diffusion coefficient and reflection coefficient in the following manner [67, 68]:

$$D_{eff,pore} = H D_\infty \quad (51)$$

$$\sigma_{pore} = 1 - W \quad (52)$$

where $D_{eff,pore}$ and σ_{pore} are the effective diffusion coefficient and the reflection coefficient for the single pore respectively. D_∞ is the standard diffusion coefficient of the solute in the liquid. H and W, which are functions of λ only, are given by:

$$H(\lambda) = \Phi\left(1 - 2.1044\lambda + 2.089\lambda^3 - 0.948\lambda^5\right) \quad (53)$$

$$W(\lambda) = \Phi(2-\Phi)\left(1 - \frac{2}{3}\lambda^2 - 0.163\lambda^3\right) \quad (54)$$

In this analysis, solute-solute and electrical charge interactions are neglected and it is assumed that the solute concentration at the pore entrance is uniform. This analysis has been found to be predictive of the real transport phenomena provided $\lambda<0.4$. For our solute-electrode pair, this criterion is well satisfied since the sodium and chloride ions are in the range of 0.18 and 0.1 nm respectively and the smallest pore size is around 1 nm.

The single pore coefficients can then be related to the overall permeability and reflection coefficient of the porous structure by the following equations:

$$P = \frac{H D_\infty \Phi \varepsilon_s}{L} \quad (55)$$

$$\sigma = 1 - W\Phi \quad (56)$$

In the particular case under consideration, the values for the different parameters are tabulated below:

$$P = 2.38\times10^{-3} \text{ mm/s} \quad (57a)$$

$$\sigma = 0.27 \quad (57b)$$

To wrap up this section, we summarize the method of analysis employed for the permeating flow discharge scheme. Eqn. (36) and (37) provide us with the velocity distribution in the channel in the presence of permeating flow. These can be plugged into the governing equation for the system, Eqn. (38), which can be solved by using a finite difference approach as outlined in the next section. The four boundary conditions to the unsteady convection-diffusion equation are obtained from Eqn. (39a) – (39d). Eqn. (39d), however, has a permeating flux term which needs

to be calculated separately with the help of the modified Kedem-Katchalsky equation, Eqn. (45). The phenomenological constants needed for the latter equation are computed using the hindered transport theory, Eqn. (53) – (57). Once the governing equation is solved, the mass of ions removed can then be calculated by employing the following equation:

$$(m_i)_{(t\to t+\Delta t)} = \int_t^{t+\Delta t}\int_0^{2h} c_i(L,y,t)\, v_x(y)\, dy\, dt + \int_t^{t+\Delta t} J_{iS}\, dt \qquad (58)$$

The first term on the RHS gives the convection-diffusion contribution while the second term computes the mass of ions removed by the permeating flow. In the limiting case when all the water is permeated through the electrodes, the first term becomes identically zero. For all cases, the net mass of ions removed can be determined by summing the masses removed for the sodium and chloride ions.

5. (d) Solution procedure

The governing concentration equations for the AFD and PFD schemes, given by Eqn. (20) (or Eqn. (24)) and Eqn. (38) respectively, are solved using the finite difference method. The physical domain is discretized into computational meshes with Δx and Δy intervals along the X and Y axes respectively. The time domain is also discretized into suitably large number of Δt intervals. Finer discretization yields better results but at the cost of computational space and time. For a number of solution methodologies including ours, discretization is not only a determining factor in the trade-off between accuracy and cost but, more importantly, a decisive influence in ensuring stability in the numerical solution.

As with any convection-diffusion problem, the governing equations posed in our analysis are parabolic partial differential equations (PDE). The speed of physical information propagation, associated with a parabolic PDE, is infinite which means that the solution at each point is affected by the solution at all other points in the physical domain at all times preceding and including the current time instant. The solution at that point, in turn, affects the solutions at every other point at all times after and including the current time. Since the domain of dependence is the finite region in front of and including the current time instant, the problem to be solved is a propagation problem and must be solved using marching methods. The Forward-Time Centered-Space (FTCS) method was employed to reduce the governing equations to algebraic equations. This is an explicit scheme, which has the following characteristics: forward in time, centered in convection and centered in diffusion. For example, the governing equation for the AFD scheme, Eqn. (20), can be restated as a FDE in the following fashion:

$$\frac{\partial c}{\partial t} + v_x \frac{\partial c}{\partial x} = D\frac{\partial^2 c}{\partial y^2}$$ (AFD governing equation written without the subscript for the i^{th} species)

$$\frac{c_{i,j}^{n+1} - c_{i,j}^{n}}{\Delta t} + v_x \frac{c_{i+1,j}^{n} - c_{i-1,j}^{n}}{2\Delta x} = D\frac{c_{i,j+1}^{n} - 2c_{i,j}^{n} + c_{i,j-1}^{n}}{\Delta y^2} \qquad (59)$$

where i, j and n are the grid point values in x, y and t respectively. Solving for $c_{i,j}^{n+1}$, we get:

$$c_{i,j}^{n+1} = c_{i,j}^{n} - \frac{c}{2}\left(c_{i+1,j}^{n} - c_{i-1,j}^{n}\right) + d\left(c_{i,j+1}^{n} - 2c_{i,j}^{n} + c_{i,j-1}^{n}\right) \qquad (60)$$

where, $c = \frac{v_x \Delta t}{\Delta x}$ gives the convection number and $d = \frac{D\Delta t}{\Delta y^2}$ gives the diffusion number.

As is evident from the above set of equations the finite difference equation derived using the FTCS method is $O(\Delta t) + O(\Delta x^2) + O(\Delta y^2)$, i.e. of order one in time and two in each of the spatial

coordinates. One could as well employ an implicit method, such as the Crank-Nicholson method, to solve the governing equations. However, the explicit FDE obtained in Eqn. (60) is clearly easier to evaluate numerically as one does not have to go through an additional set of matrix operations to obtain the values of the concentration at every point for all instants in time. Nevertheless, there is one major problem that is commonly associated with an explicit FDE and that is the question of stability. The information propagation speed for an explicit scheme is finite which is not consistent with the infinite speed of physical information propagation of the original parabolic PDE. Fortunately, only a very small amount of information is propagated at the infinite speed and the major chunk of the signal travels at a finite speed. The explicit FDE provides a close approximation to the latter provided certain criteria relating the interval sizes are met. These are called stability criteria. For a convection-diffusion equation, the stability criteria [69] can be stated as follows:

Convection number $c \leq 1$ and diffusion number $d \leq 1/2$.

$$\text{i.e. } \frac{v_x \Delta t}{\Delta x} \leq 1 \quad \text{and} \quad \frac{D \Delta t}{\Delta y^2} \leq \frac{1}{2} \tag{61}$$

Our computational meshes are discretized with $\Delta t = 0.1$s, $\Delta x = 10$ mm, $\Delta y = 0.2$ mm. v_x and D are of the order of 0.5 mm/s and 10^{-3} mm^2/s. Given these values, one can compute the resultant values of c ($5\ 10^{-3}$) and d ($2.5\ 10^{-3}$). Thus, even with large variations from the nominal values of the axial flow velocity we are in perfect shape to satisfy the stability criteria. Since one would expect relatively less variations along the flow direction, the relatively large discretization interval along the x-axis is acceptable. Further decrease in the interval along the x-axis also uses up a lot of memory space and the CAS (computer algebra simulation) software, MATLAB, used for our calculations starts to complain!

Before rounding up the discussion on the solution procedure, we must make a few comments on the boundary conditions and their effect on the corresponding FDE. Our boundary conditions in x and t specified the values of the concentration function at the respective boundaries (spatial boundary for x and temporal boundary for t). These boundary conditions, also known as Dirichlet BC, pose no problems to the formulation. The two boundary conditions in y, however, could cause some concerns, primarily because they have a specified derivative at the domain boundaries. For example, in the AFD case, Eqn (25c) provided the following BC at y = h:

$$\left(\frac{\partial c}{\partial y}\right)_{y=h} = 0$$

where the subscript i for the concentration function (denoting the i^{th} species) has been dropped. The governing FDE for the AFD case is given by Eqn. (60):

$$c_{i,j}^{n+1} = c_{i,j}^{n} - \frac{c}{2}\left(c_{i+1,j}^{n} - c_{i-1,j}^{n}\right) + d\left(c_{i,j+1}^{n} - 2c_{i,j}^{n} + c_{i,j-1}^{n}\right)$$

However, we are unable to compute the above equation for a grid point on the stated boundary because the third last term on the RHS is not defined. In other words, no grid point exists for j+1 along the Y-axis when j itself is located on the upper limit of y. In this scenario, one can introduce the FDE for Eqn.(25c) to resolve the seemingly problematic issue.

$$\left(c_y\right)_{i,j}^{n} = \frac{c_{i,j+1}^{n} - c_{i,j-1}^{n}}{2\Delta y} \tag{62}$$

where the LHS represents the first derivative of the concentration with respect to y, correct to 2^{nd} order. This can be obtained by writing the Taylor's series for the first derivative and truncating higher order terms.

Rewriting Eqn. (62) to obtain an expression for the concentration function at grid point j+1 along the Y-axis, we have:

$$c^{n}_{i,j+1} = c^{n}_{i,j-1} + 2\left(c_y\right)^{n}_{i,j}\,\Delta y \tag{63}$$

Substituting this into Eqn. (60), we can now obtain the following equation:

$$c^{n+1}_{i,j} = c^{n}_{i,j} - \frac{c}{2}\left(c^{n}_{i+1,j} - c^{n}_{i-1,j}\right) + d\left(c^{n}_{i,j-1} + 2\left(c_y\right)^{n}_{i,j}\,\Delta y - 2c^{n}_{i,j} + c^{n}_{i,j-1}\right) \tag{64}$$

This equation can now be solved for a grid point situated on the boundary y = h. Similar modifications are necessary for the PFD case as well.

Chapter 6: Results and Discussion

6. (a) Charging process

The charging experiments were performed in the no-flow state, as discussed in Chapter 4, so as to enable us to obtain the maximum possible desalination for the volume of water pumped into the channel before the start of the charging phase. Given the no-flow constraint, the main sources of meaningful information are the current characteristic graphs obtained during this period.

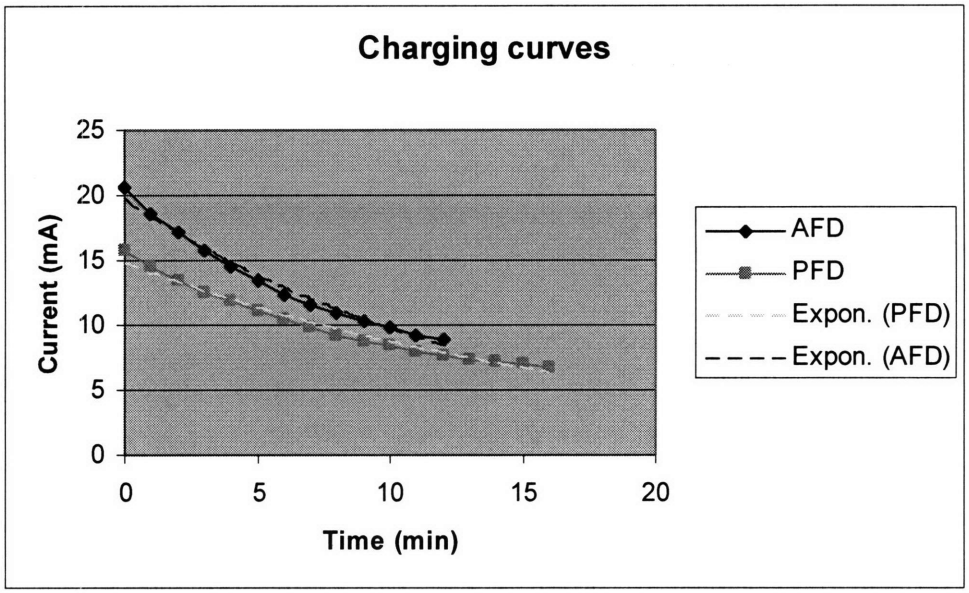

Fig. 20: Plot of current versus time obtained during the charging experiments for AFD and PFD setups. The solid lines connect the experimentally obtained data points. The dashed lines are the best fit exponential curves through these data points.

Fig. 20 reveals that the current characteristic graphs obtained using the AFD and PFD setup closely follow the classical exponential profile associated with charging of capacitors. The exponential profiles, given by the black (AFD) and green (PFD), are described by the following equation:

$$I = I_0 \exp\left(-\frac{t}{\tau}\right) \qquad (65)$$

where, $I_0 = 19.6$ mA and $\tau = 14.16$ min (for the AFD setup),
$I_0 = 14.7$ mA and $\tau = 18.9$ min (for the PFD setup).
The above curves were obtained when the setups were connected to a 1.23 V battery for 12 min (AFD) and 16 min (PFD) respectively. The charging phase was stopped when the potential difference across the carbon aerogel electrodes reached 430 mV.

We observe that the set of graphs for the AFD and PFD setups differed in their initial values as also in their rate of decline, i.e. in their time constants. This is possibly due to the switch from the single channel setup used for the AFD scheme to the three channel setup used to implement the PFD scheme. The above set of graphs seems to imply that the effective resistance is likely to be larger for the three-channel PFD setup. This could explain the drop in the initial charging current and the increment in the circuit time constant. As the solid phase (carbon aerogel) resistance is much smaller than the solution (saline water) resistance and as one would expect greater

penetration of the solution into the pores of the aerogel for the three channel setup, it would seem reasonable that the resistance in the PFD setup would be greater. An argument along similar lines can be constructed using the Newman model [51] or the De Levie model [70] for the porous electrode, where the active layer thickness increases due to greater penetration into the electrode for the PFD setup.

We also measured the difference in concentration before and after charging for the saline water fed into the channel. The measured concentration difference for the water in the AFD setup had a mean value of 35 ppm, with a standard deviation of 8 ppm. One can also compute this concentration difference by determining the mass of ions removed from the current characteristic curves in Fig. 20. It is found that the calculations based on the current versus time plots predict a concentration difference for 35.8 ppm for the AFD setup and 35.82 ppm for the PFD setup, given that the setups deionized a total volume of 160 ml. The actual volume of water withdrawn from the channel was 161 ml. As is evident from the above set of numbers, the experimentally measured concentration difference agrees excellently with the theoretically predicted concentration difference based on the charging current characteristic graphs.

Although Fig. 20 provides us with a reference point for the charging process discussions, it does not provide any significant input for the final computation of water recovery ratio and throughput. The first step towards quantification of these two performance metrics is the determination of the permissible charging time value. In other words, we need to compute the amount of time for which a charging process can be permitted to continue before the deionization system is rendered ineffective due to sufficient saturation of the electrodes. To do this, we employ Eqn. (16) of Section 5(a).

$$t_{critical} = \tau\left[10.5 - \ln\left(\frac{Q\cdot\left(c_{input} - c_{perm}\right)}{I_0}\right)\right].$$

This equation is also used to plot $t_{critical}$ versus flow rate (Q) graphs for different values of c_{perm}.

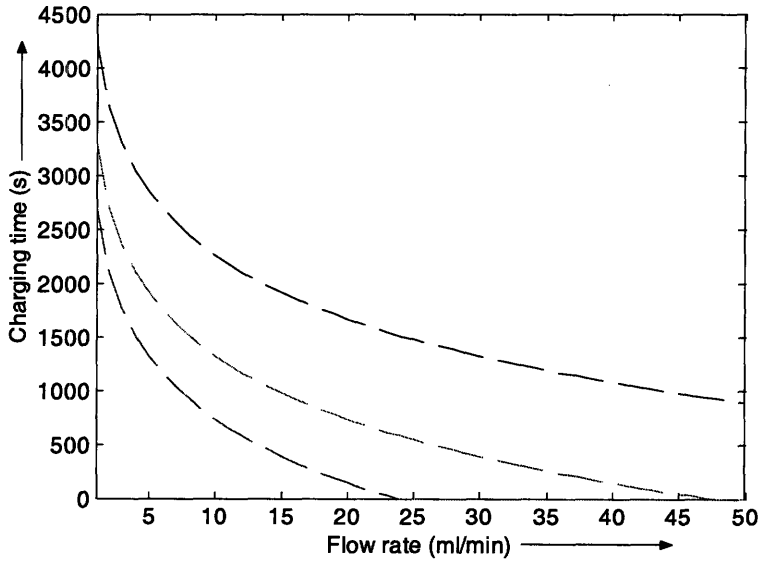

Fig. 21: Plot of permissible charging time versus flow rate for different values of permissible output concentration. The blue line, red line and black lines map the expected charging times for c_{perm} equal to 30 ppm, 15 ppm, and 5 ppm below the input concentration respectively. Charging current parameters employed: I_0 = 19.6 mA and τ = 14.16 min.

Since the current characteristic curves show similar profiles for both AFD and PFD (with slightly different values), we have drawn Fig. 21 as a master plot for the dependency of permissible charging time on the flow rate and permissible product water concentration for both AFD and PFD processes. We have used the charging current parameters obtained in our AFD experiment. However, one could just as well use the parameters obtained in our PFD charging experiment or any other set of current parameters for that matter.

The notable feature of Fig. 21 is the expected drop in permissible charging time with increase in flow rate and with decrease of permissible product water concentration. In other words, if one is pumping at a higher flow rate, less number of ions will be removed by the deionization system, relative to the number of ions being pumped, resulting in a shorter time interval for which the charging process can be fruitfully employed per cycle. Similarly, if the permissible value of product water concentration is very low, more deionization would be needed for the same input water. In such a scenario even with very little saturation of the electrodes, the deionization system might not be effective enough to carry on the charging process. This is reflected in the significant decrease in permissible charging time for any flow rate at different values of permissible product water concentration. For example, if one would like to have at least 30 ppm deionization at a flow rate of 10 ml/min, one can charge for only 600 seconds. On the other hand, if one can tolerate product water only 5 ppm below the feed water concentration, one can charge for 2200 seconds - nearly four times as long as in the previous case, given the same flow rate and charging current parameters. Obviously, if the charging current itself rises, signaling increased deionization of saline water, then the permissible charging time would need to be re-estimated. It is also critical to recognize that the charging current in the circuit is decoupled from the flow rate, as long as the number of ions in the channel is not small enough that the charging current is limited by it. The current, under normal operating conditions, depends on the resistance of the solution, which is determined by the concentration of the water in the channel.

6. (b) Axial Flow Discharging process

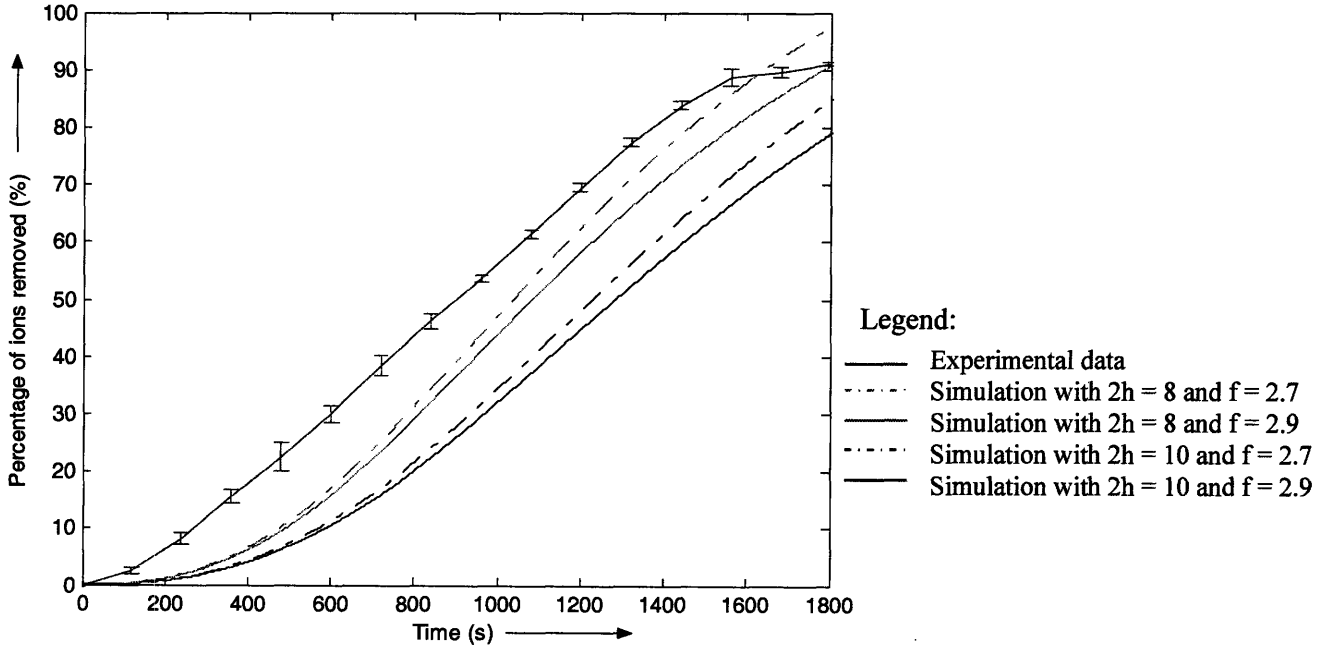

Fig. 22: Plot of percentage of ions removed as a function of time for the AFD process at a prescribed flow rate of 16 ml/min. In the legend, 2h refers to distance between the aerogel electrodes and f is the effective electrode volume, $V\varphi$.

Fig. 22 compares the numerical results with the experimental observations for the axial flow discharging process. The percentage of ions removed was calculated by converting the ratio of the mass of ions removed at any instant of time to the total mass of ions detached from the paper in three time constants to a percentage value. It is notable that in three time constants a capacitor should discharge about 95 percent of its accumulated charges. The first striking feature of the set of curves in Fig. 22 is the approximate S-shaped profile each one exhibits. On closer inspection, this is not at all different from the expected shape as the AFD process is convection-diffusion dominated and almost any diffusion process displays this kind of mass transfer characteristics as a function of time.

The initial progress is fairly slow because the diffusion phenomenon needs a certain amount of time to transfer the detached ions from the surface of the porous electrode to the bulk of the channel. This phenomenon is often referred to as the characteristic time lag for a diffusion process. Moreover, the axial flow velocity is maximum at the channel center and zero at the electrode surfaces. As a result, the convection process cannot flush out the ions till the diffusion process is able to transfer ions from the electrode surface towards the bulk. Furthermore, the initial concentration of detached ions at the aerogel surface is not very high, which means that there is no overpowering concentration gradient to accelerate the diffusion process. The electrode surface concentration rapidly picks up creating a sufficiently high concentration gradient in the lateral direction. As a consequence, the process speeds up because diffusion is able to transfer ions to the bulk, on time scales longer than the lag time, and the convective flow is able to carry away the ions that have moved away from the electrode surface. On even longer time scales, after about 1400 seconds as observed from Fig. 22, the process slows down as most of the detached ions have already been removed. The discharging current has dropped down appreciably, by this point of time, thereby releasing lesser number of detached ions into the setup. The latter implies that the concentration gradient in the lateral direction has decreased significantly, thereby hindering the diffusion process. For the AFD discharging process, our time constant, as measured from the corresponding current characteristics graph shown below in Fig. 23, was 650 seconds. After 1400 seconds, therefore the circuit has already discharged close to 87 percent of all the ions, which it had initially removed from the saline water during the charging process.

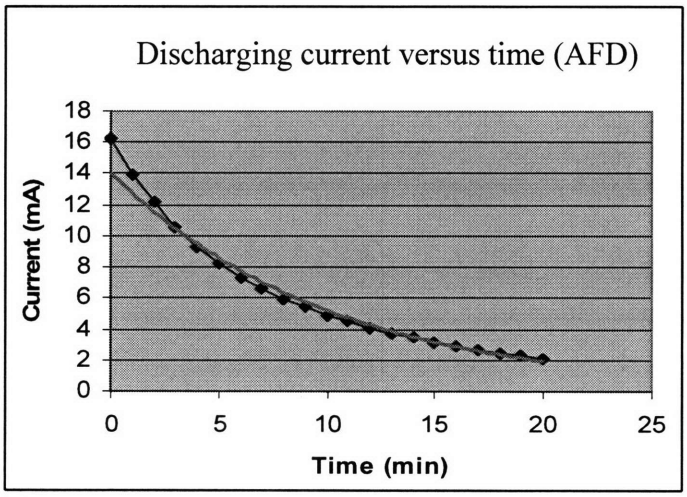

Fig. 23: Plot of discharging current versus time for the AFD setup. The blue line connects the experimental data points and the red line gives the best fit exponential through the set of data points. For the exponential curve, $I_0 = 13.39$ mA and $\tau = 10.82$ min.

One also notices from Fig. 22 that the theoretical predictions underestimate the experimental results by about 20-30 percent in the initial stages. The difference drops to around 5 percent on longer time scales. The latter can be explained in terms of resolution issues and metrological errors, coupled with concerns about the fact that a certain number of ions may have been present in the system before the charging phase even started. However, the percentage error on shorter time scales is too large to explain with the above rationale. It would seem that there is a systematic source of error in the formulation or in the experimental observations. One of the possible causes of this error is that in our theoretical formulation, we used the best fit exponential of Fig. 23 to quantify the number of ions detached at the electrode surface. Although the best fit profile provides an excellent match with the experimental observations on time scales larger than 4 min, it underestimates the observed current values by about 15 percent in the initial stages. In other words, in our formulation the number of ions detached from the paper is underestimated by about 15 percent in time scales shorter than 240 seconds. This leads to a substantial difference between the predicted value of mass of ions removed and the experimentally observed quantity in the stated time scales.

Finally, one observes that there is a significant dependence of the AFD process on the geometrical parameters, such as the width of the channel and the effective electrode volume. As we had discussed in Chapter 4, we introduce this variability in our simulations because it is difficult to estimate the exact distance between the aerogel electrodes as well as the precise volume of the aerogel electrode. One finds that introduction of this variability does not change the basic shape of the curves. The changes in the absolute values of the theoretical predictions at each instant of time are expected as the convection-diffusion phenomenon is very much dependent on the characteristic geometrical scales inside the channel as well as on the concentration values at the electrode. It is evident that the diffusion process would be slower over longer length scales (i.e. when $2h = 10$ mm) than it would be over shorter length scales (i.e. when $2h = 8$ mm). This explains the hike in the absolute values of the mass transfer when one moves from the 10 mm width to the 8 mm width channel. It is also in line with the current reasoning in CDI technologies of having extremely thin channels, which also expedites the charging process. The relationship between the percentage of ions removed and the effective electrode volume can be explained in the following manner. The concentration at the surface of the electrode is smaller when one has a larger effective electrode volume, e.g. $f = 2.9$, than when it has a smaller electrode volume, e.g. $f = 2.7$, because the number of ions detached from the aerogel remains constant in either case. The smaller concentration value at the electrode slows the diffusion process because of the corresponding drop in the net concentration gradient along the Y-direction. This relationship is reflected in the smaller absolute values on the solid lines than on the dashed lines, for any value of the distance between the aerogel electrodes (2h) (Fig. 22).

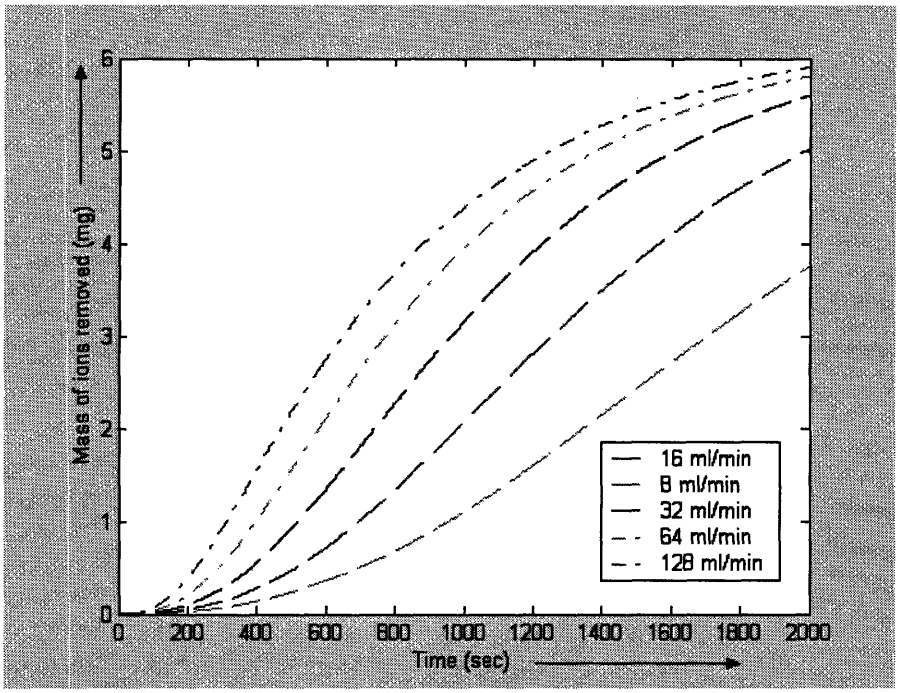

Fig. 24: Plot of mass of ion removal as a function of time for different flow rates of the AFD process.

Fig. 24 shows the variation in the mass of ions removed from the system for different flow rates. It can be seen that the characteristic lag time exists at all flow rates although it decreases appreciably for higher flow rates. The curve showing the number of ions detached from the aerogel electrode gives the upper bound on the mass transfer possible at any flow rate (and for that by any mass transfer process). Since the discharging phase is a two step process where the first step is the detachment of ions from the EDL, the number of ions that are removed from the system can never surpass the number of ions detached from the EDL. The former is calculated from the discharging current curve of Fig. 23. Lastly, we need to point out that while it is obvious that a higher flow rate does a better job of flushing out the ions at a faster pace, it tends to prove costly in terms of the amount of water used just to remove the saturating ions from the system. In other words, even if the time taken for a particular flow rate is relatively small, its higher flow rate might render it ineffective because of the net water recovery ratio of the process. We will deliberate more on this point when we analyze and compare the performance metrics of the AFD and PFD processes.

6. (c) Permeating Flow Discharging process

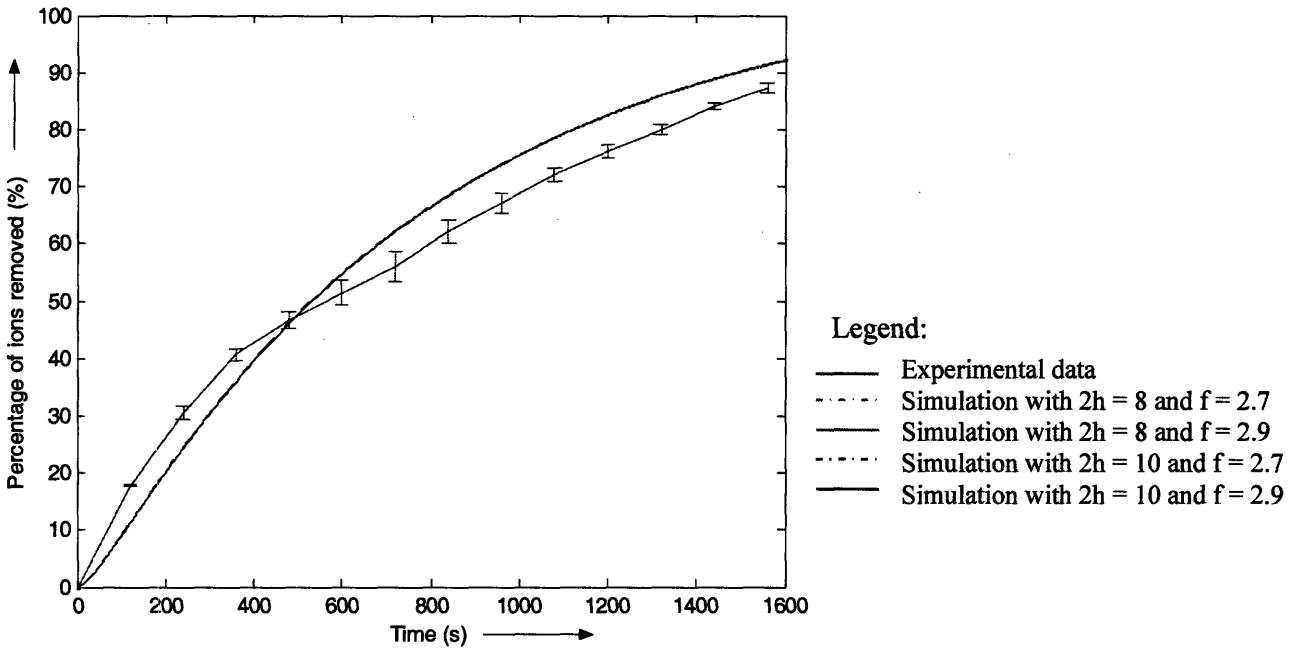

Fig. 25: Plot of percentage of ions removed as a function of time for the PFD process at a flow rate of 16 ml/min. In the legend, 2h refers to distance between the aerogel electrodes and f is the effective electrode volume, $V\varphi$. The percentage of ions removed was calculated as the number of ions removed at any instant of time divided by the total mass of ions detached from the paper in three time constants (multiplied by 100 to convert to a percentage).

Fig. 25 shows the percentage of ions removed by the permeating flow discharge process as a function of time. Before we proceed further, it must be stated that for our experiments as well as in our simulations, we considered the middle channel valve to be completely closed. This forced all the water to permeate through the aerogel electrodes. In some sense, therefore, it would be fair to call this the opposite end of the spectrum with respect to the AFD process. If the middle channel valve was only partially closed one could obtain a mixture of middle channel outlet and permeating flow which would represent some zone in the middle of the spectrum, to extend the previous analogy. Another point that needs clarification is the choice of the Y-axis not only in Fig. 25, but also in subsequent PFD process graphs. The percentage value is chosen as a more appropriate representation of the trend rather than the absolute value which could be misleading as one moves from the AFD to the PFD process, because the charging processes yields different number of adsorbed ions in the two distinct setups. In other words, the Y-axis value is a normalized value, where the normalization factor is the number of ions released in three time constants (~95% of total ions adsorbed in the setup).

The first thing we notice in Fig. 25 is the distinctly different shape of the percentage of ions removed plot obtained for the PFD process as compared to that obtained for the AFD process in Fig. 22. It spells out the obvious difference in the underlying physics of the two discharging processes. No characteristic lag can be observed in either the experimental plots or the theoretical predictions. The permeating flow discharge process removes the ions through the porous electrodes in two different ways, as discussed in Section 5(c). The first contribution comes from the solvent drag term, where the amount of ion removal is directly proportional to the

concentration on the electrode surface as per the modified Kedem-Katchalsky equation (Eqn. (45)). The second contribution is from the diffusive flux that arises due to the concentration difference across the electrodes. The lack of the characteristic lag time is because both the solvent drag and diffusion across the electrode respond to the build-up of concentration at the electrode surface. The profile here mirrors the plot of cumulative ions detached from the EDL of the aerogel electrode versus time. Depending on the concentration at the electrode, the solvent is able to drag a proportional number of ions along with the flow. Thus, there is no lag or build-up time for highest removal rate. In this case, the highest removal rate occurs when the concentration at the electrode is the highest which is, loosely speaking, when the current is maximum. Moreover, once the electrode has been crossed the ion can be considered to having been removed from the system, which is in sharp contrast to the AFD process where the diffusion was an intermediate pathway before the ion was finally flushed out by the convective flow. It is to be noted that in this regard, the solvent drag term is much more effective as it is proportional to the concentration at the electrode surface unlike the diffusive flux term which varies linearly with the difference in concentration across the electrode.

The Peclet number defined for the permeating flow gives the relative magnitude of these two contributions. For our system, if one were to consider that the outer channel concentration was significantly lower than the concentration at the electrode surface, the solvent drag term was about twice as important as the diffusive flux term for a flow rate of 16 ml/min. The importance of the solvent drag term increases linearly with the flow rate and one can visualize that at flow rates exceeding 50 ml/min in our setup the solvent drag term dominates the permeating flow process. Furthermore, the value of permeability used in our calculations is slightly higher than the typical permeability values used for similar biological membranes. Even though our theoretical predictions give a good match with the experimental observations, it is evident that if the permeability value is lower the significance of the diffusive flux term decreases even further.

It is observed, from Fig. 25, that the match between the theoretical predictions and the experimental observations is much better over the entire range for the PFD process than it was for the AFD process. Nevertheless, the theoretical predictions below 500 seconds underestimate the experimental results by about 5 percent. Subsequently, however, they are seen to overestimate the percentage of ions removed from the system. The underestimate in the initial stages can be rationalized by the same arguments made for the AFD case. This becomes more evident from Fig. 26, where one can clearly say that the best fit exponential predicts substantially lower currents (and therefore number of ions detached from the EDL) than observed experimentally in the initial stages, i.e. from the 0 to 5 min mark.

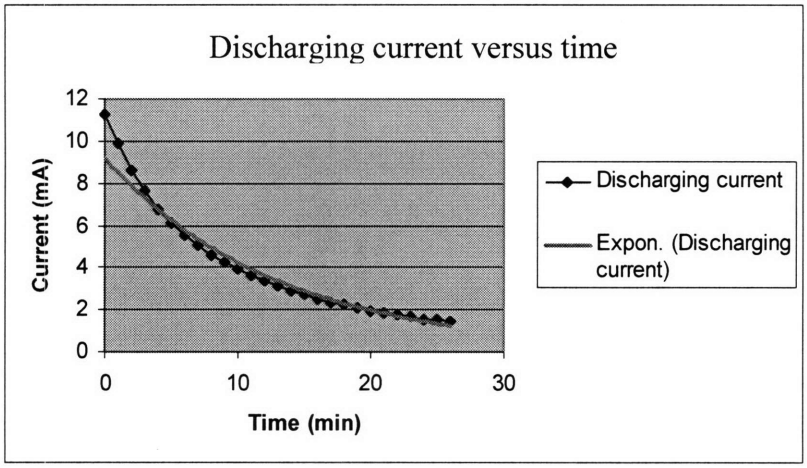

Fig. 26: Plot of discharging current versus time for the PFD setup. The blue line connects the experimental data points and the red line gives the best fit exponential through the set of data points. For the exponential curve, $I_0 = 9.20$ mA and $\tau = 12.98$ min.

It is worth mentioning, at this juncture, that the current versus time graphs for the charging process (Fig. 20) and the discharging process (Fig. 23 and Fig. 26) in the two setups – single channel AFD setup and three channel PFD setup – show a regular pattern. The currents in the circuit are the effective measures of ion attachment and detachment from the EDL in the electrode. By its very nature, the ion attachment/detachment process is independent of any ion transfer process. It only depends on the voltage and the resistance associated with the external circuit as well as within the electrochemical setup itself. Therefore, it is not entirely unexpected to observe that the AFD setup for both charging and discharging yields higher initial currents and smaller time constants than the PFD setup. Since the voltage for the charging case (the 1.23 V battery) and the discharging case (0V in the external circuit, 430 mV across the capacitor electrodes) remained the same, the resistance in the circuit must have been higher for the PFD setup than for the AFD setup, as discussed earlier in Section 6 (a). Fig. 23 and Fig. 26 thus only serve to reinforce the notion that there is a definite rise in resistance due to more penetration of the fluid into the pores.

The last notable feature of the mass transfer plot of Fig. 25 is that, unlike the AFD case, the process is very weakly dependent, if at all, on the geometrical parameters. In other words, the exact distance between the electrodes does not significantly impact the process neither does the effective electrode volume. The reason for the former is obvious. The PFD process is focused on the permeation velocity at the surface of the electrode and the concentration therein and therefore is not affected at all by the distance between the electrodes. This is very beneficial and one can envisage a system where the distance between the electrodes is not limited by the discharging process characteristics. The lack of dependency on the effective electrode volume is slightly harder to fathom. It seems contradictory at first glance to what we stated a few lines back, i.e. the solvent drag term and the diffusive flux term is directly proportional to the concentration and concentration difference at the electrode respectively. However, if the ions are removed almost as soon as they are generated (i.e. detached from the EDL in the electrode), the dependency on the actual concentration at the electrode ceases to exist. In other words, if the number of ions generated is not high enough such that there is substantial accumulation at the electrode at any instant in time, the precise concentration at the electrodes do not have a significant impact on the final outcome, i.e. the removal of the ions detached at that instant by the permeating flow. This assumption is severely restrictive and implies that the PFD process is almost completely efficient

in removing ions as soon as they are detached from the EDL, especially on smaller time scales when the ions can accumulate at the electrode very rapidly. However, if this reasoning is indeed correct then it implies that the PFD process is much superior in removing ions, especially over smaller time scales. This will form the focal point of our discussion in the coming section.

Fig. 27 and 28 below represent the important dependencies, or the lack thereof, of the mass transfer characteristics of the permeating flow discharge process on flow rate and porosity values of the material of the electrode. It is seen that there is negligible variation with change in flow rate. This can be explained in the following fashion. The higher flow rates remove somewhat more ions in the beginning. However as the concentration at the electrode drops off due to the larger number of ions removed, the number of ions removed per unit time reduces for the higher flow rates. This allows the lower flow rates to play catch up with the mass transfer characteristics. Moreover, as discussed previously, the permeability value in our case has a slightly higher value than usual which indicates a larger contribution from the diffusion across the electrodes. Most importantly, however, this result is consistent with the above hypothesis that the ions are removed almost as soon as they are released from the EDL and in essence, the detachment of ions is the restrictive term. Although it is beyond the scope of our study here, it can be proven that this is the case by computing the Damköhler number. The dependency on porosity values, shown in Fig. 28, is expected because the porosity values affect both the permeability and reflection coefficient of the porous media (Eqn. (55) and (56)).

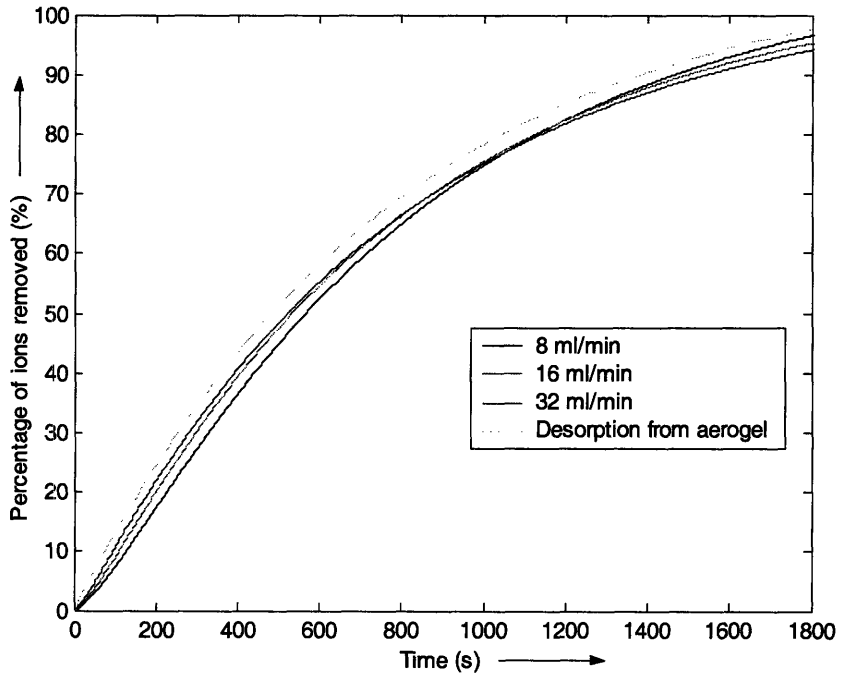

Fig. 27: Plot of percentage of ion removal as a function of time for different flow rates of the PFD process.

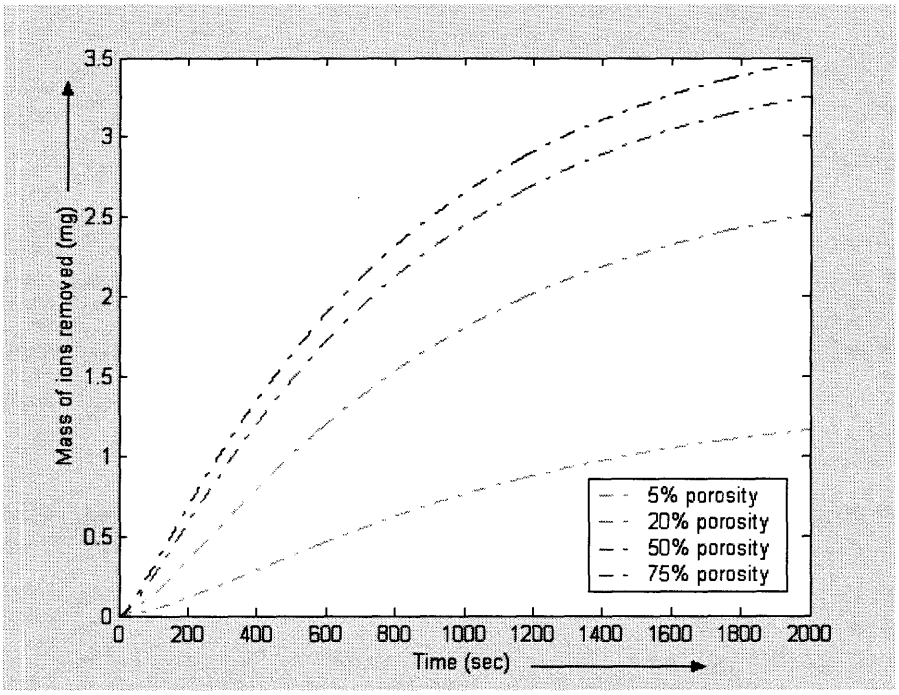

Fig. 28: Plot of mass of ion removal as a function of time for different porosity values for a PFD process employing flow rate of 16 ml/min.

6. (d) Comparison of performance metrics

In this section, we analyze the raw data collected from our experiments and the numerical predictions from our theoretical models. This leads to the computation of the performance metrics of the capacitive deionization process employing the axial flow discharge and permeating flow discharge schemes respectively, which can then be compared and contrasted quantitatively.

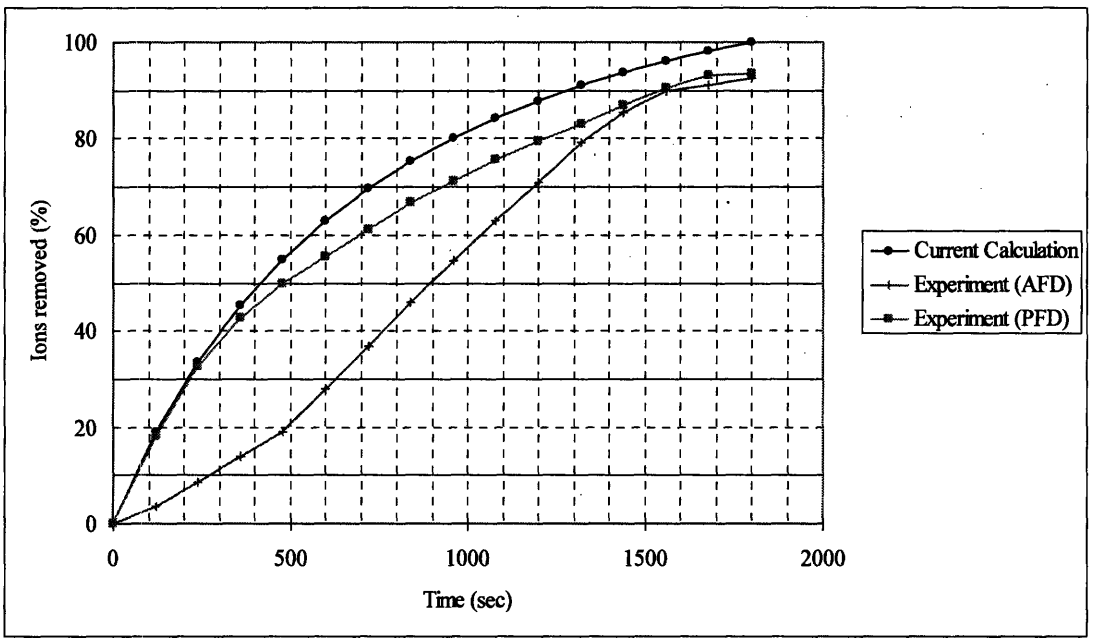

Fig. 29: Plot of percentage ion removal as a function of time for the AFD and PFD process. The topmost curve quantifies the percentage of ions detached from the electrical double layer of the capacitive electrodes.

Fig. 29 is an amalgamation of the experimental results presented in Fig. 22 (AFD) and Fig. 25 (PFD) respectively. It reveals two distinct patterns. Firstly, the topmost curve which is obtained from the experimental current calculations forms the strict upper bound to the process. In other words, our use of the two step heterogeneous reaction concept is validated. Secondly, the distinctive shapes of the AFD and PFD curves for the ion removal rate reveal that over time scales in the range of 400-800 seconds, there is a significant difference in the ion removal capability of the two processes. Over time scales longer than that the two mass transfer processes seem to merge. The reasons for these have been extensively addressed in our previous discussions. The questions we wish to answer, at this juncture, are the following:

(a) Does the distinctive shape of the curves afford any benefit in terms of the overall performance parameters?

(b) Does the time scale of 400-800 seconds have any relevance to any intrinsic time scale that can be defined for the system?

We will tackle the second question first before proceeding to discuss the relationship of the ion removal rates with the performance metrics. As revealed in Fig. 23 and Fig. 26, the time constants for the discharging circuit are in the range of 10-13 minutes, i.e. 600 – 780 seconds. We know that for the discharging of a capacitor, one time constant signifies the removal of approximately 63 percent of the initial charges on the electrodes. We can therefore state that the performance of PFD is significantly better than AFD in a time scale bordering the time constant of the

discharging circuit. This makes sense physically too, because the PFD process is fast enough to remove the ions detached during the shorter time scales, but on longer time scales due to the fall of the discharging current and the speeding up of the convection-diffusion phenomena the disparity disappears. On the shorter time scales, one can also observe that our hypothesis regarding the rapid pace of the PFD process is correct. We observe that very few ions accumulate in the porous electrode and its neighborhood as the bulk of the ions are removed as soon as they are detached from the EDL of the electrodes. This justifies the relative independence of the ion removal rate from the effective electrode volume.

The answer to the first question posed above, that is the possible benefit of the PFD process relative to the AFD process, is embedded in Fig. 29 itself. However, in order to present the information in a readily recognizable fashion we combine the theoretical predictions of the charging time (Fig. 21) and the discharging time (Fig. 22 and Fig. 25). The latter is correlated to the percent of ion removal from the system, e.g. to remove 50% of the ions from the system we need 500 seconds for the PFD process or 900 seconds for the AFD process. Thus we formulate our performance metrics, i.e. water recovery ratio and throughput as functions of discharge percentages. We must stress that a lower discharge percentage means that the charging process is able to only partially utilize the aerogel paper, e.g. if we only discharge up to 40% of the total ions, the charging can take place from 60% to the point where the current falls low enough indicating insufficient deionization from the system. In other words, permissible charging time is reduced because we do not start at zero percent charge in every case but from the point designated by the 100-discharge percent term. This implies that there will be a reduction in the throughput obtained during the charging process per cycle. However, reducing the discharge percent will increase the number of cycles that one can operate in a day. Moreover, if the water recovery ratio increases as well, the net effect of the increased water recovery ratio and number of cycles will outweigh the impact of smaller throughput per cycle. What we need to quantify is how much the water recovery ratio changes as a function of the discharge percentage.

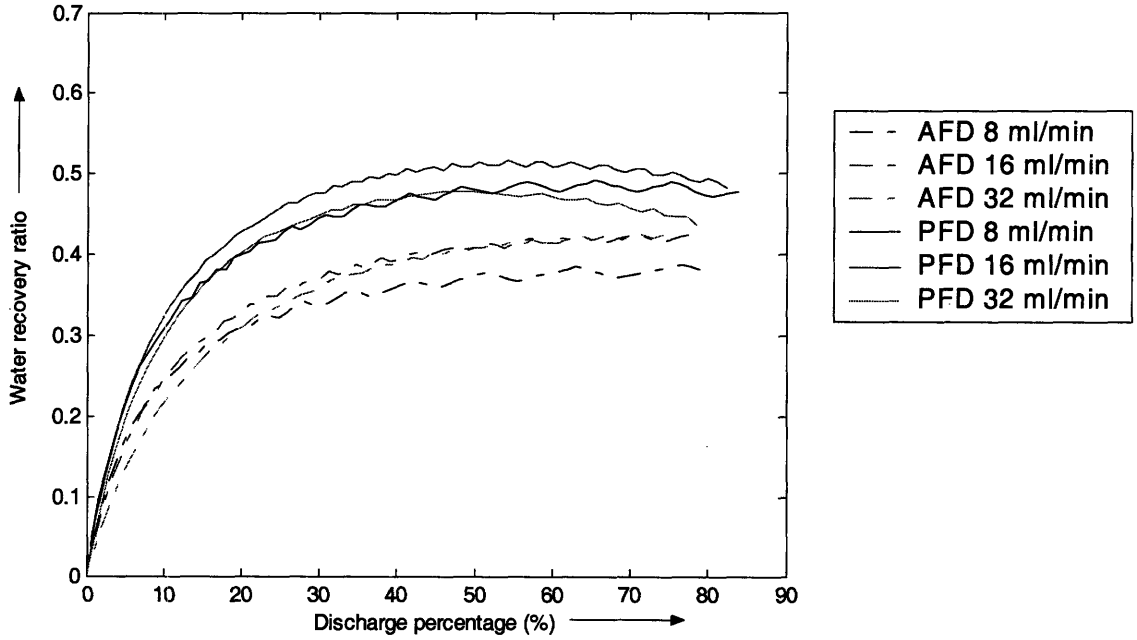

Fig. 30: Plot of water recovery ratio (standard) as a function of the discharge percentage for different flow rates of the AFD and PFD processes.

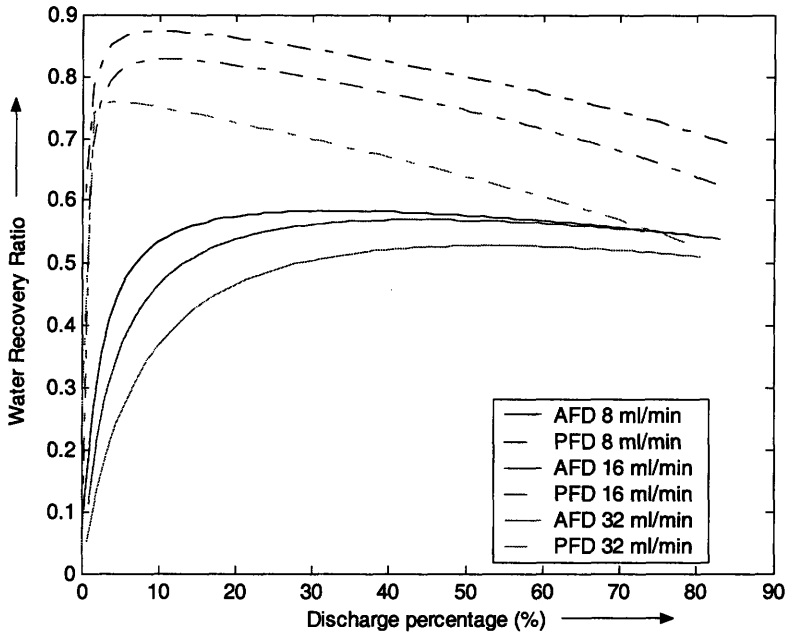

Fig. 31: Plot of modified water recovery ratio as a function of the discharge percentage for different flow rates of the AFD and PFD processes.

Fig. 30 and 31 provide us with the final piece of the puzzle. Fig. 30 charts the water recovery ratio as a function of the discharge percentage whereas Fig. 31 does the same for the modified water recovery ratio defined in Eqn. (3). The latter is physically interpreted as the water recovery ratio when no flow is permitted during the switching period. Before we go into the intricacies of what these curves do and do not reveal, let us discuss their most obvious features. From both the figures, it is obvious that a PFD process has a higher water recovery ratio than an AFD process for any flow rate. It is also evident that the PFD curves show a definite maximum, which is around the 45-50% discharge mark for the standard water recovery ratio and around the 5-10% mark for the modified water recovery ratio. The AFD curves show no such maximum leveling after an initial rise. The initial rise stops at around the same percentages stated for the optimum water recovery ratio values for the PFD process. The key point is that the difference in the maximum water recovery ratio values for the AFD and PFD processes is 20-35% for the standard water recovery ratio and 40-55% for the modified water recovery ratio over a substantial range of discharge percentage. It is but natural that the standard water recovery ratio is lower than the modified water recovery ratio as the latter has a smaller denominator.

Furthermore, Fig. 31 shows that the water recovery ratio for either process is higher for a lower flow rate than it is for a higher flow rate, which is what we predicted before we analyzed these processes. This is because of the fact that although the faster flow rate removes the ions at a faster pace, the rate is not fast enough to compensate for the higher total amount of water consumed during the discharging process, for the higher flow rates. Interestingly, the 8 ml/min and 16 ml/min AFD processes seem to follow identical curves. The reason for this is that the 8 ml/min flow rate is substantially slower in removing the ions (Fig. 24) and therefore the discharge process must continue for a disproportionately long time. This is not the case between 16 ml/min and 32 ml/min flow rates, for instance. These effects are altered to an extent by the introduction of the standard water recovery ratio in Fig. 30. This ratio accounts for the water used during the switching period. The introduction of the additional term in the denominator means that the low flow rates take even more time to come back to the charging phase, evidenced by the further fall

of the 8 ml/min AFD curve and the proportional rise of the 32 ml/min curve to the levels of the 16 ml/min curve. Due to the difference in the dependency of ion removal rate of the two processes on the flow rate, most of the above arguments made for the AFD case are not valid for the PFD case. We find that for the PFD case the 8 ml/min flow rate is substantially higher for the modified water recovery ratio curve and in the region of the 16 ml/min and 32 ml/min curves for the standard water recovery ratio because there is very little difference between the ion removal rates at different flow rates for the PFD process (Fig. 27).

There are two more notable points about these two water recovery ratio plots. Firstly, one notices the presence of slight 'tremors' in Fig. 30 while these are absent in Fig. 31. As one moves along the discharge percentage curve, it is observed that the 24 hour period, or 86400 seconds, is an integral multiple of the time period for one complete cycle for some specific values of the discharge percentage. For a discharge percentage that is slightly higher than any of the above mentioned values, the higher time period of discharging would result in a slightly larger value for the time period of one complete cycle. This slightly larger value would, in turn, mean that at least one less complete cycle can be implemented per day. Let us now look into this last incomplete cycle. If the time remaining is such that the system can be fruitfully employed in the charging phase, then the total amount of throughput water for the day is equal to the water desalinated in the charging periods for all the complete cycles plus that deionized during the charging phase of the incomplete cycle. Mathematically speaking, as long as the remaining time is less than or equal to the permissible charging time for the discharge percentage, the numerator increases with the denominator remaining constant. However, if the remaining time exceeds the charging time period the numerator becomes constant (as the charging phase has already been completed), and the denominator starts increasing, whether the time is required to discharge the setup or to switch back to the charging phase. Thus we find that within the last cycle, there is first a rise in the value for the water recovery ratio followed by a drop. It is to be noted that these tremors would be evened out over time, so if these curves were recomputed for a month or a year there would be very negligible tremors. In essence therefore the tremors are an artifact of the theoretical predictions taken for the period of a day.

Finally, we must comment on what appears to be the sudden truncation of the curves above a critical threshold (in the range of 70-80% discharge). The reason for this is two-fold. Firstly at the higher flow rates, especially 32 ml/min, this cut-off is determined by the maximum possible charging time since for a high flow rate, Eqn. (16) dictates that the permissible charging time reduces, all other parameters remaining constant. Secondly, we impose an artificial restriction that the discharging time cannot be greater than three time constants, irrespective of how many ions are taken out. This reduces the possible discharge percentage range for low flow rates, particularly for the AFD case. In other words, we do not let the 8 ml/min AFD process proceed for an irrationally high amount of time just because we would like to discharge a larger percentage of ions. The latter must be imposed because if too much time is used up in the discharging process, even if the flow rate is low, the charging process gets limited time to desalinate. This detrimental effect will not be captured in the water recovery ratio curves but can be seen while plotting the throughput of the processes as a function of the discharge percent.

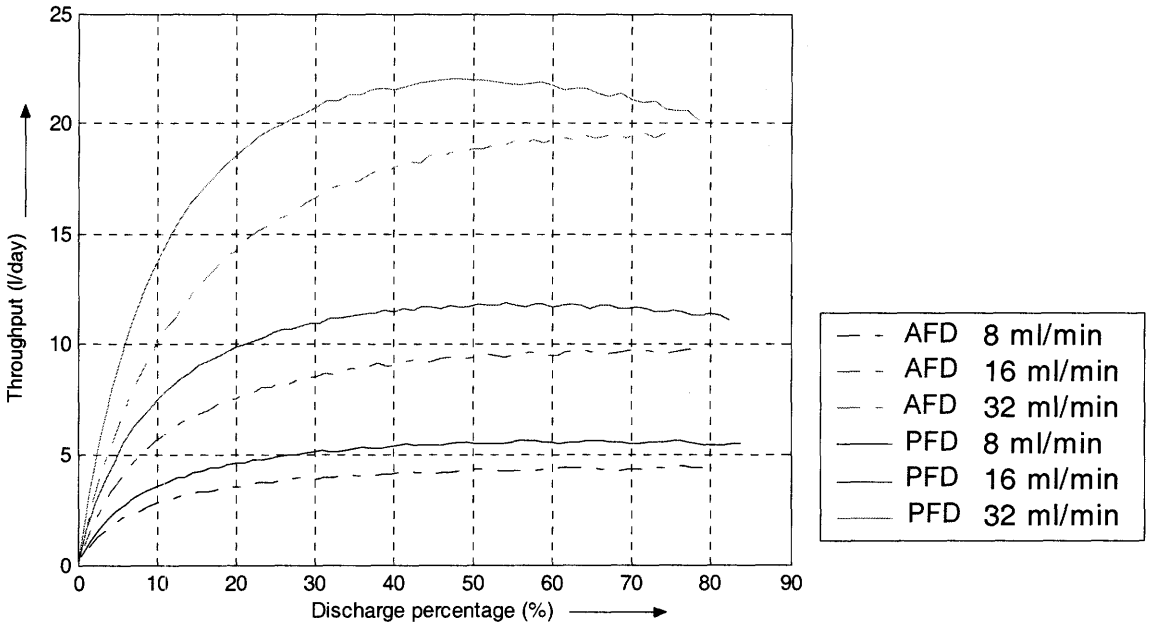

Fig. 32: Plot of throughput as a function of the discharge percentage for different flow rates of the AFD and PFD processes.

One can clearly see the effects mentioned in the previous paragraph in Fig. 32. The truncation in the AFD 8 ml/min curve as compared to the PFD 8 ml/min indicates that this is because of the disproportionately slow convection-diffusion phenomena at that axial flow rate, which results in excessive time requirements for removing higher percentage of ions from the system. The imposed restriction on the maximum time allowed for discharging results in the inability of 8 ml/min AFD process to discharge beyond 78%. The earlier truncation for the 32 ml/min curves for either process as compared to the corresponding curves for the 16 ml/min arises from the shorter permissible charging time periods. Please note that the curves, even for the 32 ml/min flow rate (where the cut-off is clearly due to the permissible charging time), for the two processes are not truncated at the exact same position for the AFD and PFD processes because the charging circuit parameters, namely initial charging current and time constant, are not the same.

More importantly, Fig. 32 reveals the usefulness of the PFD process. It predicts a 37.5 percent, 20 percent and 18.4 percent improvement in throughput for the PFD process as compared to the AFD process for 8 ml/min, 16 ml/min and 32 ml/min flow rates respectively. We note here that the comparisons have been made for the best case to best case situation, which means we compare the maximum throughput possible for a given PFD flow rate and the corresponding value for the same AFD flow rate, irrespective of where (at which value of discharge percentage) the maximum of each process occurs. Thus we can confidently state that no matter how well the AFD process performs, we can always operate the PFD process to give a 20-35 percent higher throughput, given our system and flow parameters. Again, this is not a strict upper bound and possibly one can raise the bar even further. Nevertheless, this signifies a substantial improvement and one can readily visualize that these performance metrics will have a huge bearing on the feasibility of the process on a commercial scale. If we say that a nominal 25 percent improvement in water recovery ratio can be obtained on top of the optimal 50-60 percent values for axial flow discharge (Table - 2), the net water recovery ratio can be pegged at 75-85%, which is comparable to the figures of merit for RO and EDR plants.

This figure raises hopes in a different direction as well. It is typically considered that CDI is a desalination methodology most appropriate for brackish water treatment. The reason for that is, apart from the insufficient surface area of the fabricated capacitive electrodes till date, too much water is wasted having to discharge or regenerate electrodes when one is charging with high concentration input water. For example, if a given setup can desalinate l0 liter of water, having 1000 ppm concentration, it can only produce a maximum of 1 liter throughput per cycle, for input water having 10000 ppm concentration. Now the water needed to regenerate the electrodes remains constant because the same number of ions has been adsorbed in both cases onto the EDL of the electrodes. Let us say the amount of water required to flush out the ions is 10 liter. Given this scenario, one is using up 20 liter of 1000 ppm water to produce 10 liter of acceptable water, which is acceptable. However, for 10000 ppm water, one is wasting 9 liter of water to produce a meager 1 liter of throughput, which is completely unacceptable. While we do not predict that utilization of the PFD process can cause a direct improvement from a 3000 ppm brackish water feed to a 35000 ppm seawater feed, which can only be accomplished by having a much higher surface area electrode, we estimate that a reasonable increase in the input concentration, mirroring the increase in water recovery ratio, is feasible by such an approach.

All the above improvements, however, would be to no avail if the primary advantage of capacitive deionization technique is lost in employing the permeating flow scheme. The power consumption estimates listed in Table – 2 indicate why CDI has been touted as a promising prospect for nearly a decade now. We need to re-evaluate these power consumption figures in the wake of the introduction of the new flow path. Qualitatively speaking, it is expected that the power consumption will rise because the new flow path will require additional pumping energy to ensure that the fluid crosses the porous electrode. This is over and above the electrical energy costs and the axial flow pumping costs present in the conventional process. As we only desalinate in the range of 35 ppm, it is difficult for us to guesstimate a reasonable power consumption value. However, we can use the upper limit of the various power consumption figures quoted in the literature as our reference value, to which the additional pumping costs must be added. Welgemoed and Schuttle [23] state that 0.59 kWhr/m^3 is a reasonable estimate for the power consumption per unit volume of water desalinated in an industrial module employing the capacitive deionization methodology. Let us now calculate an upper bound on the additional pumping requirements per unit volume from our knowledge of the underlying physics. We know from Eqn. (43) that the solvent flux is dependent on the net pressure difference across the porous electrodes. The net pressure difference is the difference between the hydrostatic pressure difference created by the pumping mechanism and the osmotic pressure difference due to the presence of larger number of ions on the middle channel side of the electrode than on the outer channel side. Eqn. (43) can be rewritten as:

$$\Delta P = \frac{J_V}{L_p S} + \sigma_S RT\Delta c \qquad (66)$$

Our first observation is that the first term on the RHS is fairly small for modest permeating velocities. Let us calculate this term for permeating velocity in the range of 1 mm/s, which is three orders of magnitude higher than the 8 μm/s value obtained in our experiments. Typically, the hydraulic conductivity of the carbon aerogel varies around 10^{-5} to 10^{-7} cm/s [64]. For our case, the 80% porosity would probably be higher than the upper limit mentioned here. A typical value of L_p, for the porous electrodes considered in this study for example, is thereby equal to 4 10^{-4} (/sec) for 0.025 mm thick membrane (electrode). This gives an estimated pressure requirement of the order of 2.5 m of water, which in SI units is approximately equal to 25 kPa. For experiments employing a much lower permeating velocity therefore, the pressure difference required would be proportionally reduced.

The osmotic pressure difference, therefore, necessitates the bulk of the applied gradient. Given the value of the capacitance per unit weight and the density of the material of the capacitive electrode, one can put a precise upper bound on the maximum number of ions that can be adsorbed on the surface per unit volume. For the carbon aerogel material considered in this study, the reference values were: 15-30 F/gm and 0.4-0.5 gm/cc. The reference capacitance per unit volume figure can thus be estimated to be 7.5 – 15 F/cc. With the knowledge that the voltage applied across the electrodes is 1.2 V, one can perform the following computation:

$$\Pi_{max} = 8.3\left(\frac{J}{K-mol}\right)300(K)\frac{15\left(\frac{F}{cc}\right)V_{electrode}(cc)1.2(V)}{96500(F/C)V_{electrode}(cc)(10^{-2})^3\left(\frac{m^3}{cc}\right)}\left(\frac{N}{m^2}\right) \quad (67)$$

where Π_{max} is the maximum possible osmotic pressure difference and $V_{electrode}$ is the volume of the electrode.

For the given set of data, the maximum possible osmotic pressure difference approximately equals 465 kPa. The total hydrostatic pressure difference that needs to be applied therefore equals the 25 kPa contribution (which is an extreme upper bound) from the solvent flux through the porous electrode and the 125 kPa contribution, where the osmotic reflection coefficient for the electrode material has been taken as 0.27 from Eqn. (57), from the osmotic pressure difference across the electrode. The total 150 kPa pressure difference required by the pump translates to a power requirement of 0.041 kWhr/m^3. The final outcome of these computations can therefore be stated in the following sentence:

The power requirement of the capacitive deionization process employing the axial flow discharge process, which has a base value of 0.59 kWhr/m^3, is increased by 0.041 kWhr/m^3 due to the utilization of the permeating flow discharge scheme.

In essence, therefore, there is a 7% increase in the power requirement of the process. This cannot be completely ignored but it is safe to say that the substantial power consumption advantage that is enjoyed by the conventional CDI process is still maintained, even if one employs the permeating flow discharge scheme. The total power requirement of 0.63 kWhr/m^3 is still far superior to the corresponding figures for RO and EDR processes.

Chapter 7: Conclusion

It is unquestionable that the time has come to focus our efforts and resources, on a global scale, to deal with what has increasingly turned out to be a problem of catastrophic proportions - the growing water scarcity issue. Some serious thinking over the past few decades have revealed that while desperate socio-economic measures are often the need of the hour to tackle the problem at hand, they provide only temporary relief and can sometimes even serve to worsen the problem in the long run. This provides ample motivation for a novel technological solution that can overcome the inherent barriers of water scarcity by desalinating the seemingly abundant reserves of seawater, or even, the somewhat limited quantities of brackish water. The state of the art desalination technologies, unfortunately, are unable to fill this gaping void, primarily due the prohibitive energy costs associated with these processes. Over the last decade, the capacitive deionization technique has been earmarked as a promising approach to deionize saline water. However, this technique, while enjoying almost an order-of-magnitude advantage in terms of energy costs, is plagued by its poor water recovery ratio and limited throughput characteristics. In this study, we propose a new discharge methodology which can significantly raise the water recovery ratio and throughput of the capacitive deionization technology. The significant advantage in energy costs, taken along with competitive water recovery ratio and throughput parameters, would thrust this novel technology into the forefront of growth in desalination processes and possibly cause a paradigm shift in the current opinion on desalination.

The underlying hypothesis of this novel discharge technique, which we call the permeating flow discharge scheme, is that the ions detached from the electrical double layer of the capacitive electrodes are removed at a faster rate by flow through the electrodes than by the conventional axial flow between the electrodes. Based on the physical phenomena that determine the two discharge methods, namely solvent drag and internal diffusion, it is shown that the permeating flow discharge scheme is able to decouple the intrinsically coupled capacitive deionization technology. The independence axiom, that forms the basis of the axiomatic design methodology employed in this study, states that in such a scenario, the independent control of the process parameters, in the sequence dictated by the design matrix, allows us to keep the system range within the design range without having to undertake unnecessary optimization. Motivated by this line of reasoning, we seek to employ the new discharge scheme in conjunction with the charging process of the capacitive deionization technology to obtain a complete process that can outperform the state of the art desalination technologies in terms of all the critical performance metrics, namely power consumption efficiency, water recovery ratio and throughput.

In order to verify the proposed hypothesis and determine the practical benefits extended by the permeating flow discharge technique, we performed a series of experiments to quantify the ion removal rate given consistent flow and system parameters for the two processes. Design of a table-top setup allowed us to test the two distinct flow discharge techniques, the conventional axial flow discharge and the proposed permeating flow discharge method. The experimental observations exhibit that over time scales in the range of the discharge circuit time constant (~ 10 minutes) the permeating flow scheme is able to remove twice as many ions from the setup as the conventional axial flow technique. This implies a reduction in the discharge time by up to a factor of two for discharge in the region of 50-70 percent. It might seem counter-productive, at first glance, to implement reduced discharge percent cycles, which would lead to only partial utilization of the surface area provided by the carbon aerogel for charging. However, in such a scenario both the water recovery ratio and the number of possible cycles in a day rise significantly, thereby more than compensating for the small loss in throughput on a per-cycle

basis. The mathematical formulations help to further develop this idea by making precise comparisons of the key performance metrics of the two processes.

The charging and discharging processes were mathematically formulated to characterize the impact of different flow and system parameters on the relevant physical phenomena for each process. The charging process model yields a smart tool for calculating the permissible charging time, which is an essential component in any water recovery ratio or throughput computations. An unsteady convection-diffusion model was developed to simulate the predominant phenomena in the interior of the channel surrounded by the discharging electrodes. For the permeating flow discharge case, we undertook an additional transmembrane flux analysis to account for the ions being taken away from the system due to the flow through the electrodes. The characterization of these processes provides us with not only a deeper insight into the system behavior but also valuable predictions for the performance metrics for the two discharge processes.

The finite difference solutions to the differential equations formulated in the theoretical models show very good agreement with the experimental observations from our table-top setup. We find that the reduced discharge percent cycles are indeed very beneficial not only for the permeating flow discharge process but also for the traditional axial flow discharge process as it prevents having to waste valuable time for the removal of a few more ions from the system. It is observed that, in the water recovery ratio versus discharge percent graphs, the water recovery ratio for the permeating flow discharge process is about 20-35 percent better than that for the axial flow discharge process. Furthermore, if one were to install an upstream valve in the system that could prevent the flow of water during the switching period, the extent of benefit in terms of water recovery ratio rises to about 40-55 percent. The throughput analysis also reveals a rise mirroring the 20-35 percent advantage for the water recovery ratio of a standard process (without additional valves). The ranges described herein reflect the dependency of the process metrics on the flow and system parameters. Moreover, we observe that the water recovery ratio curves for the permeating flow discharge process show a definite optimal discharge percentage, whereas no such maximum exists for the axial flow discharge process, although below a critical threshold the water recovery ratio shows a significant fall. It is to be noted that these figures are indicative of our setup and experiments and are by no means optimized as such. In other words, the advantages in employing the permeating flow discharge could supersede the benefits predicted here by a further 5-10 percent.

The study shows that based on the power consumption needs quoted in the literature, the increase in energy costs may not be negligible but the order-of-magnitude differential with the existing desalination techniques is by no means surrendered. This is a significant result as it prevents us from stepping into the trade-off zone where benefit in a couple of performance metrics might have been rendered useless by the loss felt along another. One can, at this point, clearly visualize the salient features of using the permeating flow discharge approach. We are able to implement a desalination technology, which is competitive with the reverse osmosis and electrodialysis reversal processes in terms of water recovery ratio and throughput, while maintaining a stranglehold over the power consumption ratings. The competitive nature of the former performance metrics is brought about by the 25-30 percent rise on top of the existing optimized figures of 50-60 percent observed by other investigators. The net water recovery ratio stands at a mean of 75 percent which is definitely comparable to the 80 percent mark set by the reverse osmosis process. Again, if one were to optimize the permeating flow discharge process, one might be able to not only reach but possibly cross the reference mark cited above. Moreover, the significant improvement in water recovery ratio would imply that the capacitive deionization process can be used to desalinate higher concentrations of input water. The introduction of this new discharge scheme would therefore reduce the bottleneck of the process, whereby only low

concentrations of saline water are considered to be suitable for desalination by this process. In conclusion, it would be fair to say that if these figures can be optimized and scaled up for an industrial plant, the desalination contribution would swing from a meager 0.3 percent of the global consumption figures to one more appropriate for a panacea for the water scarcity problem.

Evidently, further work needs to be done along a number of directions to consolidate this approach. It seems the best way forward is to construct a scaled-up experimental facility where one can not only test the above predictions about water recovery ratio, power consumption and throughput but also determine the long term operational effectiveness of the capacitive deionization approach coupled with the permeating flow discharge scheme. One would naturally look at a completely automated facility which can switch from one process to another depending on the time allotted for each part of a cycle, the concentration measurements made during the cycle or some combination of these two factors. The scaled-up facility would further allow us to test whether it is feasible to desalinate higher concentration input water. Finally, it would be easier to identify possible flaws with the proposed approach that might have been overlooked at the initial conceptual level. For example, one issue that would need to be addressed is the more frequent maintenance of a plant employing the permeating flow discharge approach due to the expected rise in the incidence of fouling of the porous electrodes. At this juncture, it is impossible to say how much this is likely to affect the economics of the process.

On the modeling side, one would need to find the theoretical bounds of the performance metrics that could be arrived at by employing the permeating flow discharge process. Characterization of the maximum benefits will not only establish the optimal operating conditions for a plant but also will provide figures that can be more comprehensively compared with the standard performance parameters of the existing desalination technologies. Before one can proceed to that stage, however, it is to be noted that the formulations herein might need some modification to account for other processes that could play a bigger role in scaled up systems, e.g. turbulence in the channel flow. In this context, it is also pertinent to mention that a more involved modeling of the porous electrodes is warranted to eliminate several of the simplifications that have been made for this initial study. The ultimate goal in the theoretical studies would be to establish a simulation model that can provide a walkthrough for a plant performance, whose flow and system parameters can be set by the end user. Such a model would be of great help in guiding the design and construction for an industrial level facility.

Other areas of research that would lead to substantial development of these conceptual ideas include the development of an enormously high surface area per unit flat surface area capacitive electrode. Possibly ideas of supercapacitors can be incorporated into material research in this direction. It would also be reasonable to investigate porous electrodes that come at lesser capital investments, even if it means a moderate reduction in the electrosorption capacity. As described in Chapter – 4, other design concepts, such as shell and tube type, could be employed in order to extract further benefit form this approach. On a more fundamental level, one could also investigate other phenomena, besides solvent drag for example, that could lead to similar improvements in the performance metrics of the system or, in the best case scenario, turn the batch operational mode of capacitive deionization into a continuous mode, where throughput can be obtained during the entire cycle. The final motivation is to establish a clear cut desalination methodology that can transform both seawater and brackish water to potable, agricultural and industrial water at prices competitive with the public water supply. Ideally, such a system could be hooked with solar power generation systems so that the effective energy costs reduced to a minimum.

References

[1] Howe, E.D., "Fundamentals of water desalination", M. Dekker, New York, 1974.

[2] "Water Crisis", World Water Council, http://www.worldwatercouncil.org/index.php?id=25 (6th May, 2007).

[3] "Global Water Use and Demand", Water Resources and Use in Australia, http://www.ozh2o.com/h2use.html (6th May, 2007).

[4] Spiegler, K. S., "Principles of desalination", Academic Press, New York, 1966.

[5] deMan, J. M., "Principles of food chemistry", 3rd edition, Aspen Publishers Inc., Maryland, 1999.

[6] "World water resources at the beginning of the 21st century", State Hydrological Institute, http://webworld.unesco.org/water/ihp/db/shiklomanov/summary/html/summary.html (6th May, 2007).

[7] Ortega-Guerrero, A., Rudolph, D. L., Cherry, J. A., "Analysis of long-term land subsidence near Mexico City: Field investigations and predictive modeling", Water Resources Research, Vol. 35 (11), 3327-3342, 1999.

[8] "Where we work", Water Partners International, http://www.water.org/waterpartners.aspx?pgID=881 (6th May, 2007).

[9] Kasper, D.L., Braunwald, E., Fauci, A.S., Hauser, S.L., Longo, D.L., Jameson, J.L., "Harrison's Principles of Internal Medicine", McGraw-Hill, New York, 2005.

[10] "Water for people, Water for life", World Water Development Report, United Nations, 2003.

[11] "Pilot Analysis of Global Ecosystems", World Resources Institute Report, 2001.

[12] "Global water supply and sanitation assessment 2000 report", WHO/UNICEF Joint Monitoring Programme for Water Supply and Sanitation, 2000.

[13] Klio, N., "Water resources and conflict in the Middle East", Routledge, Oxfordshire, England, 2001.

[14] "Contested environments", ed.: Bingham, N., Blowers, A., Belshaw, C., John Wiley & Sons, Inc., Chichester, UK, 2003.

[15] "The Helsinki Rules on the uses of the waters of international rivers", adopted by the International Law Association, 52nd Conference, Helsinki, August 1966.

[16] Rothfeder, J., "Our water is running out", The Boston Globe, 6th January, 2002.

[17] "The 19th IDA Worldwide Desalting Plant Inventory", Global Water Intelligence, Aug 2006.

[18] "Desalination and water purification technology roadmap", Sandia National Laboratories and U.S. Department of Interior, Bureau of Reclamation, Desalination and Water Purification Research and Development Program report #95, 2003 (http://www.sandia.gov/water/desal/docs/DesalRdmap04a.pdf (6th May, 2007)).

[19] "The 18th IDA Worldwide Desalting Plants Inventory", Wangnick Consulting, 2004.

[20] "Electrodialysis and electrodialysis reversal technology", ed.: Meller, F. H., Ionics, Watertown, MA, 1984.

[21] Vrijenhoeka, E. M., Hongb, S., Elimelech, M., "Influence of membrane surface properties on initial rate of colloidal fouling of reverse osmosis and nanofiltration membranes", Journal of Membrane Science, Vol. 188 (1), 115-128, June 2001.

[22] Farmer, J. C., Pekala, R. W., Fix, D. V., Mack, G. V., Poco, J. F., Grant, W. J., Pomernacki, C. L., Savoye, C. F., "Capacitive deionization with carbon aerogel electrodes", LLNL Report, 1995: http://www.llnl.gov/tid/lof/documents/pdf/226878.pdf (6th May, 2007).

[23] Welgemoed, T. J., Schutte, C. F., "Capacitive desalination technology: an alternative desalination solution", Desalination 183, 323- 340, 2005.

[24] Lee, J-B., Park, K-K., Eum, H-M., Lee, C-W., "Desalination of a thermal power plant wastewater by membrane capacitive deionization", Desalination 196, 125-134, 2006.
[25] Allison, R. P., "High water recovery with electrodialysis reversal," Proceedings, American Water Works Assoc. Membrane Conference, Baltimore, MD, Aug. 1-4, 1993.
[26] Buros, O. K., "The ABCs of Desalting", 2nd edition, IDA and SWCC, 2000.
[27] "The 17th IDA Worldwide Desalting Plants Inventory", Wangnick Consulting, 2002.
[28] "Desalination Technology- Multi-Effect Distillation", Oceanit Desalination Technology, http://www.e-monitoring.com/bws/desalinationTechnology/multiEffectDistillation.htm (6th May, 2007).
[29] Khan, A.H., "Desalination Processes and Multistage Flash Distillation Practice", Elsevier, Amsterdam, 1986.
[30] "Electrodialysis", Wikipedia, http://en.wikipedia.org/wiki/Electrodialysis (6th May, 2007).
[31] "Electrodialysis Reversal (EDR)", GE Water and Process Technologies, http://www.gewater.com/products/equipment/ed_edr_edi/edr.jsp (6th May, 2007).
[32] Clark II, E. H., "Water prices rising worldwide", Earth Policy Institute, http://www.earth-policy.org/Updates/2007/Update64.htm (6th May, 2007).
[33] Johnson, A. M., Newman, J., "Desalting by means of porous carbon electrodes", J. Electrochem. Soc., Vol. 118(3), 510-517, 1971.
[34] Andelman, M. D., "Flow-through capacitor", U.S. Patent No. 5,415,768, 1995.
[35] Andelman, M. D., "Non-fouling flow through capacitor system", U.S. Patent No. 5,779,891, 1998.
[36] Farmer, J., "Method and apparatus for capacitive deionization, electrochemical purification, and regeneration of electrodes", US Patent No. 5,425,858, 1995.
[37] Farmer, J. C., "Method and apparatus for capacitive deionization and electrochemical purification and regeneration of electrodes", U.S. Patent No. 5,954,937, 1999.
[38] Andelman, M. D., "Non-fouling flow-through capacitor", U.S. Patent No. 5,620,597, 1997.
[39] Van Konynenburg, R. A., Farmer, J. C., "Means for limiting and ameliorating electrode shorting", U.S. Patent No. 5,980,718, 1999.
[40] Hanak, J. J., "Apparatus and method for electrocoriolysis the separation of ionic substances from liquids by electromigration and coriolis force", U.S. Patent No. 5,858,199, 1999.
[41] Faris, S. M., "Movable electrode flow through capacitor", U.S. Patent No. 6,805,776, 2004.
[42] Tran, T. D., Farmer, J. C., Murguia, L., "Method and apparatus for capacitive deionization and electrochemical purification and regeneration of electrodes", U.S. Patent No. 6,309,532, 2001.
[43] Andelman, M. D., Walker, G. S., "Charge barrier flow-through capacitor", U.S. Patent No. 6,709,560, 2004.
[44] Max, M. D., "Segregated flow, continuous flow deionization", US Patent Application No. 20060049105, 2006.
[45] Suh, N. P., "Axiomatic Design: Advances and Applications", Oxford University Press, 2001.
[46] Farmer, J. C., Tran, T. D., Richardson, J. H., Fix, D. V., May, S. C., Thomson, S. L., "The application of carbon aerogel electrodes to desalination and waste treatment", LLNL, 1997 (http://www.osti.gov/bridge/servlets/purl/563143-U3gqnw/webviewable/563143.pdf (6th May, 2007)).
[47] "SEM photos – Carbon aerogel paper", MarkeTech International Inc., http://www.mkt-intl.com/aerogels/pages/semphotos.html (6th May, 2007).

[48] Yang, K.-L., Ying, T.-Y., Yiacoumi, S., Tsouris, C., Vittoratos, E. S., "Electrosorption of ions from aqueous solutions by carbon aerogel: an electrical double-layer model", Langmuir, Vol. 17, 1961-1969, 2001.

[49] Yoon, B.-J., Jeong, S.-H., Lee , K.-H., Kim, H. S., Park, C. G., Han, J. H., "Electrical properties of electrical double layer capacitors with integrated carbon nanotube electrodes", Chemical Physics Letters, Volume 388 (1-3), 170-174, 2004.

[50] Probstein, R. F., "Physicochemical Hydrodynamics: An Introduction", 2nd edition, John Wiley & Sons, New Jersey, 193, 1994.

[51] Newman, J., "Electrochemical Systems", Prentice-Hall, Inc., Englewood Cliffs, N.J., 454-495, 1991.

[52] Farahmandi, C. J., "A mathematical model of an electrochemical capacitor with porous electrodes," Proceedings on the Symposium on Electrochemical Capacitors, ed.: Delnick, F. M., Tomkiewicz, M., Electrochemical Society, 1997.

[53] Srinivasan, V., Weidner, J. W., "Mathematical modeling of electrochemical capacitors", Journal of Electrochemical Society, Vol. 146, 1650-1658, 1999.

[54] Vol'fkovich, Yu. M., Serdyuk, T. M., "Electrochemical capacitors", Russian Journal of Electrochemistry, Vol. 38(9), 935–958, 2002.

[55] Langlois, S., Coeuret, F., "Flow-through and flow-by porous electrodes of nickel foam. II. Diffusion-convective mass transfer between the electrolyte and the foam", Journal of Applied Electrochemistry, Vol. 19(1), 51-60 ,1989.

[56] Schlichting, H., "Boundary Layer Theory", McGraw-Hill, New York, 1968.

[57] Berman, A. S., "Laminar flow in channels with porous walls", Journal of Applied Physics, Vol. 24(9), 1953.

[58] Yuan, S. W., "Further investigation of laminar flow in channels with porous walls", Journal of Applied Physics, Vol. 27(3), 1956.

[59] Kedem, O., Katchalsky, A., "Thermodynamic analysis of the permeability of biological membranes to non-electrolytes", Biochimica et Biophysica Acta, Vol. 27 (229), 413-430, 1958.

[60] Patlak, C. S., Goldstein, D. A., Hoffman, J. F., "The flow of solute and solvent across a two-membrane system", Journal of Theoretical Biology, Vol. 5, 426-442, 1963.

[61] Kedem, O., Katchalsky, A., "A physical interpretation of the phenomenological coefficients of membrane permeability", The Journal of General Physiology, Vol. 45, 143-179, 1961.

[62] Teorell, T., "Transport processes and electrical phenomena in ionic membranes", Progress in Biophysics and Biophysical Chemistry, Vol. 3, 305, 1953.

[63] Meyer, K. H., Sievers, J. F., "*La perméabilité des membranes I. Théorie de la perméabilité ionique*", Helvetica Chimica Acta, Vol. 19(1), 649-665, 1936.

[64] Al-Muhtaseb, S. A., Ritter, J. A., "Preparation and properties of Resorcinol-Formaldehyde organic and carbon gels", Advanced Materials, Vol. 15(2), 101-114, 2003.

[65] Kong, F.-M., LeMay, J. D., Hulsey, S. S., Alviso, C. T., Pekala, R. W., "Gas permeability of carbon aerogels", Journal of Materials Research, Vol. 8(12), 3100-3105, 1993.

[66] "Carbon nanofoam", MarkeTech International Inc., http://mkt-intl.com/aerogels/pages/carbon.html (6th May, 2007).

[67] Deen, W. M., "Hindered transport of large molecules in liquid-filled pores", AIChE J, Vol. 33, 1409-1425, 1987.

[68] Anderson, J. L., Quinn, J. A., "Restricted transport in small pores: A model for steric exclusion and hindered particle motion", Biophys J, Vol. 14, 130-150, 1974.

[69] Hoffman, J. D., "Numerical Methods for Engineers and Scientists", 2nd edition, Marcel Dekker, Inc., New York, 2001.

[70] De Levie, R., "Advances in Electrochemistry and Electrochemical Engineering", ed: Delahay, P., Interscience Publishers, New York, Vol. 6, 1967.